Journal of Medicinal Chemistry

Article

Salicylic Acid Derivatives Inhibit Oxalate Production in Mouse Hepatocytes with Primary Hyperoxaluria Type 1

Maria Dolores Moya-Garzon, Cristina Martin Higueras, Pablo Peñalver, Manuela Romera, Miguel Xavier Fernandes, Francisco Franco-Montalban, José A. Gómez-Vidal, Eduardo Salido, and Mónica Díaz-Gavilán

J. Med. Chem., **Just Accepted Manuscript** • DOI: 10.1021/acs.jmedchem.8b00399 • Publication Date (Web): 20 Jul 2018

ACS Publications

is published by the American Chemical Society. 1155 Sixteenth Street N.W., Washington, DC 20036

Salicylic Acid Derivatives Inhibit Oxalate Production in Mouse Hepatocytes with Primary Hyperoxaluria Type 1.

María Dolores Moya-Garzón,[†¥] *Cristina Martín Higueras,*[‡¥] *Pablo Peñalver,*[†§] *Manuela Romera,*[†] *Miguel X. Fernandes,*[‡#] *Francisco Franco-Montalbán,*[†] *José A. Gómez-Vidal,*[†] *Eduardo Salido,*[*‡] *Mónica Díaz-Gavilán*[*†].

[†]Departamento de Química Farmacéutica y Orgánica, Universidad de Granada, Campus de Cartuja s/n, 18071 Granada, Spain.

[‡]Hospital Universitario de Canarias, Universidad La Laguna & Center for Rare Diseases (CIBERER), 38320 Tenerife, Spain.

ABSTRACT: Primary Hyperoxaluria Type 1 (PH1) is a rare life-threatening genetic disease related to glyoxylate metabolism and characterized by accumulation of calcium oxalate crystals. Current therapies involve hepatic and/or renal transplantation, procedures that have significant morbi-mortality and require long-term immunosuppression. Thus, a pharmacological treatment is urgently needed. We introduce here an unprecedented activity of salicylic acid derivatives, as agents capable of decreasing oxalate output in hyperoxaluric hepatocytes at the low micromolar range, which means a potential use in the treatment of PH1. Though correlation of this phenotypic activity with glycolate oxidase (GO) inhibition is still to be verified, most of the salicylic acids described here are GO inhibitors with IC_{50} values down to 3 μM. Binding mode of salicylic acids inside GO has been studied using *in silico* methods and preliminary structure-activity relationships have been established. The drug-like structure and ease of synthesis of our compounds make them promising hits for structural optimization.

INTRODUCTION

Primary hyperoxaluria type 1 (PH1) is a rare and life-threatening genetic alteration of glyoxylate metabolism that is due to a deficit of the enzyme alanine-glyoxylate aminotransferase (AGT). This enzymatic defect leads to an accumulation of glyoxylate, which is then converted to the end-product oxalate by lactate dehydrogenase (LDH).[1] When oxalate levels exceed renal excretion capacity, insoluble crystals of calcium oxalate accumulate, first in kidneys and secondly in extra-renal tissues. No pharmacological treatment addressing the pathogenesis of PH1 exists currently, although in some PH1 cases, administration of pyridoxine restores AGT enzymatic activity.[2,3,4] Double kidney-liver transplantation is the only curative option, but patients must be subjected to extensive immunosuppressive treatments for the rest of their life, with a survival rate of 86, 80 and 69 % at 1 year, 5 years and 10 years, respectively.[5,6] New molecular strategies aim to avoid the risks and limitations of surgery and immunosuppression in PH1. In such sense, current research focuses on two main lines. One of them is the recovery of AGT activity[7] and the other one the palliative diminution of oxalate production by inhibiting glyoxylate formation (substrate reduction therapy, SRT) or glyoxylate oxidation to oxalate (LDH inhibition).[8,9] SRT is a useful approach in inborn errors of metabolism characterized by substrate accumulation.[10,11] Enzymes glycolate oxidase (GO) and hydroxyproline dehydrogenase (HYPDH) are being explored as targets for SRT in PH1.[11,12,13] The FMN-dependent enzyme GO, which catalyzes oxidation of glycolate to glyoxylate, has recently been validated as a safe and efficient target for SRT in PH1 using genetically modified mice.[11] GO-deficient mice (*Hao1*$^{-/-}$) developed normally without adverse phenotypic effects and double KO mice (*Agxt1*$^{-/-}$*Hao1*$^{-/-}$) showed low levels of oxalate excretion compared to hyperoxaluric mice (*Agxt1*$^{-/-}$). In addition, the small GO inhibitor (GOi) CCPST (Figure 1), with an IC_{50} = 43.5 μM and K_i = 20.3 μM

against purified recombinant mouse GO (mGO), significantly reduced the production of oxalate in *Agxt1*$^{-/-}$ mouse hepatocytes *in vitro* [EC_{50}(24 h) = 25.3 μM, (48 h) = 33 μM, (72 h) = 34 μM]. Oral administration of CCPST to *Agxt1*$^{-/-}$ mice produced a 30-50% reduction in urine oxalate.[11] However treatment with CCPST needs a high dose which could lead to unwanted side effects and therefore special emphasis on the need of more potent GOi's has been made.[11]

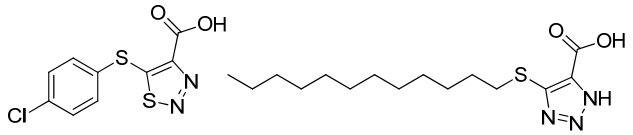

CCPST CDST

Figure 1. Structures of GO inhibitors CCPST and CDST.

Though the idea of using GOi's for the treatment of PH1 has been suggested before[14] and several small-molecule GOi's have been described, no useful drug has been identified for the treatment of PH1 patients. Non-favorable physicochemical properties, such as poor aqueous solubility contribute to this in molecules such as CDST[15] (Figure 1) (K_i = 15 nM). Available structures of spinach (sGO)[16] and human enzymes (hGO)[17,] co-crystallized with inhibitors such as CCPST[18] and CDST[15] has allowed the establishment of some structure-activity relationships.[15,19,20,21,22] Known GOi's bear a polar head with an acidic functionality; the presence of a protonated heteroatom located β with respect to the acidic function is beneficial.[18,22] Flat, electron rich fragments stabilize ternary complex enzyme-cofactor-substrate by π-π interactions with FMN flavin ring, and hydrophobic aliphatic or aromatic groups hang from the polar head. The polar moiety of these inhibitors must enter into the GO active site while the side chain remains in the hydrophobic access channel causing a disorder that prevents its closure.[15] Therefore, a two-region binding site is envisaged for GOi's.[18] According to crystallographic

data,[15,18] CDST and CCPST mimic glyoxylate interactions in the active site of hGO (Figure 2). Carboxyl groups of CDST, CCPST and glyoxylate overlay interacting with residues Arg167, Arg263 and Tyr26 while the N atoms at position 3 of the heterocyclic rings of CDST and CCPST overlay with the keto group in glyoxylate and interact with His260. Thiadiazole ring of CCPST does not carry a proton and neither does the glyoxylate keto group. Therefore, interaction of these two molecules would require the protonation of His260 and this would contribute to the weaker binding of CCPST compared to CDST.[22] CDST and CCPST also hydrogen bond to Tyr132 *via* the ring N2. This group of aminoacids constitutes the first of the two binding regions for GOi's. The second binding region establishes hydrophobic interactions with the side chain of the inhibitor and is constituted by variable aminoacids for each GOi. Trp110, Leu205, Tyr208 are noteworthy residues interacting with CCPST and CDST. Within this second binding site, flexible chains such as the one of CDST would help to a better accommodation of the inhibitor.[22]

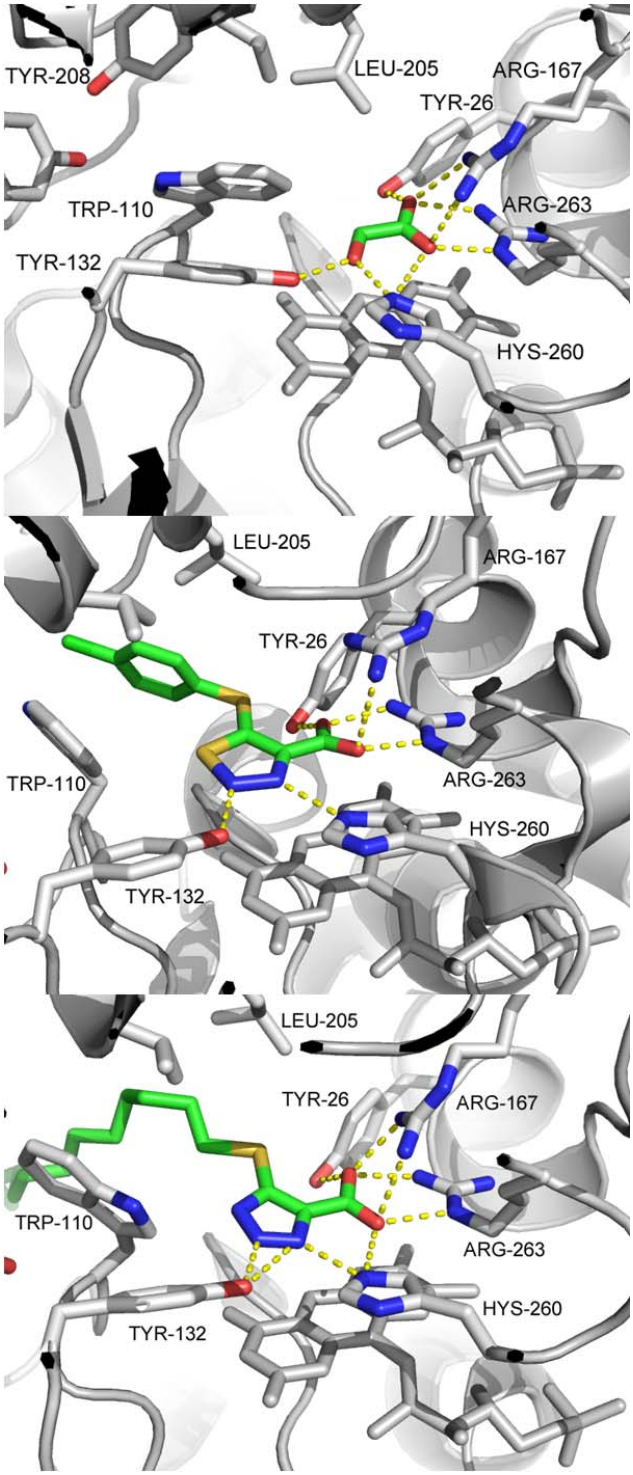

Figure 2. Interactions of glyoxylate (up), CCPST (center) and CDST (down) in hGO active site. Obtained from crystallographic data (PDBid: 2RDU; 2W0U; 2RDT from top to bottom).

Small proline-like inhibitors for HYPDH have also been prepared and their IC_{50}s on isolated enzyme found to be around 0.30 mM.[23] No data on cells have yet been published for this type of inhibitors.

Apart from GO and HYPDH inhibition using small molecules, development of siRNA[24,25,26,27,28] and antisense oligonucleotides against these enzymes are currently under research.[29] Better ADME properties and an easier delivery into affected cells favors small molecules over nucleotide molecules. However, it is also possible that synergistic effects could arise from small drug/siRNA co-administration.

In our search for novel GOi's as possible drugs for the treatment of PH1, we looked for structural motifs matching the required characteristics of this type of inhibitors. We envisaged the salicylic core as a promising candidate as it presents a protonated heteroatom located β relatively to an acidic functionality.[22] Its flat electron-rich ring bears a carboxylic acid that could reproduce interactions at Arg167, Arg263 and Tyr26 while the protonated oxygen of the phenolic function could act as hydrogen donor in the interaction with His260. As in the case of CDST, no energetically costly protonation of His260 would be required. In addition, salicylate derivatives are broadly used as therapeutic agents[30] and the preparation of new compounds based on this structure would easily lead to drug-like hits with good ADME properties. Our preliminary docking studies for salicylic acid agreed with this presumption, showing favorable interactions within hGO crystallographic structure and a binding pattern comparable to the one of CDST and CCPST in the binding regions 1 and 2 (Figure 3). Using the same docking methodology, interaction figures were obtained for CDST and CCPST agreeing with the interaction profile already described from crystallographic studies (Figure S1).

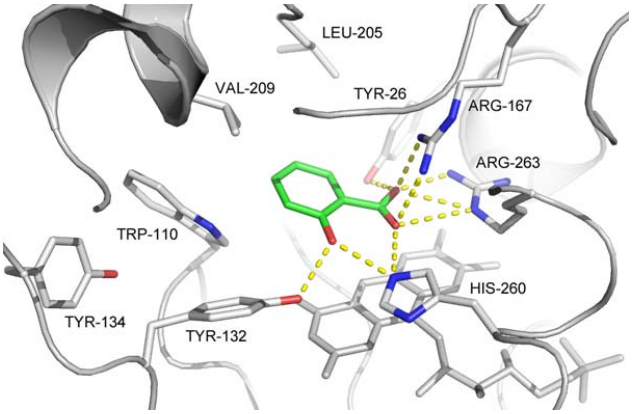

Figure 3. Docked salicylic acid inside hGO active site (PDBid: 2RDT).

We describe the design, synthesis and biological evaluation of salicylic acid derivatives as novel agents decreasing oxalate output from PH1-mouse primary hepatocytes in a more effective way than CCPST. The drug-like structures of these compounds make them promising hits for structural modification. This finding opens the gate for salicylic acid derivatives to be used in the treatment of PH1. No bibliographic precedent could be found relating salicylate core with this kind of biological activity.[31] Therefore a new target for salicylates as well as a novel application in the decrease of oxalate production is herein introduced.

RESULTS AND DISCUSSION

For all the compounds included in this study, we have evaluated their inhibitory activity on recombinant mGO as well as their capacity to diminish oxalate production in hyperoxaluric mouse hepatocyte cultures. In the cell-based assay, glycolate added to the cell culture medium is metabolized to glyoxylate by GO and this last one oxidized to oxalate mainly by LDH. Excreted oxalate is quantified from the extracellular medium using a colorimetric assay. When a good GOi is added, the first step is blocked and a decrease of oxalate release is then observed. We

have used theoretical partition coefficients (expressed as $logP_{th}$), corresponding to unionized species, as an empirical indicator to discard too lipophilic molecules (logP > 5) which could be retained in the cellular membrane. Favorable $logP_{th}$ values (between 0 and 5) would help good membrane permeability. Additionaly, we have made *in silico* calculations about binding mode inside the human enzyme. Mouse and human GO proteins share 89.5 % sequence identity.[32] We have chosen purified mGO as a high-quality tool for the screening of potential inhibitors as activity results can be safely translated in to a human setting and, at the same time, the comparability of our findings can be assured when the biological testing is escalated to the available mouse cellular systems. On the other hand, prediction of the binding mode for each compound inside hGO has allowed comparison with glyoxylate, CCPST and CDST crystallographic data.[18]

Our work on salicylates began with the screening of a small group of salicylic-related compounds (**1**-**17**, Figure 4) for a preliminary outlook on their GO inhibitory activity and their capacity to reduce oxalate production in *Agxt1*$^{-/-}$ mouse primary hepatocytes. The group included simple salicylic acids (**1**-**9**), benzofused derivatives (**10**-**16**) and the structuraly related chloroquinoline (**17**), which were chosen according to structural diversity criteria. These aromatic systems aim at exploring different types of interaction at the enzymatic active site. Differently sized, rigid or flexible, aliphatic, aromatic and heteroaromatic side chains with polar and hydrophobic functionalities were searched to explore interaction modes at the access channel. Except for **16**, all of them were obtained from commercial sources.

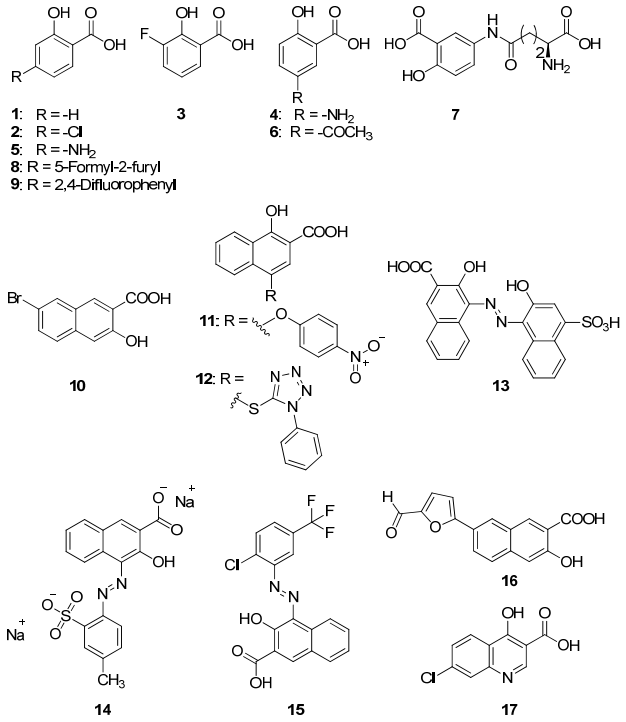

Figure 4. Structures of salicylate-related compounds selected for a preliminary screening on primary and secondary assays.

Salicylic acid (**1**) showed a low inhibitory effect (less than 30 %) at 25 μM over mGO catalytic activity, lower than the activity found for CCPST (34.8 %) (Table 1). Neither halogen substitutions on the phenyl ring (**2**, **3**) nor chloride-quinoline (**17**) showed inhibitory increases compared to compound **1**. Addition of an amine group on C5 (**4**) instead of C4 (**5**) did indeed yield higher inhibition of the enzymatic activity (71.9 ± 3.2 % at 25 μM), with an IC_{50} of 7.8 ± 1.2 μM, but did not decrease oxalate release in *Agxt1*$^{-/-}$ cells. In turn, 5-acetyl (**6**) and polar 5-glutamine (**7**) substitutions did not improve GO inhibition compared to **1**. Insufficient hydrophobic interactions may be the reason for the low GO inhibitory activity observed for these compounds. Compounds **8** and **9** (diflunisal)[33] present hydrophobic side chains, a key feature for GO inhibition. Compound **9** still presented an inhibition percentage lower than 30 %, but

compound **8** inhibited 82.8 ± 5.6 % GO enzymatic activity at 25 μM with an IC_{50} of 34.5 ± 1.2 μM. However, even with a favorable $logP_{th}$ value, it was neither efficient decreasing oxalate output of *Agxt1*$^{-/-}$ hepatocytes (Table 1).

Table 1. Biological data of the first set of compounds and CCPST and *in silico* prediction of partition coefficient ($logP_{th}$). Biological determinations: (i) Enzymatic inhibition on purified mouse glycolate oxidase (mGO), assays either at single concentration (25 µM) and IC_{50} calculation after fitting dose-response curves. (ii) Excreted oxalate in *Agxt1*$^{-/-}$ mouse primary cultured hepatocytes, compared to control (relative oxalate).

Compound	mGO[a] (%)	IC_{50} (µM)	R^2	Relative oxalate[b]	$logP_{th}$
CCPST	34.8 ± 4.8	43.5 ± 1.1		0.63 ± 0.16[c]	n/a
1	18.5 ± 13.7	n/a		n/a	1.46
2	20.8 ± 4.4	n/a		n/a	1.98
3	13.5 ± 4.6	n/a		n/a	1.60
4	71.9 ± 3.2	7.8 ± 1.2	0.93	0.88 ± 0.02	0.68
5	14.9 ± 7.9	n/a		n/a	0.68
6	22.1 ± 1.0	n/a		n/a	0.77
7	7.8 ± 2.8	n/a		n/a	0.42
8	82.8 ± 5.6	34.5 ± 1.2	0.88	0.88 ± 0.18	0.29
9	27.9 ± 0.6	n/a		0.88 ± 0.08	3.42
10	42.3 ± 1.1	39.9 ± 1.1	0.94	0.99	3.25
11	96.3 ± 0.5	2.9 ± 1.1	0.97	0.77 ± 0.01	1.00
12	75.3 ± 2.6	11.1 ± 1.1	0.98	0.99 ± 0.01	5.93
13	75.1 ± 2.3	n/a		1.11 ± 0.03	4.87
14	1.5 ± 2.1	n/a		n/a	4.62
15	47.4 ± 2.3	n/a		0.91 ± 0.04	6.17
16	26.2 ± 1.6	n/a		n/a	0.72
17	24.8 ± 5.9	n/a		n/a	2.53

[a]Percentage of inhibition of purified mGO at 25 µM of the drug, after 1 min. [b]Oxalate output tested at 24h post-treatment with 10 µM of the drug in *Agxt1*$^{-/-}$ mouse primary hepatocytes cultured with 5 mM glycolate, in 6-well plates. Data are represented as mean ± SD of n = 3 replicates. One-way ANOVA statistical analysis, $p<0.05$ was considered statistically significant. [c]Data at 12.5 µM in *Agxt1*$^{-/-}$ mouse primary hepatocytes. IC_{50}: Calculated on mouse glycolate oxidase in saturated conditions of glycolate (22.2 mM). R^2: IC_{50} curve-fitted score. n/a: Not assessed.

A total of seven commercial benzofused salicylates (naphthylic acids) with different substitution patterns were included in the preliminary screening (**10**-**16**, Figure 4). The additional

benzene ring was thought to possibly reinforce the binding of the molecule to the target via hydrophobic interactions. The increase in the hydrophobicity consequent to the adition of the fused benzene is in fact reflected in higher $logP_{th}$ values (Table 1). The simplest of these molecules carried a bromine group bound to the naphthalene core (**10**), while more complex structures had an electron-rich linker (azo group, sulfur or oxygen atom) to aromatic cycles (tetrazole, benzene or naphthalene). 4-Substituted 1-hydroxy-2-naphthylic acids with flexible ether or thioether linkers, **11** and **12**, presented good inhibition percentages on isolated mGO (96.3 ± 0.5 and 75.3 ± 2.6 %, respectively) (Table 1). Compounds **13-15** are 4-arylazo-3-hydroxy-2-naphthylic acids with rigid azo linkers; **13** and **14** bear polar sulfonic functionalities on the aromatic side chain while **15** contains lipophilic halogens. Within this group, compound **13** yielded a 75.1 ± 2.3 % mGO inhibition at 25 μM, the activity of **15** remained close to 50 %, while **14** dramatically lost inhibition activity. Finally, compound **10**, with no extended side chain, showed an inhibitory activity below 50 %. Replacing the bromine atom on the C7 of **10** with an aromatic side chain **(16**), using Suzuki-Miyaura cross-coupling, led to lower inhibitory activity. From this first set of compounds, we found the naphthyl derivative **11** to be the best GOi (IC_{50} = 2.9 ± 1.1 μM), which also resulted in the most efficient hit *in vitro*, but still limited to only 23 % reduction of excreted oxalate at 10 μM.

Predicted binding modes show that compounds **1-17** reproduce with only slight differences the interactions of glyoxylate, CCPST and CDST in the active site of hGO (Table S1) (representative 2D-interaction diagrams for group **1-17** are shown in Figure 5; 2D-interaction diagrams for the whole group **1-17** in Figure S2). Electrostatic and/or hydrogen bond interactions with Arg167 and Arg263 can be established through both carboxy and hydroxy groups of the β-hydroxybenzoic fragment of **1-17**. Salicylic acids **1-9** also establish hydrogen bond interactions

with His260 through the heteroatoms in the salicylic head although they lack interaction with Tyr26 (except **6** and **7**). Contrary to what had been initially envisaged, interactions at His260 are established, like glyoxylate and CCPST, by hydrogen donation from the aminoacid. Except **6** and **9**, they all interact with Tyr132 but, differently to CDST and CCPST, they do it by hydrophobic bonding. Quinoline **17** followed a similar interaction pattern than compounds **1-9** in this binding region 1.

A different binding pattern was found for β-hydroxy naphthylic derivatives (**10-16**) in this first binding region (Table S1). While interactions at Arg167 and Arg263 were conserved, interaction with His260 could not be observed for these compounds. However, a hydrogen bond interaction with Tyr26, which was not observed in **1-9** or quinoline **17**, was found to be established now (except for compound **12**), happening through the β-OH and/or the carboxy group of the salicylic head. In all cases, Tyr26 appears to behave as hydrogen donor. Compound **11** only interacts with Tyr26 through the carboxylate group, remaining the β-OH functionality free for interaction with Tyr132 (Figure 5). This interaction βOH-Tyr132 is not observed in any other naphthylic or salicylic derivative and it happens by hydrogen donation from the β-hydroxy group of **11**. It is remarkable as **11** was also the most potent mGOi within this first group of compounds (**1-17**). Compounds **10**, **13** and **16** interact with Tyr132 by hydrophobic while **15** interacts via π-π stacking interactions. Compounds **12** and **14** lack any type of interaction with Tyr132 (Figure 5).

About interactions in the binding region 2, compounds **1-7** and **10**, lacking a hydrophobic tail establish hydrophobic interactions with Trp110, through the salicylic aromatic ring (ring A), except for compound **6** that uses the acetyl group for this interaction. Interestingly, when a second aromatic ring is bonded to the salicylic head, interaction with Trp110 normally happens

through the ring in the side chain (ring B), except for compound **15**, which presents no interaction with Trp110 (Figure 5). Bonding to this aminoacid happens by means of π-π stacking in all the compounds that present ring B (**8**, **11**-**14**) except in **9** and **16**, that interact *via* hydrophobic forces. Only compounds with a side chain pending from the β-hydroxybenzoic fragment interact at Leu205 and Tyr208 (**1**-**6** *vs* **7**-**16**, Table S1). Quinoline **17** is the only exception able to interact at Leu205 without presenting a hydrophobic side chain.

The choice of testing 2-hydroxynaphthoic acids *vs* single-ring salicylic acids was aimed at establishing novel hydrophobic interactions that would eventually increase the binding affinity of the molecules. Prediction models showed naphthoic derivatives **12**, **13**, **15** and **16** could establish hydrophobic (**12**, **13**, **16**) or π-π stacking (**15**) interactions through the extended aromatic system (Figure 5). These interactions could produce a slight increase of the GO inhibitory activity (**12**, **13** or **15** *vs* **14** or **17**, Table 1) but are not essential (**12** *vs* **11**, Table 1). Furthermore, they are not related to a capacity of decreasing oxalate release. On the other hand, the presence of the condensed aromatic system is detrimental for the aqueous solubility of the compounds and complicates the synthetic process. Thus, we decided to concentrate our efforts on the structural optimization of simple salicylic acids. Predicted binding modes for group **1**-**17** indicated that aromatic rings, either electron-rich or electron-poor carbocycles or heterocycles, attached to the salicylic head reinforce binding to hGO by interaction at the binding region 2. Both, aryl and heteroaryl rings have led to mGO inhibitors such as the furylsalicylate **8** (IC_{50} = 34.5 ± 1.2 μM), or the naphthoic acids **11** and **12** with nitrophenyl and phenyltetrazole side chains (IC_{50} = 2.9 ± 1.1 and 11.1 ± 1.1 μM, respectively) (Table 1). Taking all this into account, we focused on the preparation of salicylic acids bearing aromatic heterocycles and carbocycles as hydrophobic tails (heteroaryl and biphenyl analogues, respectively).

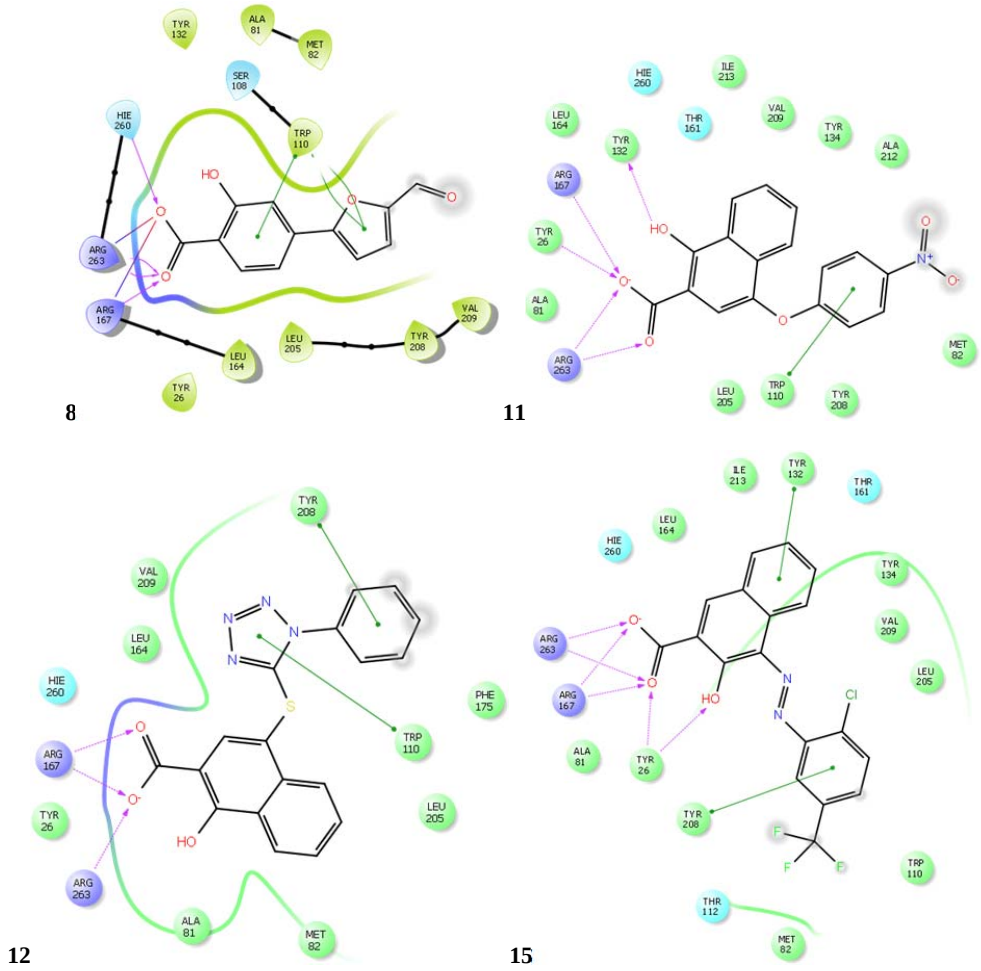

Figure 5. 2D Diagrams of interactions between compounds **8**, **11**, **12**, **15** and human glycolate oxidase residues (purple: basic, cyan: polar uncharged, green: non-polar). Grey shadow represents interaction with solvent. Hie260: His260 protonated on N_ε [Maestro software (Schrödinger)].

Synthesis of salicylic acid derivatives. Most of our final compounds were prepared, in moderate to high yields, following an easy one-step procedure based on Suzuki-Miyaura cross-coupling, starting with commercial aryl halides (**18**) and boronic acids (**19**) (Scheme 1). Three different standard methods were followed depending on easiness of purification and yield

criteria. These methods differ in the catalytic system, reaction solvent and the use of conventional or microwave heating. Palladium acetate was used to catalyze this process, either in complex with triphenylphosphine or microencapsulated in polyurea (PdEnCat®). The use of microencapsulated palladium acetate (PdEnCat®) was preferred due to its economic and environmental advantages derived from its easy removal/reuse and the environmentally friendly ligand-free solvent system.[34] PdEnCat® reactions were developed in an ethanol/water mixture while soluble palladium acetate was used in dimethylformamide/water systems. In all reactions self-coupling processes were minimized by displacement of oxygen with argon in the reaction system.

Scheme 1. Synthesis of aryl salicylates by Suzuki-Miyaura cross-coupling[a]

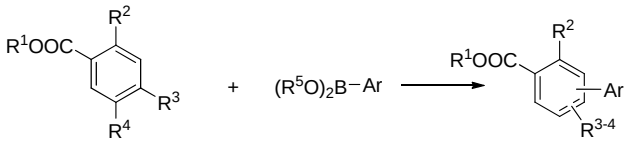

18 **19** **20-55**

[a]Reagents and conditions: Method A: i) K_2CO_3, $Pd(OAc)_2$, PPh_3, DMF/H_2O (1/1), 100 ºC; ii) HCl 10 %, H_2O, 0 ºC. Method B: i) K_2CO_3, PdEnCat®30 0.4 mmol/g, EtOH/H_2O (1/1), 100 ºC; ii) HCl 10 %, H_2O, 0 ºC. Method C: i) K_2CO_3, $Pd(OAc)_2$, PPh_3, DMF/H_2O (1/1), 100 ºC microwave; ii) HCl 10 %, H_2O, 0 ºC. Detailed structures of **18** and **19** in Table S2.

When 2-hydroxyesters were used as starting materials type **18** (R_1 = -CH_3, R_2 = -OH) (e.g. methyl 5-iodosalicylate **18a**: R^3 = -H, R^4 = -I), hydrolysis of the ester functionalities happened in the mildly basic aqueous medium of the Suzuki reaction. This way, the final coupled free carboxylic acids were obtained in a two-step (coupling-hydrolysis) one-pot procedure. However,

when 2-alkoxybenzoates were used as starting materials type **18** (R^1 = -CH_3, R^2 = -OCH_3), ester hydrolysis did not happen in the Suzuki coupling conditions. These results can be explained by means of a neighbor group participation process. Basic hydrolysis of salicylate esters seems to be mediated by the neighboring free hydroxy group, probably by hydrogen bridging to the basic carbonyl group. This intramolecular bond is not possible in the case of 2-alkoxybenzoates and thus the hydrolysis of this type of esters requires more drastic conditions.

Reaction yields expressed in this work refer to purified products and have been calculated considering only product presenting more than 95 % purity in HPLC. For that reason, some yields fall below 50 %. Purification at the low scale used in this work was the major issue found in the synthetic protocol of our compounds, due to low solubility in organic solvents and high affinity for polar stationary phases of chromatographic systems. Eventual large-scale production however, could allow the use of non-chromatographic purification methods and the consequent increase of yield. In this work, further reaction optimization studies were not carried out as the most active compounds in terms of mGO inhibition and oxalate decrease were obtained in satisfactory yields, ranging between 72-100 %.

Heteroaryl analogues. Taking **8** (Figure 4) as the reference heteroaryl compound, we started making minor structural modifications to explore the influence of each structural fragment on the biological activity of this compound. In order to determine to what extent is the salicylic head necessary for the GO inhibitory activity of **8**, we synthesized the non-salicylic derivatives **20**-**25** (Figure 6), i) with no phenolic or carboxy functionalities (**20**[35], **21**[36]); ii) with decreased or null hydrogen donor capacity at C2 (**22**-**23**); iii) unable to ionize at physiological pH (**24**); iv) with increased hydrogen donor capacity on the phenolic group (**25**).

Compounds **20-25** were prepared according to the general procedure indicated in Scheme 1. Under these conditions ester **24**, lacking a free neighboring hydroxy group (Figure 6), did not undergo hydrolysis. Compound **23** (Figure 6) was prepared from **24** by treatment with sodium hydroxide.[37]

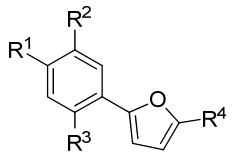

	R^1	R^2	R^3	R^4
8	-COOH	-OH	-H	-CHO
20 (42 %)	-H	-COOK	-H	-CHO
21 (76 %)	-OH	-H	-H	-CHO
22 (30 %)	-COOH	$-CH_2OH$	-H	-CHO
23	-COOH	$-OCH_3$	-H	-CHO
24 (57 %)	$-COOCH_3$	$-OCH_3$	-H	-CHO
25 (48 %)	-COOH	-OH	$-NO_2$	-H

Figure 6. Structures of the non-salicylic compounds tested. In brackets: isolated yields in Suzuki-Miyaura coupling (method A: **21-25**; method C: **20**).

Like before, the biological activity of **20-25** on recombinant mGO and on hyperoxaluric mouse hepatocytes was evaluated (Table 2) and binding modes (Table S3, Figures 7 and S3) were calculated. Unfavorable negative values of $logP_{th}$ were found for some of the compounds in this set (Table 2).

Table 2. Biological data of non-salicylic compounds **20**-**24** and **25,** and *in silico* prediction of partition coefficient ($logP_{th}$). Comparison with CCPST and **8**. Biological determinations: (i) Enzymatic inhibition on purified mouse glycolate oxidase (mGO); (ii) Excreted oxalate in *Agxt1*$^{-/-}$ mouse primary cultured hepatocytes, compared to control (relative oxalate).

Compound	mGO[a] (%)	Relative oxalate[b]	$logP_{th}$
CCPST	34.8 ± 4.8	0.63 ± 0.16[c]	n/a
8	82.8 ± 5.6	0.88 ± 0.18	0.29
20	22.7 ± 8.7	0.86 ± 0.11	0.00
21	24.2 ± 5.4	**0.32 ± 0.06***	0.01
22	0	0.98 ± 0.23	-0.54
23	0	0.82 ± 0.04	-0.26
24	17.5 ± 4.8	0.90 ± 0.10	-0.22
25	5.9 ± 3.1	0.86 ± 0.04	-2.24

[a]Percentage of inhibition of purified mGO at 25 μM of the drug, after 1 min. [b]Oxalate output decrease tested at 24h post-treatment with 10 μM of the drug in *Agxt1*$^{-/-}$ mouse primary hepatocytes cultured with 5 mM glycolate, in 6-well plates. Data are represented as mean ± SD of n = 3 replicates. One-way ANOVA statistical analysis, *$p<0.05$ was considered statistical significant. [c]Data at 12.5 μM in *Agxt1*$^{-/-}$ mouse primary hepatocytes. N/A: Not assessed.

None of the compounds **20**-**25** presented satisfactory activities against purified mGO (Table 2).

The experimental values indicate the need to maintain the carboxylic acid and the free phenol in any derivative prepared from **8** in order to preserve the inhibitory activity against mGO (**8** *vs* **20**, **21**, **23** and **24**); they also suggest the irreplaceability of the phenolic group by a benzylic hydroxy group (**8** *vs.* **22**). These data mean the carboxy and the aromatic β-OH groups are playing essential roles in the interaction with the enzyme. From the experimental data it would be reasonable to think the β-OH is behaving as a hydrogen donor (**8** *vs* **22** and **23**). In this line, compound **25**, in which an electron-withdrawing nitro group is situated *para* with respect to the phenolic OH, would be expected to be a better inhibitor. However, it resulted in a drastic loss of

GO inhibition activity (Table 2). Binding mode predictions for **8** (Figure 5) did not show interaction through the β-OH. Analysis of the 2D-interaction diagram for **22**, **23** and **25** show that the benzylic alcohol in **22** behaves as a hydrogen acceptor from Tyr132 (Table S3, Figure S3). When this benzylic hydroxy group is substituted by a methoxy group (**23**), the hydrogen bond with Tyr132 disappears and instead the methyl group appears involved in hydrophobic interactions with the same aminoacid (Table S3, Figure S3). In the case of compound **25** (Figure 7), the presence of the nitro group displaces the molecule in the active center and avoids the essential interactions at Arg167 and Arg263 and the interaction with His260, all of which are established by the carboxy groups of **8**, **22** and **23**. Thus according to the predicted binding mode, the β-OH group of **8** would not participate in hydrogen bonding to the enzyme while the benzylic alcohol in **22** and the methoxy group in **23** would interact with the enzyme *via* hydrogen bond or hydrophobic forces. The better mGO inhibitory activity found for **8** *vs* **22** and **23** could then be due to the less bulky group at the β position, which allows a better accommodation of the molecule inside the active site of mGO, rather than to hydrogen donation through the phenolic functionality. However, the presence of the β-OH is needed as its removal leads to a loss of inhibitory activity (**8** *vs* **20**) (Table 2). 2D-Interaction diagram for compound **20** (Table S3, Figure S3) suggests a lack of interaction with His260 and Tyr26 that could be the reason for the absence of activity of this compound. Thus, a suitably sized substituent situated β relatively to the carboxylic acid in ring A, seems to be necessary to allow the right disposition of the essential interacting groups of inhibitor and enzyme. It could not be clarified at this point whether interaction through that β-substituent could improve the potency of the inhibitors.

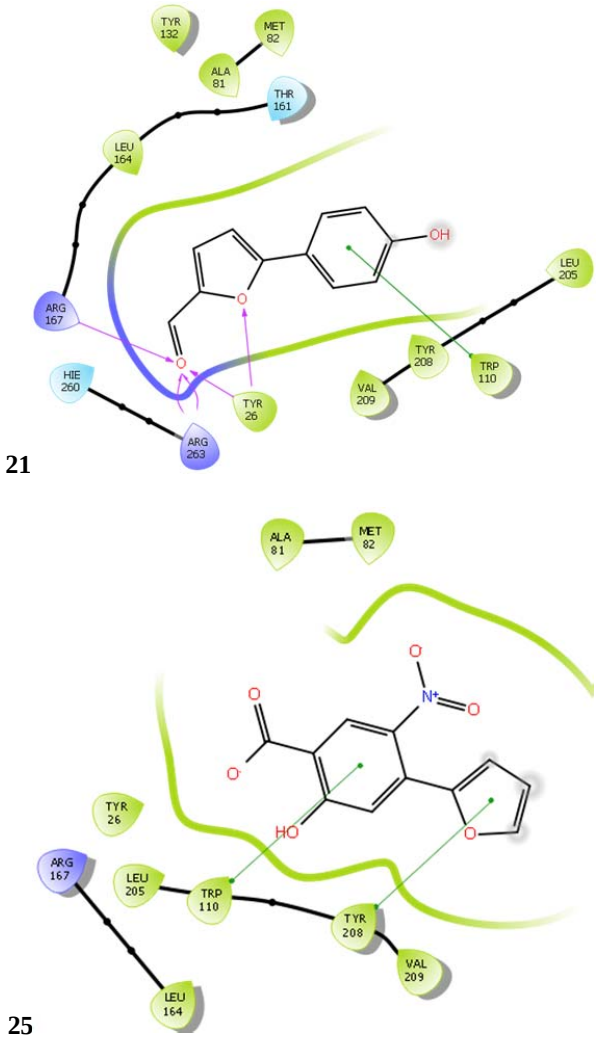

Figure 7. 2D Diagrams of interactions between compounds **21** and **25** and human glycolate oxidase residues (purple: basic, cyan: polar uncharged, green: non-polar). Grey shadow represents interaction with solvent. Hie260: His260 protonated on N_ε [Maestro software (Schrödinger)].

Compounds **21** and **24** have no free carboxylic acid in the polar head; in **21** it has been removed while in **24** it has been esterified into a methylcarboxylate. Thus, these two molecules are expected to interact poorly at Arg167 and Arg263. The binding mode predictions show the two molecules turn around in the binding site of hGO, drawing the formylfuran moiety towards

the binding region 1 and leaving the polar head orientated towards the binding region 2. With this disposition, **21** uses the formyl group in the side chain to interact with both Arg167 and Arg 263 as hydrogen acceptor. Also, **21** interacts as hydrogen acceptor from Tyr26 through both, the formyl and the furan oxygen atoms while lacks interaction with His260 (Table S3, Figure 7). Formyl group of compound **24** binds to His260 and Tyr132 acting as acceptor in hydrogen bonds. No interaction between **24** and Arg167 or Arg 263 was predicted (Table S3, Figure S3). Both, **21** and **24** establish π-π stacking bonds to Trp110 (Table S3).

In the binding region 2, compounds **20**-**25** interact with Trp110 and Tyr208, but only some of them do the same with Leu205 (Table S3, Figure S3).

Compound **21** was the only one in this group (**20**-**25**) to produce oxalate decrease on PH1-mouse primary hepatocytes (Table 2). Compound **21** resulted more effective than CCPST at the cellular level, lowering oxalate output to 32 % at 10 μM on cell-based assays, without cytotoxic effects. However, **21** is not a potent GOi. This finding suggests compound **21** may exert its biological effect by interaction with an alternative biological target, a possibility that deserves further investigation. Possible interferences of **21** in the biological methods were investigated and discarded (see *Assay interference test* in Experimental Section and Tables S4-S5).

Once the need to maintain the salicylic polar head to achieve GO inhibition was confirmed, we explored modifications of the side chain. First was moving it to the C5 position of the salicylic head, the *para* position with respect to the phenol function (C5 isomers). Compound **26**[35] (Figure 8), C5 isomer of **8**, was prepared as described in Scheme 1 using **18a** and 5-formyl-2-furanboronic acid (**19a**: Ar = 2-furyl, R^5 = -H) (Table S2) as starting materials (method B, quantitative yield). The use of PdEnCat® allowed a drastic increase of the reaction yield *vs* non-encapsulated palladium acetate.

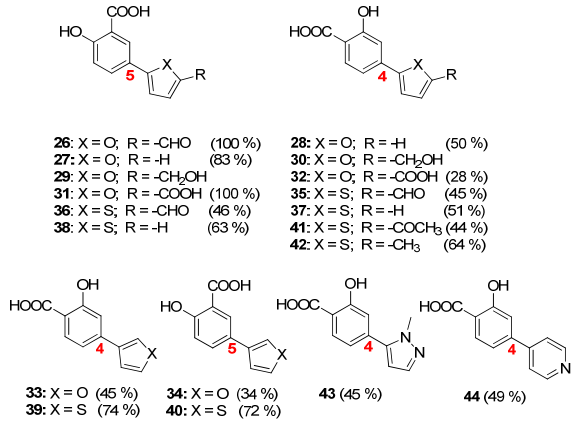

Figure 8. Structures of the heteroarylsalicylates tested. In brackets: Isolated yields in Suzuki-Miyaura coupling. Method A: **33**-**38** and **40**. Method B: **26**, **31** and **32**. Method C: **27**, **28**, **39** and **41**-**44**. For compounds **39**, **41**-**44**, yields are referred to their isolation as potassium carboxylates.

Upon evaluation against mGO, **26** resulted in a slightly less potent inhibitor than its C4 isomer (**8**), but still with an IC_{50} value lower to the one of CCPST (Table 3). In turn, the *in vitro* efficacy on oxalate diminution was remarkably improved, showing an EC_{50} value of 3.45 μM, 5-fold better than CCPST (see *Calculation of EC_{50} and cytotoxicity test for **26** and **27*** section below*)*. If compared to CCPST, **26** represents a marked improvement of the phenotypic effect on cells with only a slight increase of the inhibitory activity on mGO. Using Cornish-Bowden and Dixon plots we determined that **26** behaves as a competitive inhibitor with an inhibition constant (K_i) on mGO of 47.2 μM. As in the case of **21**, this discrepancy between the enzymatic potency of **26** and its efficiency on cells deserves further investigation as it could mean the existence of alternative target(s) for this compound. The interaction diagram obtained for **26** inside hGO (Figure S4) indicates this compound binds to Arg167, Arg263 and His260, through the carboxy and the β-OH groups, and establishes hydrophobic interactions with Tyr132, Trp110, Leu205

and Tyr 208 through both, the salicylic ring (ring A) and the furan ring (ring B). The formyl group establishes no interaction to the target and appears solvated. Compared to its C4 isomer, **8**, a more important participation of the β-OH in the attachment of the molecule to the target can be observed in **26** as it participates as hydrogen acceptor in the binding to His260. The main binding difference between CCPST and **26** is the lack of interaction of compound **26** at Tyr26 (Table S7).

Table 3. Biological data of heteroarylsalicylates **26-44** and *in silico* prediction of partition coefficient ($logP_{th}$). Comparison with **8** and CCPST. Biological determinations: (i) Enzymatic inhibition on purified mouse glycolate oxidase (mGO), at single concentration and IC_{50} calculation. (ii) Excreted oxalate in *Agxt1*$^{-/-}$ mouse primary hepatocytes, compared to control (relative oxalate).

Compound	mGO[a] (%)	IC_{50} (μM)	R^2	Relative oxalate[b]	$logP_{th}$
CCPST	34.8 ± 4.8	43.5 ± 1.1		0.63 ± 0.16[c]	n/a
8	82.8 ± 5.6	34.5 ± 1.2	0.88	0.88 ± 0.18	0.29
26	42.7 ± 12.8	38.2 ± 1.2	0.81	0[d]	2.59
27	n/r	n/r		0[d,e]	-0.29
28	35.8 ± 6.9	39.3 ± 1.0	0.94	0.87 ± 0.15	0.65
29	98.0 ± 1.6	4.6 ± 1.1	0.96	0.88 ± 0.19	-0.11
30	85.7 ± 9.3	7.9 ± 1.1	0.98	0.88 ± 0.01	-0.11
31	0	n/a		0.68 ± 0.14*	0.13
32	0	n/a		n/a	0.13
33	22.8 ± 5.6	n/a		1.02 ± 0.3	0.56
34	26.6 ± 1.9	n/a		0.89 ± 0.16	0.56
35	28.7 ± 1.3	n/a		1.00 ± 0.20	0.06
36	52.1 ± 13.4	9.4 ± 1.3	0.87	0.93 ± 0.18	0.06
37	35.4 ± 7.2	32.5 ± 1.1	0.96	0.74 ± 0.16*	0.99
38	30.0 ± 2.4	39.5 ± 1.1	0.91	0.82 ± 0.01	0.99
39	41.4 ± 7.8	21.6 ± 1.3	0.80	0.99 ± 0.12	0.90
40	25.2 ± 5.0	n/a		0.94 ± 0.10	0.90
41	28.1 ± 9.3	n/a		0.89 ± 0.14	1.02
42	28.7 ± 10.3	n/a		0.95 ± 0.02	1.02
43	16.2 ± 6.2	n/a		0.93 ± 0.01	0.34
44	22.7 ± 2.3	n/a		0.88 ± 0.03	2.76

[a]Percentage of inhibition of purified mGO at 25 μM, after 1 min. [b]Oxalate output decrease 24h after treatment with 10 μM of the drug in *Agxt1*$^{-/-}$ mouse primary hepatocytes cultured with 5 mM glycolate, in 6-well plates. Data represented as mean ± SD of n = 3 replicates. One-way ANOVA statistical analysis, *$p<0.05$ was considered statistical significant. [c]Data at 12.5 μM in *Agxt1*$^{-/-}$ mouse primary hepatocytes. [d]Values below the detection limit of the colorimetric method. [e]No interference due to the low concentration of the drug. IC_{50}: Calculated in saturated conditions of glycolate (22.2 mM). R^2: IC_{50} curve-fitted score. n/a: Not assessed. n/r: Not reliable data due to interference.

To check the role of the formyl group on **26** and how its suppression or replacement would affect the biological activity of this molecule, compound **27** (Figure 8) with an unsubstituted furan side chain, was prepared using the Suzuki protocol (Scheme 1). Contrarily to **26**, the use of PdEnCat® was not effective for the preparation of **27**, with most of the starting materials remaining unreacted after 24 h. Instead, **27** could be obtained in good yield (83 %) by catalysis using non-encapsulated palladium acetate. Formyl removal led to a 4-fold increase in the mGO inhibitory activity while the *in vitro* efficacy (EC_{50} = 3.56 μM) remained unchanged if compared to **26** (Table 3). However, these results must be interpreted carefully as compound **27** interferes in both biological assays, GO-inhibition and oxalate quantification on cells, by inhibiting the horseradish peroxidase (HRP) that is used in the evaluation protocols (calculated IC_{50} of **27** against the oxalate determination kit = 18 μM) (see *Assay interference test* in Experimental Section and Tables S4-S6). This interference prevents us from giving a faithful value of activity for this compound against mGO, as to obtain an IC_{50} value against mGO, concentrations of at least 40 μM of **27** had to be used, exceeding the IC_{50} value found for **27** against HRP. For the same reason, calculation of K_i was not accomplished for compound **27**. However, in the case of oxalate determination on cells, the activity values reported above can be considered indicative as the effect of the interference is not significant at concentrations up to 5 μM of **27** (Table S6). This fact suggests the formyl group in **26** is not essential for achieving oxalate decrease and therefore this group could be replaced to obtain structurally diverse analogues. The binding prediction of **27** inside hGO suggests a similar interaction profile to **26**, except for an extra interaction at Tyr26, established by the carboxylate group of **27**, and a better hydrophobic wrapping in the binding region 2 (Figure S4). The equivalent elimination of the formyl group in the C4 isomer of **26**, compound **8**, resulted in compound **28**. In this case, the removal of the

formyl group did not mean any improvement of the inhibitory activity against mGO and, additionaly, **28** is inactive on PH1 mouse primary hepatocytes (Table 3). Comparison of the predicted binding profiles of **28** and **27** (C4/C5 isomers) shows, as it happened in the pair of isomers **8**/**26**, a more important binding participation of the β-OH in the case of the C5 isomer (Table S7, Figure S4). In both C5 compounds, **26** and **27**, the β-OH group behaves as hydrogen acceptor in the binding to His260 (Table S7, Figure S4).

No enzymatic or colorimetric interference was found for compound **26** in any of the biological assays (see *Assay interference test* in Experimental Section and Tables S4-S5). This different behavior of **26** and **27** against HRP could be due to a lower selectivity derived from the smaller size of **27**. At this point we wanted to check whether **26** could be producing **27** after metabolism, so we could have the same misleading effect on the oxalate decrease results obtained *in vitro* for **26**. Metabolite profiling of compound **26** using mouse liver microsomes, showed the formation of two main metabolites corresponding to reduction and oxidation of the formyl group (**29** and **31**, Figure 8), meaning 40.1 % and 48.2 % of the total metabolites after 60 min. A minor metabolite could be also observed, accounting for 11.6 % after 60 min (Figure S5). This metabolite, which presents a different retention time than **27** in LC-MS analysis (Figures S5-S6), seems to correspond to a formyl group oxidation plus decarboxylation on the salicylic ring. The samples were analyzed by LC-HRMS in negative ionization mode. Compound **26** showed a high intrinsic clearance with an elimination half-life of 13.3 min while **27** showed a medium intrinsic clearance with an elimination half-life of 61.9 min (Tables S8 and S9, Figure S7). No metabolites could be detected for compound **27** after 60 min incubation.

We then proceeded to prepare the main metabolites of **26**, structures **29** and **31** (Figure 8), in order to examine their biological activity and their capacity to produce interferences in the

biological testing process. The primary alcohol **29** and its C4 isomer **30** (Figure 8), were made by reduction of the formyl group in **26** or **8** respectively. Both presented satisfactory GO inhibitory activities (IC_{50} = 4.6 ± 1.1 μM for **29** and IC_{50} = 7.9 ± 1.1 μM for **30**) but low decrease of oxalate output in PH1 mouse hepatocytes in culture (Table 3). No interference could be observed for these compounds (see *Assay interference test* in Experimental Section and Table S10). Oxidized derivatives of **26** and **8**, carboxylic acids **31** and **32** (Figure 8), were totally inactive as mGOi's and therefore interference by inhibition of HRP was discarded. The absence of interference found for the metabolites of **26** (**29** and **31**) confirms the activity of this compound. Thus **26** is a moderate mGOi with a high capacity to decrease oxalate production in hyperoxaluric hepatocytes. Interestingly, its metabolite **31** presents the same activity profile, with null activity as mGOi but with capacity to decrease oxalate production in approximately 30 % after 24 h incubation with cells at 10 μM (Table 3). Thus, in the cell system, metabolism of the aldehyde **26** happens in favor of the less active carboxylic acid **31**, causing the time-dependant loss of activity of **26**. A common mechanism of action could be involved in the phenotypic activity of compounds **26**, **27** and **31** on cells, which is higher than their activity as mGOi's on pure enzyme. For these compounds, possible interactions with alternative biological targets, different from GO, should be considered.

Since the orientation of the ring in the binding site can be crucial for a good interaction with GO, the furan ring was also bound to the salicylic molecule by its carbon atom C3'. Compounds **33** and **34** (Figure 8), C3' isomers of **28** and **27** respectively, were prepared by Suzuki-Miyaura coupling. None of them presented satisfactory mGO inhibitory activity or capacity to decrease the production of oxalate in cells (Table 3).

We then replaced the furan ring in **8** and **26** by different nitrogen or sulfur heterocycles. The latter contains a sulfur atom in a similar position to CCPST. We prepared thiophene (**35-42**), pyrazole (**43**) and pyridine derivatives (**44**) (Figure 8) according to the general procedure indicated in Scheme 1. Isosteric change in the formylfuran **8** (C4 isomer) to give the formylthiophene **35** (C4 isomer) (Figure 8), led to loss of the mGO inhibitory activity and the efficacy on cell-based assays (Table 3). Differently, formylthiophene derivative **36**[38] (C5 isomer) (Figure 8) (IC_{50} = 9.4 ± 1.3 μM) was a 4-fold more potent mGO-inhibitor than its formylfuran isoster **26** (C5 isomer) (IC_{50} = 38.2 ± 1.2 μM). Unfortunately, it did not decrease oxalate excretion in PH1 hepatocytes (Table 3). The same isosteric change in the nonformylated furan **27** (C5 isomer) raised thiophene **38**[39] (Figure 8), which showed a huge decrease of efficacy (0.82 ± 0.01 *vs.* 0 relative oxalate) while conserving the same potency as mGOi (IC_{50} = 39.5 ± 1.1 μM) (Table 3). As we did with the furan derivatives, we checked the importance of the orientation of the thiophene by binding it to the polar head by its C3' carbon atom (compounds **39** and **40**, Figure 8). C3'-Thienyl derivatives did not improve the potency of their C2' counterparts (**37** and **38**) (Table 3). Exploration of different substitution on the C2'-bound thiophene ring, such as acetyl (**41**) or methyl (**42**) groups, led to poor mGOi's without activity on cells (Table 3). Nitrogen heterocycles pyrazol (**43**) and pyrimidine (**44**) produced no improvement in the mGO inhibitory activity or the oxalate decrease capacity. In summary, although the C5 formylthiophene derivative **36** represented an increase of the mGO inhibitory activity with respect to its formylfuran isoster **26**, any of the other sulphur or nitrogen derivatives **35-44** presented relevant activities on mGO inhibition or any improvement with respect to the furan analogues. Neither oxalate decrease activities were obtained, pointing out the crucial role of the

heteroatom present in the heterocycle ring to produce potent and, to some extent, effective inhibitors.

Amongst compounds **26**-**45**, unfavorable negative logP_{th} values were found only for **27**, **29** and **30** (Table 3).

In silico predictions of the binding mode of heteroarylsalicylates **26**-**44** showed these compounds can establish interaction with key residues in the binding regions 1 and 2 (Table S7, Figure S4). As a general rule they interact with Arg167, Arg263 (except **36**), His260, Tyr208 and Leu205. Most of them interact with Trp110, excep for the C5 alcohol **29**, the C5 2-thienyl **38** and its isomer the C5 3-thienyl **40**. Less frequent is the interaction at Tyr132 that is not established by 2-thienyl and 3-thienyl derivatives **30**, **37**, **40**, **41** and **45**, the C4/C5 isomers **33** and **34** containing 3'-furyl side chains and the pyridinyl derivative **44**. Finally, just five compounds bind to Tyr26. These are the C5 2-furyl derivative **27**, the C4/C5 5-carboxy-2-furyl derivatives **31** and **32**, and the C4/C5 pair of 5-formyl-2-thienyl derivatives **35** and **36**. Polar groups located at the terminal heterocycles such as the formyl group on **26** or **35**, the hydroxy group on **29** or **30**, or the nitrogen atoms in the heterocycles of **43** and **44** get solvated. Other than with the solvent, nitrogen containing heterocycles give no additional interaction to hGO, and the terminal ring of **43** and **44** establishes only the usual Van der Waals interactions to the target. Compound **32** presents a special binding mode as it uses the furoic moiety to interact at the binding region 1 and the salicylic fragment to interact at the binding region 2.

A characteristic binding pattern differing C4 *vs* C5 substitution could be found in these heteroarylsalicylates. If we compare binding mode predictions for the pairs of C4/C5 isomers (**8**/**26**, **28**/**27**, **30**/**29**, **32**/**31**, **33**/**34**, **37**/**38**, **39**/**40**) (Table S7, Figures 9 and S4) it is found that: (i) only C5 isomers, except compound **31**, use the β-OH to interact with His260, (ii) only C4

isomers establish π-π stacking interactions with Trp110. This means interaction at His260 is reinforced in C5 isomers as they use both, the carboxylate and the β-OH group, as hydrogen acceptors from this aminoacid. However, C4 isomers establish more efficient π-π stacking interactions with Trp110 compared to the hydrophobic interactions of the C5 isomers. These observations do not apply to the C4/C5 couple of 5-formyl-2-thienyl derivatives **35**/**36**. While **35** matches the binding pattern of a C4 isomer, **36** presents an unsual binding mode with interaction between the carboxy group of the salicylic head and the residues Trp110 and Tyr132 instead of the usual interaction with Arg167 and Arg263 (Figure S4). However, this different binding mode predicted for C4 and C5 isomers, did not translate into significantly different potency against mGO (Table 3).

No common binding pattern could be observed for the best GOi's in this group **29**, **30** and **36** (Table S7).

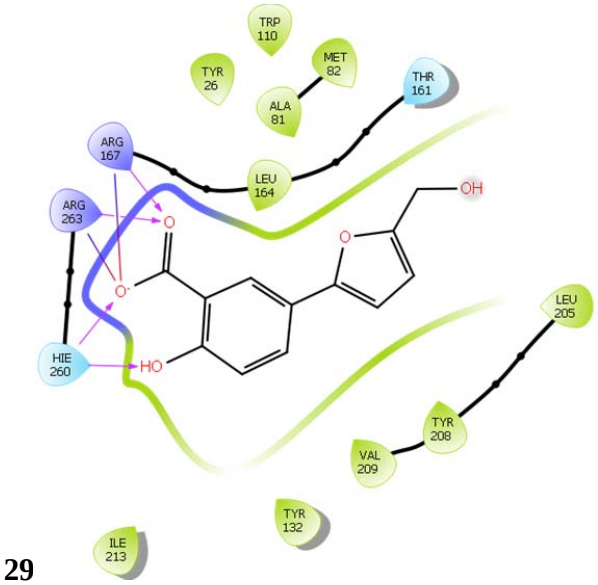

29

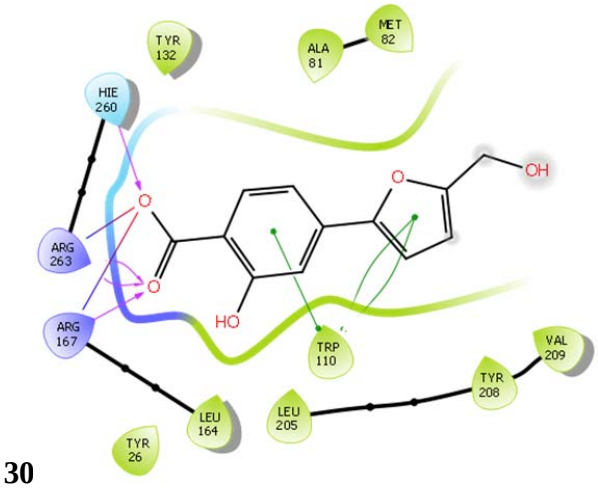

30

Figure 9. 2D-Diagram of interactions between the most potent mGO inhibitors heteroarylsalicylates, the C4/C5 isomers **30** and **29**, and hGO active site residues (purple: basic, cyan: polar uncharged, green: non-polar). Grey shadow represents interaction with solvent. Hie260: His260 protonated on N_{ε} [Maestro software (Schrödinger)]. 2D-Interaction diagrams for the whole group **26**-**44** in Figure S4.

The phenotypic activity of the most efficient oxalate decreasing heteroarylsalicylates (**26** and **27**) was studied further.

Calculation of EC_{50} and cytotoxicity test for 26 and 27. After **26** and **27** showed significant reduction of excreted oxalate in the first screening at 10 μM, we performed full *in vitro* dose-response curves for both compounds, following previously reported methodologies.[11] In parallel, we carried out cytotoxicity assays to assure that oxalate was diminished by the inhibitor and not by a decrease in the number of viable cells. Compound **26**, with a formyl group, could potentially produce toxic effects by reaction with proteins.[40] Compound **26** at 6.25 μM significantly reduced excreted oxalate levels by 67.3 ± 32% after 24 h of treatment. At concentrations of 12.5 μM, significant reduction was achieved at 24 h and 48 h of treatment (105.8 ± 29.2 % and 62.3 ± 24.4 %, respectively) (Figure 10a). Cells did not show any sign of cytotoxicity within the concentration range tested (Figure 10b). Calculated EC_{50} for each time point was: 3.45 ± 1.17 μM at 24 h, 8.36 ± 1.12 μM at 48 h and 11.19 ± 1.18 μM at 72 h (Figure S8). Compound **27** showed similar efficacy as **26**. It could reduce to 26.5 ± 6.3 % oxalate levels at 2.5 μM after 24 h of treatment, and 5 μM was enough to keep significant low levels of oxalate at least during 72 h post-treatment (Figure 11a). Calculated EC_{50} at each time point was: 3.59 ± 1.06 μM at 24 h, 7.88 ± 1.04 μM at 48 h and 9.2 ± 1.04 μM at 72 h (Figure S9). Cytotoxicity was observed only when treated with 80 μM of compound (Figure 11b). The more noticeable time-dependent loss of activity of **26** *vs* **27** is predictable from the chemical and metabolic instability observed for **26** (above).

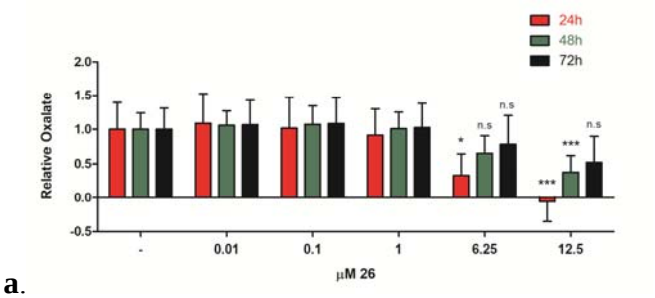

a.

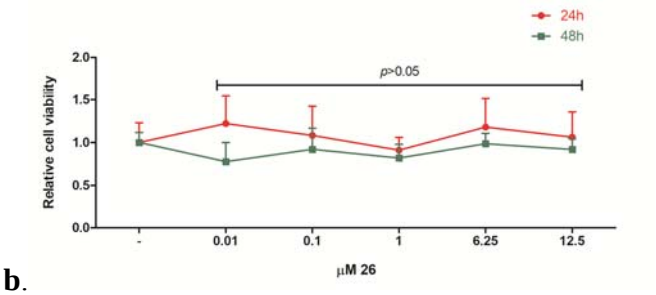

b.

Figure 10. *Agxt1*$^{-/-}$ mouse hepatocytes treated with **26**. (a) Relative oxalate excreted after 24 h, 48 h and 72 h of treatment. (b) Cell viability within the same range of concentrations. Data are represented as mean ± SD, from two independent experiments, with three replicates in each one. ANOVA statistical signification: *P < 0.05, **P < 0.01, ***P < 0.001, NS = not significant, relative to control at each time point.

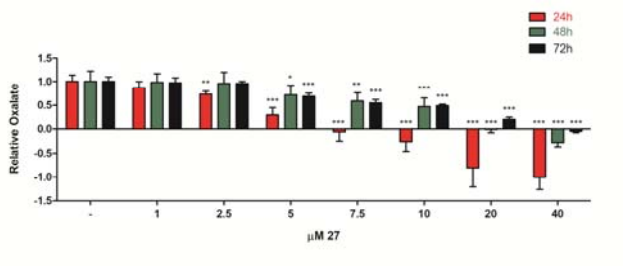

a.

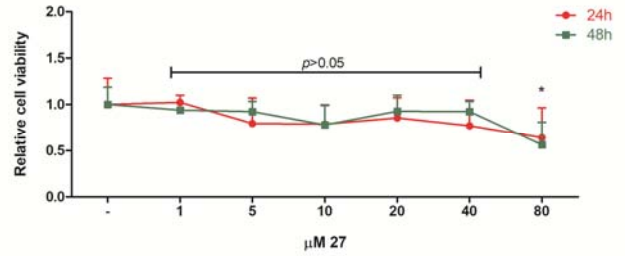

b.

Figure 11. *Agxt1*$^{-/-}$ mouse hepatocytes treated with **27**. (a) Relative oxalate excreted after 24 h, 48 h and 72 h of treatment. (b) Cell viability within the same range of concentrations. Data are represented as mean ± SD, from two independent experiments, with three replicates in each one. ANOVA statistical signification: *P < 0.05, **P < 0.01, ***P < 0.001, relative to control at each time point.

Compounds **26** and **27** can decrease oxalate excretion levels on *Agxt1*$^{-/-}$ mouse primary hepatocytes with the lowest EC_{50} value described so far by small molecules in a SRT strategy. Compared to CCPST, in the same experimental conditions, **26** and **27** are around 7-fold more efficient oxalate decreasing agents. In contrast, the mGO inhibitory activity of CCPST and **26** is comparable[11] (Table 4).

Table 4. Comparison of biological activities of CCPST and compounds **26** and **27**.

	IC_{50} (μM)	EC_{50} (μM)		
		24h	48h	72h
CCPST	43.5	25.3	33.0	34.0
26	38.2	3.5	8.4	11.2
27	-	3.6	7.9	9.2

IC_{50}: Calculated on mouse glycolate oxidase oxidase in saturated conditions of glycolate (22.2 mM). EC_{50}: For oxalate output decrease tested at 24h post-treatment with each drug in *Agxt1*$^{-/-}$ hepatocytes cultured with 5 mM glycolate.

Summarizing the results for heteroarylsalicylates, we obtained maximum mGO inhibitory activities ranging 4-40 μM. Furylsalicylates **29** and **30**, and thienylsalicylate **36** gave the best results (IC_{50}s 4.6 ± 1.1, 7.9 ± 1.1 and 9.4 ± 1.3 μM, respectively). All of them present electron-rich five membered not-nitrogen heterocycles side chains that can be attached to C4 (**30**) or C5 (**29** and **36**) of the salicylic polar head through the C2' position of the heterocycle. Attached to C5' they present aldehyde (**36**) or hydroxymethyl (**29** and **30**) functionalities. However, these inhibitory potencies were not enough to produce decrease of oxalate excretion in hyperoxaluric mouse hepatocytes. A special case is the one of 5-furylsalicylate **26** (and related **27**) that, despite being only moderate mGOi's on recombinant protein *in vitro*, they are able to drastically reduce oxalate production by hyperoxaluric hepatocytes at 10 μM. Compound **31**, a metabolite of **26**, shows the same activity profile, producing a 30 % decrease of oxalate level at 10 μM, with null mGO inhibitory activity on recombinant protein *in vitro*. This suggests the phenotypic activity of **26**, **27** and **31** might be compounded by interaction with other(s) biological target(s). Future research will explore feasible alternative targets involved in glyoxylate metabolism such as LDH or HYPDH. Other explanations such as slow-binding inhibition kinetics should be also considered.[41]

Biphenyl or arylsalicylate analogues (**45-55**, Figure 12). In the group of biphenyl analogues we include those compounds in which an aromatic carbocycle is attached to the salicylic polar head. They are thus formed by a biphenyl system which rings we have denominated A (salicylic ring) and B (side chain ring). They take after compound **11** (Figure 4), which presents good potency against purified mGO (IC_{50} = 2.9 ± 1.1 μM) and certain activity on oxalate reduction on cells (0.77 ± 0.08 relative oxalate at 10 μM). In the design of biphenyl analogues we disregarded the naphthylic head of compound **11** in favor of the simpler and more hydrophilic salicylic one. This way, the biphenyl analogues or arylsalicylates can also be considered structural derivatives of compound **9** (Figure 4). All biphenyl analogues were prepared by Suzuki-Miyaura coupling as described in Scheme 1. Calculated $logP_{th}$ values experiment an increase for the biphenyl systems (Table 5), especially when ring B is attached to a third aromatic ring (ring C) or halogens substituents are introduced (compounds **48**-**55**). 2D-Interaction diagrams for the whole group **45**-**55** are given in Figure S10.

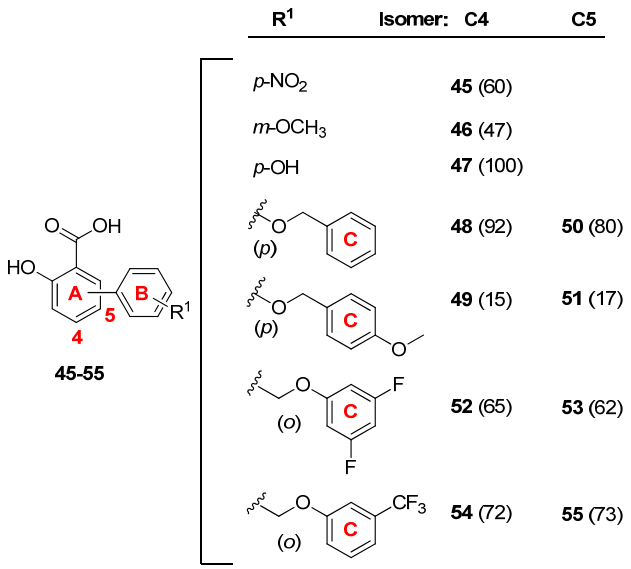

Figure 12. Structures of the arylsalicylates prepared. In brackets, isolated yields (%) for their preparation by Suzuki-Miyaura coupling. Method A: **50**, **52**, **53** Method C: **45**-**49**, **51**, **54**, **55**. For compounds **45**-**49**, **51**, **54**, **55** yields are referred to their isolation as potassium carboxylates.

Compound **11** bears a *p*-nitrophenoxy side chain. We prepared the corresponding arylsalicylate with the same electron-withdrawing *p*-nitro (**45**) and also derivatives with electron-donating *m*-methoxy (**46**) and *p*-hydroxy (**47**)[42] groups on ring B (Figure 12). The three compounds contain hydrogen acceptor substituents but only the hydroxyl group on **47** could act as a hydrogen donor. The electron-withdrawing character of the *p*-nitro increases the acidity of the carboxylic acid and the phenol in **45**, while the electron-donating *p*-hydroxy in **47** decreases it. The *m*-methoxy electron-donor group in **46** has little influence on ring A and only increases the electron-density in ring B. These three derivatives, with IC_{50}s between 10 and 20 μM, resulted less potent that **11** but increased the mGO inhibitory activity of **9**, which presents a difluorophenyl ring B (Table 5). Compound **47** resulted the most potent mGOi of the three new analogues **45**-**47**. Binding

predictions for **45-47**, suggest none of the substituents on ring B interact with aminoacidic residues of hGO while all the 4-nitro, 3-methoxy and 4-hydroxy groups of **45**, **46** and **47** respectively, get solvated (Figures 13 and S10). This goes against the idea that the higher potency of **47** *vs* **45** and **46** could be due to the presence of a H-bond donor atom in C4' of the biphenylic system. According to the theoretical predictions, the carboxylate groups of **45-47** participate in electrostatic interactions with Arg167, Arg263 and they are also hydrogen acceptors from His260 (Table S11). Thus, the *p*-hydroxy group in **47** could assist these interactions by increasing the electronic density of the carboxylate group *vs* the electron withdrawal played by the *p*-nitro group of **45**. None of these compounds, **45-47**, showed promising efficacy results on relative oxalate output by hyperoxaluric hepatocytes (Table 5).

Table 5. Biological data of arylsalicylates **45-55** and *in silico* prediction of partition coefficient ($logP_{th}$). Comparison with **9**, **11** and CCPST. Biological determinations: (i) Enzymatic inhibition on purified mouse glycolate oxidase (mGO), at single concentration and IC_{50} calculation. (ii) Excreted oxalate in *Agxt1*$^{-/-}$ mouse primary hepatocytes, compared to control (relative oxalate).

Compound	mGO[a] (%)	IC_{50} (μM)	R^2	Relative oxalate[b]	$logP_{th}$
CCPST	34.8 ± 4.8	43.5 ± 1.1		0.63 ± 0.16[c]	n/a
9	27.9 ± 0.6	n/a		0.88 ± 0.08	3.42
11	96.3 ± 0.5	2.9 ± 1.1	0.97	0.77 ± 0.01	1.00
45	41.9 ± 9.2	19.7 ± 1.2	0.87	0.91 ± 0.05	0.26
46	50.9 ± 7.3	19.5 ± 1.1	0.86	0.83 ± 0.03	2.89
47	61.3 ± 8.8	13.5 ± 1.1	0.95	0.82 ± 0.01	2.86
48	83.4 ± 8.5	10.4 ± 1.2	0.85	1.11 ± 0.18	4.67
49	65.0 ± 6.3	13.8 ± 1.2	0.89	0.90 ± 0.16	4.42
50	70.9 ± 7.8	14.8 ± 1.1	0.93	0.80 ± 0.16	4.67
51	83.8 ± 10.1	9.5 ± 1.2	0.81	1.07 ± 0.32	4.42
52	77.7 ± 7.3	8.3 ± 1.2	0.95	0.72 ± 0.16*	4.95
53	84.5 ± 4.0	5.8 ± 1.2	0.89	0.92 ± 0.08	4.95
54	98.6 ± 0.7	4.4 ± 1.2	0.95	0.62 ± 0.29*	5.52
55	96.2 ± 2.4	3.5 ± 1.2	0.86	0.68 ± 0.21*	5.52

[a]Percentage of inhibition of purified mGO at 25 μM, after 1 min. [b]Oxalate output decrease 24h after treatment with 10 μM of the drug in *Agxt1*$^{-/-}$ mouse primary hepatocytes cultured with 5 mM glycolate, in 6-well plates. Data represented as mean ± SD of n = 3 replicates. One-way ANOVA statistical analysis, *$p<0.05$ was considered statistical significant. [c]Data at 12.5 μM in *Agxt1*$^{-/-}$ mouse primary hepatocytes. IC_{50}: Calculated in saturated conditions of glycolate (22.2 mM). R^2: IC_{50} curve-fitted score. n/a: Not assessed.

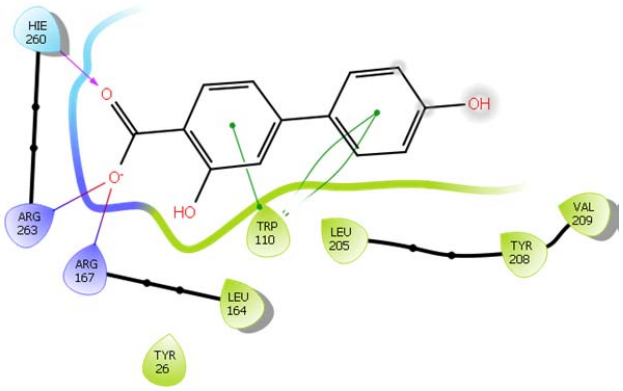

47

Figure 13. 2D-Diagram of interactions between the arylsalicylate **47** and hGO active site residues (purple: basic, cyan: polar uncharged, green: non-polar). Grey shadow represents interaction with solvent. Hie260: His260 protonated on N_{ε} [Maestro software (Schrödinger)].

We then prepared compounds **48**-**55** (Figure 12) in which the *p*-hydroxy group on ring B of **47** is etherified with benzyl groups yielding flexible structures with three aromatic rings: a biphenyl system (rings A and B) bonded to a benzene (ring C) through a two-atom flexible linker. This ring C constitutes a novel distant point for π-π stacking or hydrophobic interaction. Substitution pattern on ring B of **48**-**51** is *para* and thus these molecules present a linear geometry. Compounds **48** and **49** are C4 isomers (ring A substituted on C4). Compound **48** with a plain ring C (Figure 12) had a slight increase of potency against mGO if compared to **47** (Table 5). These data support the idea that it is not a hydrogen bond donation from the substituent on ring B what determined the activity of **47** but the electron-donating character of such substituent. Compound **49** with a more electron-rich *p*-methoxyphenyl ring C, showed similar inhibitory potency than **47**. Corresponding C5 isomers of **48** and **49**, compounds **50**[43] and **51** (Figure 12), presented only slightly different inhibitory activities to their C4 counterparts (Table 5). Binding mode predictions for compounds **48**-**51** inside hGO show the benzylic moieties added on the

biphenyl core get solvated. Thus, hydrophobic interactions with the enzyme are mainly established through the biphenyl fragment of the molecule (Figures 14 and S10). A noteworthy binding feature of this group of compounds is matching the specific characteristics for C4/C5 isomers described before. Both C4 isomers, **48** and **49**, establish π-π stacking interactions with Trp110, using the biphenyl core (rings A and B) while C5 isomers, **50** and **51**, do not interact with this residue. On the other hand, C5 isomers interact more efficiently with His260, by hydrogen bonding using both the carboxy and β-OH functionalities *vs* C4 isomers that only use the carboxy group. However, C5 isomers **50** and **51** do not interact with Tyr26 in the binding region 1, nor Leu205 or Tyr208 in the binding region 2. Unfortunately, none of these linear three-ring derivatives **48**-**51**, with IC_{50} against mGO ranging 9-15 μM, had significant impact on oxalate production decrease by hyperoxaluric hepatocytes *in vitro* (Table 5).

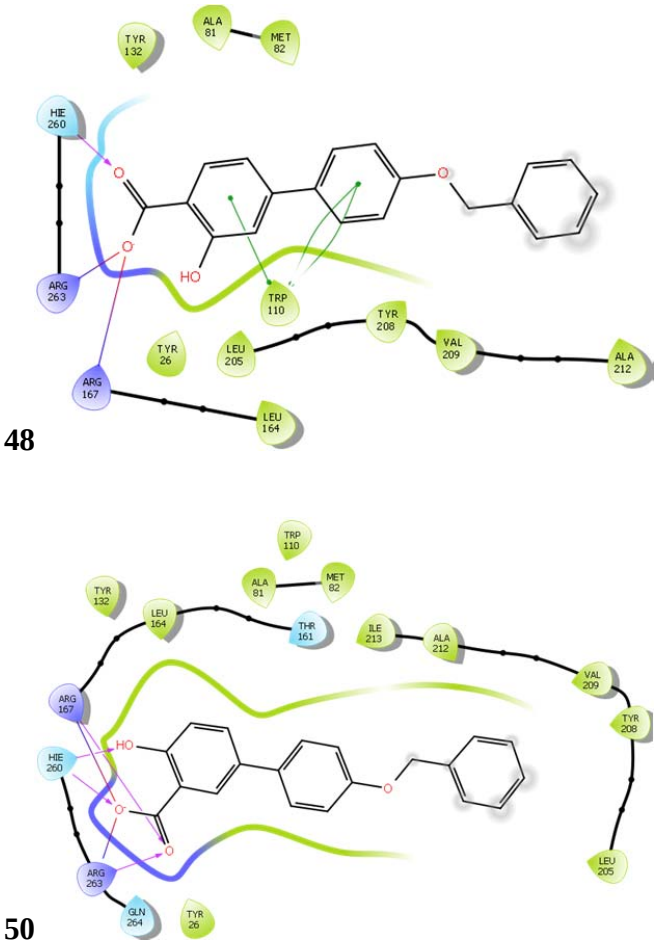

Figure 14. 2D-Diagram of interactions between the C4/C5 isomers three-ring linear arylsalicylates **48** and **50,** and hGO active site residues (purple: basic, cyan: polar uncharged, green: non-polar). Grey shadow represents interaction with solvent. Hie260: His260 protonated on N_{ε} [Maestro software (Schrödinger)].

Compounds **52-55** are also three-ring systems with the same biphenylic core bonded to a third benzene ring (rings A-C). In this case, *ortho* substitution on ring B gives them angled structure (V-shaped) with rings A and C oriented in a *syn* manner *vs* the linear structure of

compounds **48**-**51** (Figure 12). Ring C in **52** and **53** is a π-deficient difluorophenyl ring. Compound **52** can be considered a benzologue of compound **9** (Figure 4), with an extra methoxy linker. Compound **53** is the corresponding C5 isomer of **52**. Both considerably enhanced the potency of **9** and became the most potent mGOi's with arylsalicylate structure prepared to that moment, though still less potent than **11** (IC_{50} = 8.3 and 5.8 μM for **52** and **53** *vs* IC_{50} = 2.9 μM for **11**) (Table 5). Binding mode predictions for **52** and **53** show no interaction at His260, as it also happened in the case of **11** (Table S11). Compound **53** presents atypical binding pattern with (i) no interaction at Arg167 or Arg263, (ii) a hydrogen bond by donation from its β-OH to Tyr26 and (iii) a hydrogen bond by donation from Tyr132 to the carboxylate functionality of **53** (Table S11, Figure S10). In both, **52** and **53**, a π-π stacking interaction to Trp110 is predicted to be established through ring B of the molecule, independently of being C4 or C5 isomers. In the case of the C5 isomer **53**, this interaction with Trp110 is reinforced by hydrogen donation from this aminoacid to the carboxylate group of **53** (Table S11, Figure S10). Compound **52** slightly decreased excreted oxalate levels in *Agxt1*$^{-/-}$ primary hepatocytes (Table 5).

Other π-deficient halogenated V-shaped derivatives such as **54** and **55**[44] (Figure 12) were prepared by substitution of the difluorophenyl rings of **52** and **53** with trifluoromethylphenyl groups. In this case, potency increased reaching IC_{50} values below 5 μM, and *in vitro* efficacy considerably increased, all this without compromising cellular viability (Table 5). Interference test for these most potent and efficient arylsalicylates resulted negative, verifying thus the activity of these compounds (see *Assay interference test* in Experimental Section and Table S4). As it happened with **52** and **53**, π-π stacking interaction with Trp110 happens in both C4 and C5 isomers (Table S11). It means that the previously observed rule for which only C4 isomers π-stack to Trp110 does not apply to the angled three-ring systems **52**-**55**. In the case of **54**/**55**,

while **54** (C4) uses rings A and B for this interaction to Trp110, **55** (C5) uses rings A and C (Figure 15). Consistent with the trend observed before, **55** (C5) interacts more efficiently than **54** (C4) with His260, using both carboxylic and β-OH functionalities. In fact, like CDST and CCPST did, **55** interacts with all the considered aminoacids in the binding regions 1 and 2. We must highlight hydrogen acceptance from Tyr26 (comparable to **11**, CDST and CCPST) and hydrogen bond donation to Tyr132 (comparable to **11**) (Table S11, Figure 15).

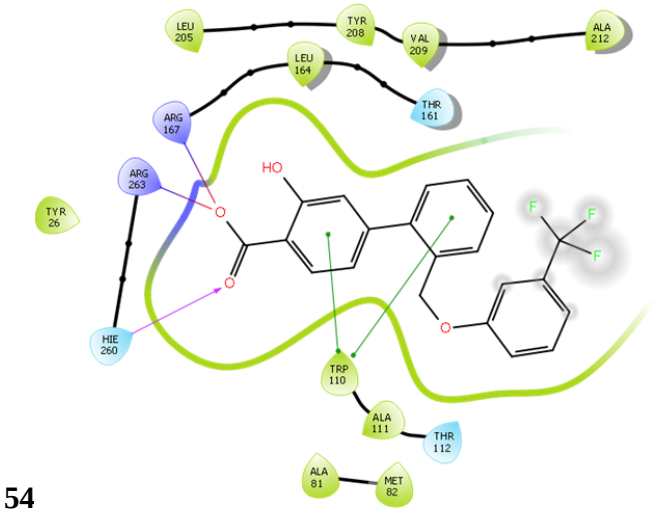

54

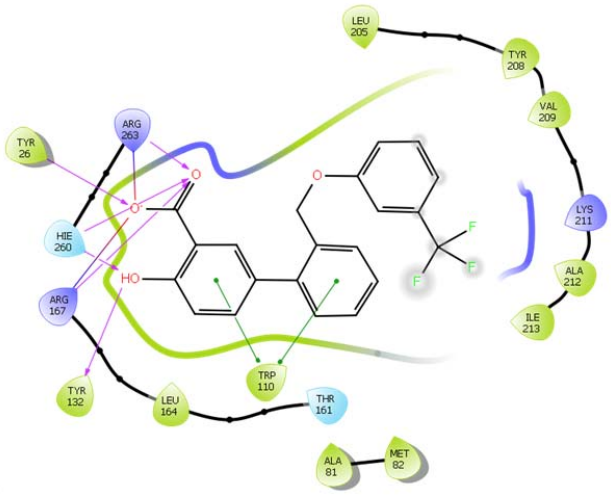

55

Figure 15. 2D-Diagram of interactions between the C4/C5 isomers three-ring V-shaped arylsalicylates **54** and **55**, and hGO active site residues (purple: basic, cyan: polar uncharged, green: non-polar). Grey shadow represents interaction with solvent. Hie260: His260 protonated on N_{ε} [Maestro software (Schrödinger)].

In summary, the biphenyl derivatives behave as GOi's with potencies ranging between 3 and 20 μM. In this group, the most potent GOi's, **54** and **55**, are also the most efficient agents in cells, producing a 30 % decrease of oxalate release in hyperoxaluric mouse hepatocytes at 10 μM (Table 5). In the case of the biphenyl derivatives we have found compatibility between mGO

inhibitory activity and capacity to reduce oxalate production in cells, allowing the phenotypic activity to be rationalized from mGO inhibition. Due to its effective predicted binding to hGO and its capacity to decrease oxalate production, compound **55** can be considered a suitable hit for the preparation of more potent GOi's with oxalate decrease capacity.

About binding mode predictions for the arylsalicylates **45**-**55** (Table S11, Figure S10), most of them present the usual interactions with Arg167 and Arg263 (except **53**) and His260 (except **52** and **53**). This last aminoacid interacts with the carboxy group of the salicylic head in all cases, and additionally with the phenolic group in **50**, **51**, and **55** (C5 isomers). Interaction with Tyr206 and Tyr132 is not a general feature of the group but both interactions happen in the most active compound **55**. Leu205 and Tyr208 interact with most of the compounds in this group or appear leaning close to them (except **50**). Trp110 establishes π-π stacking bonds with most of the compounds, except **50** and **51** (C5 isomers). These stacking bonds happen at rings A and B in all cases but it is worth highlighting that in the most potent inhibitor **55**, they happen at rings A and C. Simultaneous interaction of Trp110 at the two distal rings is possible due to the angled shape of the molecule that allows the spatial proximity of both rings. This interaction could be favored by the π-deficiency of ring C, as it is known that π-deficient aromatic systems generally form stable π-π interactions.[45] Another special characteristic of **55** is the high number of interactions established through the salicylic head. Apart from cation-π interaction to Arg167 and π-π stacking interaction with Trp110 established through the ring, the carboxylate group establishes electrostatic interaction with Arg167, and is acceptor in hydrogen bonds with Arg167, Arg263, Tyr26 and His260. The phenolic function is hydrogen acceptor with His260 and donor with Tyr132. Compound **55** is the C5 isomer of **54**. According to *in silico* data, in this case by changing the hydrophobic tail from C4 (**54**) to C5 (**55**), the proximity to hydrophobic

residues is also changed, being C5-binding more favorable. Establishment of these hydrophobic interactions happens mostly through the linker containing ring B.

Binding mode and biological activity

Hydroxynaphthoic acid **11** and salicylate **55** are our most potent mGOi's corresponding also to a more effective decrease of oxalate release (leaving apart heteroaryl compounds **21**, **26**, **27** and **31** which might also act by a different mechanism of action). Both, **11** and **55** contain a flexible linker that facilitates the accommodation of the molecule inside the enzyme and both adopt an angled V-shape, with *syn* disposition of the target-binding aromatic rings, when they establish bonds with hGO active site residues (Figures 5 and 15). Binding mode prediction for **55** is much more favorable with an extensive network of interactions established through the salicylic head and the hydrophobic tail, including the linker between rings B and C. A special binding feature that has been observed only in these two compounds but not in any other molecule studied here is the fact that they are hydrogen donors to Tyr132 through the hydroxy group of the salicylic head (**55**) or the corresponding naphthylic head (**11**). Only compound **22** uses the β-hydroxymethyl function to establish H-bond to Tyr132, but in this case the amino acid is the donor part. CCPST and CDST bind to Tyr132 as hydrogen acceptors through their ring N2.[18] Compound **11** does not establish bond to His260, while **55** binds to this aminoacid as hydrogen acceptor through both, the carboxylic and phenolic functions of the salicylic head. It means that, as it happens with CCPST and glyoxylate, binding of **55** happens after protonation of His260. This fact was described as thermodynamically unfavorable and accounts for the lower potency of CCPST when compared to the hydrogen donor CDST.[18] This could as well contribute to the lower potency of **55** if compared to CDST. Both, **11** and **55**, interact with Trp110 by π-π

stacking in the first case through ring B (side chain) and in the second case through rings A and C (salicylic head and hydrophobic tail, respectively). Though binding to Trp110 is a general feature observed in many of the compounds included in this work, **55** is the only one in which this residue simultaneously interacts with two distal rings in the structure.

The 3D diagram of interactions for **55** shows its active conformation inside GO and shows an offset stacking geometry in the interaction between ring C and Trp110[45] (Figure 16). In the bound conformation rings A and C are placed perpendicular to each other. The fragment between them, containing ring B, plays three main roles: (i) behaves as a flexible linker facilitating the spatial disposition of rings A and C, (ii) provides the suitable length for simultaneous binding of rings A and C at GO active site and Trp110 and (iii) reinforces the binding to the target by means of hydrophobic interaction (Figures 15 and 16).

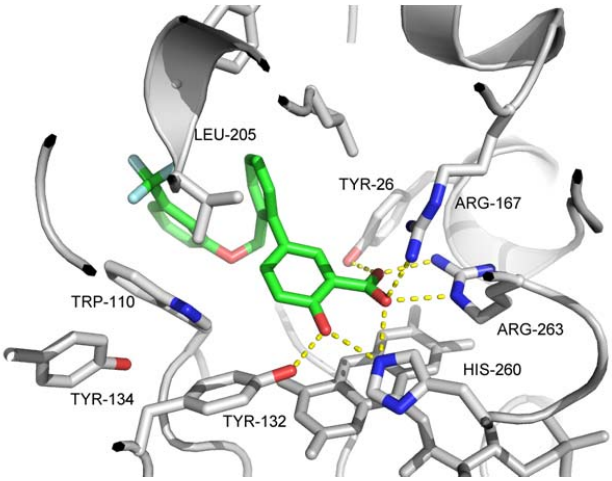

Figure 16. 3D-Diagram of interactions of **55** inside human glycolate oxidase (PDBid: 2RDT).

Preliminary structure-activity relationships

Considering the experimental activities and calculated binding modes for all the molecules in this study, preliminary structure-activity relationships can be outlined to aid the design of novel salicylic mGOi's with oxalate decreasing activity (Figure 17). The salicylic fragment must

be conserved and the phenolic and carboxylic functions must be maintained free for a good interaction at the binding region 1; substitution on C5 is preferred over C4 as it allows a better interaction of the hydrophobic tail with the binding region 2 residues; the structure must contain a second aromatic ring that can interact with Trp110 by π-π stacking and therefore electron-deficient aromatic systems are preferred (in this sense, arenes with electron-withdrawing substituents are preferred over the electron-poor pyridine); a flexible linker must be introduced between both rings to facilitate the accommodation of the molecule inside the enzyme, and to allow the *syn* disposition and free rotation of the aromatic rings. The optimum length of the flexible ring and its nature must still be determined. The linker has been predicted to interact *via* hydrophobic forces, but the possibility of other interactions such as hydrogen bonding in linkers containing heteroatoms should be evaluated. Except specific issues, the metabolism process of this structure (Figure 17) would mainly depend on the rate of oxidation of benzylic positions and aromatic rings. Eventually, the life time of these molecules could be increased or reduced as needed, by steric hindrance or strategic location of metabolism resistant/labile groups.

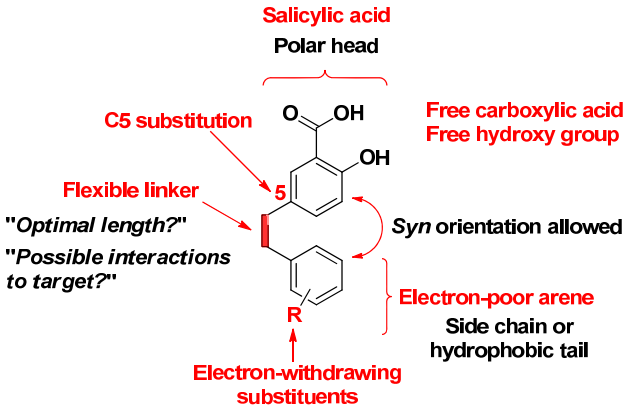

Figure 17. Summary of preliminary structure-activity relationships extracted for salicylates with activity as glycolate oxidase inhibitors and capacity to reduce oxalate production in hyperoxaluric hepatocytes.

CONCLUSION

We have identified the salicylate fragment as a drug-like structural core able to exert mGO inhibition and to reduce the production of oxalate in PH1 mouse hepatocytes, therefore with possible application in the treatment of PH1. Docking studies indicate that salicylic acid can interact with polar aminoacids at the GO active site using its carboxy and hydroxy groups and experimental results show that both are essential to achieve GO inhibition. Aryl and heteroaryl hydrophobic tails attached to this polar head can establish interactions at the hydrophobic access channel of the enzyme. Good mGOi's present hydrophobic tails with five-membered electron rich heterocycles (furan **8**, **29** and **30** or thiophen **36**), though the most potent molecules carry π-deficient arenes (**11**, **54** and **55**) (IC_{50}s 2-5 μM). *In silico* calculations inside hGO suggest flexible molecules that can adopt a V-shaped conformation with *syn* orientation of the rings in the polar head and the hydrophobic tail interact more effectively. We have observed that salicylic acid derivatives that can produce a reduction of the oxalate output in *Agxt1*$^{-/-}$ mouse hepatocytes, present experimental IC_{50} values lower than 4.5 μM against mGO (**11**, **54** and **55** with IC_{50}s 2.9,

4.4 and 3.5 μM, respectively). Still, these low micromolar mGOi's produce a moderate 20-30 % decrease of oxalate at 10 μM. We have highlighted compound **55**, which is a 12-fold more potent GOi than CCPST and reduces oxalate output to 68 % at 10 μM, as a qualified hit for structural optimization in the future preparation of more potent GO inhibitors with oxalate decreasing activity.

5-Furylsalicylates **26** and **27,** and 4-furylphenol **21**, are potent agents decreasing oxalate in *Agxt1*$^{-/-}$ mouse hepatocytes (70-100 % diminution at 10 μM). This is of great importance as oxalate decrease is the main objective chased with a pharmacological treatment of PH1. Compounds **26** and **27** ($EC_{50} \approx 3$ μM) are 7-fold more efficient than CCPST in oxalate output decrease in the cell assay 24 h after treatment, and their activities are barely altered for at least 72 h. No cytotoxic effect could be found for these compounds at the effective doses. However, **21**, **26** and **27** present poor mGO inhibitory activity ($IC_{50} > 35$ μM). These results suggest an off-target or multi-target mechanism could be behind the phenotypic effect of these compounds. Further studies aimed at its elucidation are currently being conducted, firstly considering the logical off-targets LDH or HYPDH, which are involved in glyoxylate metabolism. We have highlighted compound **26** as a qualified hit for structural optimization in order to eliminate non-favorable features such as its short half-life, due to chemical and metabolic instability, or its potential toxicity due to the presence of the unnecessary formyl functionality. Compound **21**, with non-salicylic structure opens the door to a novel family of effective oxalate decreasing agents.

Outstanding features of the salicylic acid derivatives are their drug-like structure and their ease of synthesis that endow them with industrial applicability. Most of our salicylates can be prepared using a single step procedure. Compounds **26** and **55** have been obtained with high to

quantitative yields. Since our active hits are salicylic acid derivatives, their antiinflamatory activity should be assessed for eventual unrelated beneficial or detrimental side effects. No previous data on antiinflamatory activity of furylsalicylates has been reported. Salicylic acid is a much weaker inhibitor of cyclooxygenase isoforms (COX-1 and COX-2) than acetylsalicylic acid[46] and its antiinflamatory activity has been attributed to interaction with alternative targets[47] and modulation of gene expression.[48] Renal toxicity associated to chronical administration is reported to be less agresive for salicylic acid *vs* other nonsteroidal anti-inflammatory drugs.[49] Beyond the scope of this article, in which a novel biological activity of salicylates is introduced, evaluations of anti-inflammatory activity and renal toxicity will be conducted in the short-term research using suitable candidate molecules. The information obtained in this evaluation will help the design of future drug candidates.

EXPERIMENTAL SECTION

General Experimental Methods. All solvents and chemicals were used as purchased without further purification. The progress of the reactions was controlled by thin layer chromatography (TLC) on aluminium plates (Merck AL de Silicagel 60 F254) and detected by UV lamp (254 nm) or employing a solution of vanillin (6g) and concentrated sulfuric acid (2.5 mL) in ethanol (250 mL) and heating. *R*f values refer to these TLC plates developed in the solvents indicated. Small scale microwave-assisted synthesis was carried out in sealed vessels using a Biotage Initiator Microwave with automatic arm and controlled irradiation at 2.450 GHz (Biotage AB, Upsala). These parameters were established following the basic principles of microwave assisted organic synthesis. The temperature was measured with an IR sensor on the outside of the reaction vessel. Purification by flash chromatography was performed on Silicagel Merck 60 (230-400 mesh

ASTM). The non-crystalline compounds were shown to be homogeneous by chromatographic methods and characterized by NMR and HRMS. For some samples the purification process involved the use of an Eppendorf 5418R centrifuge. ^{1}H-NMR and ^{13}C-NMR spectra have been recorded in a 2-channel 300 MHz Varian Inova Unity, a 2-channel 400 MHz and a 3-channel 500 MHz Varian Direct Drive spectrometers using CD_3OD, $(CD_3)_2SO$, $(CD_3)_2CO$ $CDCl_3$ or D_2O. Chemical shifts (δ) are quoted in parts per million (ppm) and are referenced to residual H in the deuterated solvent as the internal standard. Coupling constants (*J*) are expressed in Hz. Splitting patterns are designated as follows: s, singlet; d, doublet; dd, double doublet; ddd, double double doublet; t, triplet; ddt, double double triplet; tt, triple triplet; q, quartet; m, multiplet and b, broad. High resolution mass spectra (HRMS) were recorded by time of flight (TOF) mass spectrometry with electrospray ionization (ESI) in positive or negative mode, using a time of flight apparatus with orthogonal acceleration LCT Premier^{TM}. Low resolution mass spectra (LRMS) were recorded by ESI in positive or negative mode, coupled to high resolution liquid chromatography (LC-MS) in a simple quadrupole Agilent 6110 instrument equipped with a Zorbax Eclipse XDB-C18 4.6 x 150 mm column. Purity of the compounds was assessed by HPLC using an Agilent 1200 instrument with diodo-array detector equipped with a Zorbax Eclipse XDB-C18 4,6 x 150 mm column. Column temperature was set at 25 ºC. Absorbance was measured at 214, 254 or 280 nm, as suitable for each compound. Purity of most final compounds was higher than 95% and, in every case, higher than 90%. For colorimetric interference test, absorbance was measured at 515 and 590 nm. Melting points (mp) were taken in open capillaries on a Gallenkamp Melting Point Apparatus and are uncorrected.

HPLC methods for purity determination:

General HPLC set up: Flow 0.8 mL/min; solvent A [water (0.1% HCOOH)/acetonitrile (0.1% HCOOH)]; solvent B [acetonitrile (0.1% HCOOH) 100%].

For **16**, **18f**, **20**, **21**, **23**, **24**, **25**, **26**, **27**, **31-33**, **35-38**. **HPLC set up**: Detector λ = 214, 254 nm; solvent A [water (0.1% HCOOH)/acetonitrile (0.1% HCOOH) 80/20]. Isocratic A 2 min + gradient A→B 17 min + isocratic B 2 min.

For **22**, **40**: **HPLC set up**: Detector λ = 214, 254 nm; solvent A [water (0.1% HCOOH)/acetonitrile (0.1% HCOOH) 80/20]; Isocratic A 2 min + gradient A→B 17 min + isocratic B 2 min.

For **28**, **29**, **30**, **39** (potassium salt), **41-46** (potassium salts), **49** (potassium salt), **54** (potassium salt): **HPLC set up**: Detector λ = 214, 254, 280 nm; solvent A [water (0.1% HCOOH)/acetonitrile (0.1% HCOOH) 60/40]; Isocratic A 2 min + gradient A→B 15 min + isocratic B 4 min.

For **34**: **HPLC set up**: Detector λ = 214, 254 nm; solvent A [water (0.1% HCOOH)/acetonitrile (0.1% HCOOH) 70/30]; Isocratic A 2 min + gradient A→B 17 min + isocratic B 2 min.

For **48**, **54**, **55**: Detector λ = 214, 254 nm; solvent A [water (0.1% HCOOH)/acetonitrile (0.1% HCOOH) 60/40]; Isocratic A 2 min + gradient A→B 17 min + isocratic B 2 min.

For **50**, **52**, **53**: Detector λ = 214, 254 nm; solvent A [water (0.1% HCOOH)/acetonitrile (0.1% HCOOH) 50/50]; Isocratic A 2 min + gradient A→B 11 min + isocratic B 4 min.

Colorimetric interference test for compounds **21**, **26** and **27**: **HPLC set up**: Detector λ = 515, 590 nm; solvent A [water (0.1% HCOOH)/acetonitrile (0.1% HCOOH) 80/20]. Isocratic A 2 min + gradient A→B 17 min + isocratic B 2 min.

Colorimetric interference test for compounds **54** and **55**: Detector λ = 515, 590 nm; solvent A [water (0.1% HCOOH)/acetonitrile (0.1% HCOOH) 60/40]; Isocratic A 2 min + gradient A→B 17 min + isocratic B 2 min.

General procedure for small scale Suzuki-Miyaura (SM) cross-coupling (20-22, 24-28, 31-55).

Method A: A solution of K_2CO_3 (3 equiv) in water (4 mL/mmol of **18**) was prepared in a glass tube equipped with a stirring bar. After dissolution, DMF was added (2 mL/mmol of **18**) and the mixture was degassed by bubbling with argon. Consecutively the corresponding halide (**18**) (1 equiv), the boronate derivative (**19**) (1.2 equiv), PPh_3 (15 mol%), $Pd(OAc)_2$ (5 mol%) and DMF (2 mL/mmol of **18**) were added in that sequence. The mixture was then degassed by argon bubbling during 10 min after which the tube was sealed. The reaction was heated at 100 ºC during 24 h. After this time, the reaction crude was washed with methanol or acetonitrile on a filter plate and the filtrate was evaporated under vacuum. The residue was dissolved in water, cooled to 0 ºC and acidified with HCl 10%. After evaporation under vacuum, the final crude was purified by flash column chromatography on silica gel.

Method B:[34b] A solution of K_2CO_3 (3 equiv) in water (4 mL/mmol of **18**) was prepared in a glass tube equipped with a stirring bar. After dissolution, ethanol was added (4 mL/mmol of **18**) and the mixture was degassed by bubbling with argon. Consecutively the corresponding halide (**18**) (1 equiv), the boronate derivative (**19**) (1.5 equiv) and Pd EnCat® 30 (6 mol%) were added in that sequence. The mixture was then degassed by argon bubbling during 10 min after which the tube was sealed. The reaction was heated at 80 ºC during 24 h. After this time, the reaction crude was filtered (washing with methanol) and the filtrate was evaporated under vacuum. The residue

was dissolved in water, cooled to 0 ºC and acidified with HCl 10%. After evaporation under vacuum, the final crude was purified by flash column chromatography on silica gel.

Method C: The reaction was set up as described in method A, using a microwave vial instead of a sealed tube. The reaction was programmed in a microwave instrument for heating at 100 ºC during 3 h (45 seconds pre-stirring). After this time, the reaction crude was washed with methanol on a filter plate and the filtrate was evaporated under vacuum. The residue was dissolved in water, cooled to 0 ºC and acidified with HCl 10%. After evaporation under vacuum, the final crude was purified by flash column chromatography on silica gel.

7-(5-Formylfuran-2-yl)-3-hydroxy-2-naphthoic acid (**16**). Method A (SM). Reagents: **10** (60 mg, 0.225 mmol), **19a** (37.8 mg, 0.27 mmol), K_2CO_3 (93.29 mg, 0.675 mmol), PPh_3 (8.92 mg, 0.034 mmol), $Pd(OAc)_2$ (2.47 mg, 0.011 mmol), and DMF/H_2O 1/1 (2 mL). Column chromatography: DCM/MeOH (20:1→8:2). Solid 22% yield (14 mg, 0.05 mmol), mp 200 ºC (decomposition). ^{1}H NMR (400 MHz, $(CD_3)_2SO$] δ = 9.60 (s, 1H), 8.44 (bs, 1H), 8.32 (bs, 1H), 7.83 (d, *J* = 8.7 Hz, 1H), 7.72 (d, *J* = 8.7 Hz, 1H), 7.67 (d, *J* = 3.8 Hz, 1H), 7.29 (d, *J* = 3.8 Hz, 1H), 7.04 (bs, 1H); ^{13}C NMR [101 MHz, $(CD_3)_2SO$] δ 177.3 (CHO), 170.3 (C), 161.2 (C), 159.1 (C), 151.4 (C), 136.7 (C), 131.4 (CH), 126.4 (CH), 125.9 (CH), 125.7 (C), 125.5 (CH), 123.5 (C), 123.3 (CH), 122.1 (C), 109.2 (CH), 108.0 (CH). HRMS (TOF ES$^-$): *m/z* calcd for $C_{16}H_9O_5$ $(M\text{-}H^+)^-$ 281.0450, found 281.0432. HPLC (λ = 214): 100%; (λ = 254): 99.7% purity, t_R 13.52 min.

4-Bromo-2-(hydroxymethyl)benzoic acid (**18d**). 5-Bromophthalide (95 mg, 0.446 mmol) was refluxed in THF/aqueous NaOH 1N 1/1 (4.5 mL) for 6 h. Once the reaction finished, THF was evaporated under vacuum. The mixture was taken in water (10 mL) and it was acidified with

HCl 10%. The crude after evaporation was purified by flash chromatography using DCM/MeOH (20:1→9:1) followed by EtOAc/CH_3CN/MeOH/H_2O (70:10:5:5). White solid, 97% yield (100 mg, 0.45 mmol), mp 162-166 °C. ^{1}H NMR [400 MHz, $(CD_3)_2CO$] δ = 7.98 (s, 1H), 7.93 (d, *J* = 8.3 Hz, 1H), 7.57 (dd, *J* = 8.3, 1.9 Hz, 1H), 4.98 (s, 2H). ^{13}C NMR [101 MHz, $(CD_3)_2CO$] δ = 167.7, 148.0, 133.3, 130.7, 130.2, 127.6, 127.5, 62.4. HRMS (TOF ES$^-$): *m/z* calcd for $C_8H_6O_3Br$ $(M\text{-}H^+)^-$ 228.9500, found 228.9492.

2-Hydroxy-4-iodo-5-nitrobenzoic acid (**18f**).[50,51] 2-Hydroxy-4-iodobenzoic acid (30 mg, 0.114 mmol) was dissolved in AcOH (3 mL). The mixture was then cooled to 0 °C and 8 µL of HNO_3 60 % (0.114 mmol) and 12 µL de H_2SO_4 95-97 % (0.228 mmol) were added. The reaction was allowed to stir at rt for 48 h. The mixture was then concentrated in rotavapor and the crude residue was purified by flash chromatography using EtOAc/CH_3CN/MeOH/H_2O (70:10:5:5→60:10:10:10). Yellow solid, 73% yield (26 mg, 0.084 mmol). ^{1}H NMR [300 MHz, $(CD_3)_2CO$] δ = 8.51 (s, 1H), 7.41 (s, 1H). HRMS (TOF ES$^-$): *m/z* calcd for $C_7H_3NO_5I$ $(M\text{-}H^+)^-$ 307.9056, found 307.9076. HPLC (λ= 254 nm): 93.8%; (λ= 214 nm): 93.4% t_R = 11.68 min.

Potassium 3-(5-formylfuran-2-yl)benzoate (**20**). Method C (SM). Reagents: 3-Bromobenzoic acid (**18b**) (50 mg, 0.249 mmol), **19a** (41.83 mg, 0.299 mmol), K_2CO_3 (103.24 mg, 0.747 mmol), PPh_3 (9.705 mg, 0.037 mmol), $Pd(OAc)_2$ (2.69 mg, 0.012 mmol), and DMF/H_2O 1/1 (2 mL). Column chromatography: DCM/MeOH (30:1→20:1). Orange solid 42% yield (27 mg, 0.113 mmol), mp 266 ºC. ^{1}H NMR (400 MHz, CD_3OD) δ = 9.62 (s, 1H), 8.51 (t, *J* = 1.5 Hz, 1H), 8.08 (ddt, *J* = 10.6, 7.8, 1.1 Hz, 2H), 7.60 (t, *J* = 7.8 Hz, 1H), 7.53 (d, *J* = 3.8 Hz, 1H), 7.17 (d, *J* = 3.8 Hz, 1H); ^{13}C NMR (101 MHz, CD_3OD) δ 179.3 (CHO), 169.2 (CO), 159.7 (C), 153.8 (C), 131.7 (CH), 130.8 (C), 130.4 (CH), 130.2 (CH), 127.3 (CH), 125.7 (C), 109.8 (CH), 78.9 (CH). HRMS

(TOF ES$^-$): *m/z* calcd for $C_{12}H_7O_4$ (M-H$^+$)$^-$ 215.0344, found 215.0354. HPLC (λ = 214): 95.2%; (λ = 254): 100% purity, t_R 10.72 min. Experimental data agree with those reported.[35]

5-(4-Hydroxyphenyl)-2-furaldehyde (**21**). Method A (SM). Reagents: 4-Bromophenol (**18c**) (60 mg, 0.343 mmol) and **19a** (56.89 mg, 0.412 mmol), K_2CO_3 (142.22 mg, 1.029 mmol), PPh_3 (13.37 mg, 0.051 mmol), $Pd(OAc)_2$ (3.82 mg, 0.017 mmol) and DMF/H_2O 1/1 (2 mL). Column chromatography: EtOAc/hexane (1:5→1:3). Yellow solid, 76% yield (49 mg, 0.260 mmol), mp 170 ºC. ^{1}H NMR [400 MHz, $(CD_3)_2CO$] δ = 9.60 (s, 1H), 8.86 (s, 1H), 7.78 – 7.72 (m, 2H), 7.48 (d, *J* = 3.7 Hz, 1H), 6.99 – 6.94 (m, 3H); ^{13}C NMR [101 MHz, $(CD_3)_2CO$] δ = 177.2, 160.4, 159.9, 152.7, 127.8, 125.3, 121.8, 116.8, 106.9. Spectroscopic data agree with the ones found in bibliography.[36] HRMS (TOF ES$^-$): *m/z* calcd for $C_{11}H_7O_3$ (M-H$^+$)$^-$ 187.0395, found 187.0381. HPLC (λ= 254 nm): 100%; (λ= 214 nm): 100%; t_R = 10.64 min.

4-(5-Formylfuran-2-yl)-2-(hydroxymethyl)benzoic acid (**22**). Method A (SM). Reagents: **18d** (22 mg, 0.095 mmol), **19a** (15.95 mg, 0.114 mmol), K_2CO_3 (39.39 mg, 0.285 mmol), PPh_3 (3.67 mg, 0.014 mmol), $Pd(OAc)_2$ (1.076 mg, 0.005 mmol) and DMF/H_2O 1/1 (2 mL). Column chromatography: DCM/MeOH (20:1→9:1) followed by EtOAc/CH_3CN/MeOH/H_2O (70:2.5:1.25:1.25→70:5:2.5:2.5). Brown solid, 30% yield (7 mg, 0.028 mmol). ^{1}H NMR [300 MHz, $(CD_3)_2CO$] δ = 9.72 (s, 1H), 8.23 (s, 1H), 8.12 (d, *J* = 8.1 Hz, 1H), 7.87 (d, *J* = 8.2 Hz, 1H), 7.56 (d, *J* = 3.7 Hz, 1H), 7.31 (d, *J* = 3.6 Hz, 1H), 4.99 (s, 2H); ^{13}C NMR (126 MHz, CD_3OD) δ = 179.3, 159.8, 154.0, 145.5, 133.2, 132.7, 132.6, 125.2, 124.5, 112.0, 110.6, 108.6, 63.7. HRMS (TOF ES$^-$): *m/z* calcd for $C_{13}H_9O_5$ (M-H$^+$)$^-$ 245.0450, found 245.0443. HPLC (λ = 214): 96.9%, (λ = 254): 100% purity; t_R 11.29 min.

4-(5-Formylfuran-2-yl)-2-methoxybenzoic acid (**23**). Compound **24** (22 mg, 0.084 mmol) was dissolved in THF/aqueous NaOH 1N 1/1 (0.84 mL) and was stirred at 60 °C for 2 h. Once the

reaction had finished, the THF was removed in rotavapor. The residue was taken in water (10 mL) and acidified with HCl 10%. The resultant solid was filtered and purified by flash chromatography on silica gel using DCM/MeOH (20:1→9:1) followed by EtOAc/CH_3CN/MeOH/H_2O (70:10:5:5). Orange solid, 29% yield (6 mg, 0.024 mmol). ^{1}H NMR [300 MHz, $(CD_3)_2CO$] δ = 9.72 (d, *J* = 2.3 Hz, 1H), 8.05-7.95 (m, 1H), 7.67 (s, 1H), 7.64-7.55 (m, 2H), 7.37 (d, *J* = 3.6 Hz, 1H), 4.11 (d, *J* = 2.2 Hz, 3H). HRMS (TOF ES$^-$): *m/z* calcd for $C_{13}H_9O_5$ $(M\text{-}H^+)^-$ 245.0450, found 245.0436. HPLC (λ = 214): 96.9% and (λ = 254): 98.5% purity, t_R 10.18 min.

Methyl 4-(5-formylfuran-2-yl)-2-methoxybenzoate (**24**). Method A (SM). Reagents: 5-Bromofurfural (**18e**) (60 mg, 0.343 mmol), 4-methoxycarbonyl-3-methoxyphenylboronic acid (**19c**) (86.31 mg, 0.398 mmol), K_2CO_3 (142.2, 1.029 mmol), PPh_3 (13.37, 0.051 mmol), $Pd(OAc)_2$ (3.82 mg, 0.017 mmol) and DMF/H_2O 1/1 (2 mL). Column chromatography: EtOAc/hexane (1:4→1:2). Yellow solid, 57% yield (51 mg, 0.20 mmol), mp 126 ºC. ^{1}H NMR (400 MHz, $CDCl_3$) δ = 9.69 (s, 1H), 7.86 (d, *J* = 8.0 Hz, 1H), 7.41 (d, *J* = 1.5 Hz, 1H), 7.39 (dd, *J* = 8.0, 1.5 Hz, 1H), 7.34 (d, *J* = 3.8 Hz, 1H), 6.94 (d, *J* = 3.7 Hz, 1H), 4.00 (s, 3H), 3.91 (s, 3H). ^{13}C NMR (101 MHz, $CDCl_3$) δ = 177.5, 166.1, 159.7, 158.0, 152.6, 133.6, 132.5, 123.3, 120.8, 117.2, 109.5, 108.4, 56.4, 52.3. HRMS (TOF ES$^+$): *m/z* calcd for $C_{14}H_{12}O_5Na$ $(M+Na)^+$ 283.0582, found 283.0591. HPLC (λ = 214): 97.7%, (λ = 254): 96.0% purity; t_R 12.97 min.

4-(Furan-2-yl)-2-hydroxy-5-nitrobenzoic acid (**25**). Method A (SM). Reagents: **18f** (41 mg, 0.133 mmol), **19b** (31.04, 0.160 mmol), K_2CO_3 (55.15 mg, 0.399 mmol), PPh_3 (5.25mg, 0.020 mmol), $Pd(OAc)_2$ (1.57 mg, 0.007 mmol) and DMF/H_2O 1/1 (2 mL). Column chromatography: DCM/MeOH (15:1→9:1) and EtOAc/CH_3CN/MeOH/H_2O (70:5:2.5:2.5→70:10:10:10). Brown solid, 48% yield (16 mg, 0.064 mmol), mp 187 ºC. ^{1}H NMR [400 MHz, $(CD_3)_2CO$] δ = 8.40 (s,

1H), 7.63 (d, *J* = 1.0 Hz, 1H), 6.99 (s, 1H), 6.76 (d, *J* = 3.2 Hz, 1H), 6.56 (dd, *J* = 3.2, 1.7 Hz, 1H). ^{13}C NMR [101 MHz, $(CD_3)_2CO$] δ = 172.8 (CO), 166.4 (C), 150.3 (C), 144.7 (CH), 139.1 (C), 129.7 (C), 129.0 (CH), 118.9 (C), 117.5 (CH), 112.6 (CH), 110.7 (CH). HRMS (TOF ES$^-$): *m/z* calcd for $C_{11}H_6NO_6$ $(M\text{-}H^+)^-$ 248.0195, found 248.0206. HPLC (λ = 254): 94.0%, (λ = 214): 92.1% purity; t_R 12.38 min.

5-(5-Formylfuran-2-yl)-2-hydroxybenzoic acid (**26**). Method B (SM). Reagents: **18a** (60 mg, 0.216 mmol), **19a** (45.32 mg, 0.324 mmol), K_2CO_3 (89.56 mg, 0.648 mmol), PdEnCat® 30 (32.5 mg, 0.113 mmol; 0.4 mmol/g Pd) and EtOH/H_2O 1/1 (2 mL). Column chromatography: DCM/MeOH (20:1→8:2). Brown solid, 100% yield (50 mg, 0.215 mmol), mp 232.6 ºC. ^{1}H NMR [400 MHz, $(CD_3)_2SO$]: δ = 9.51 (s, 1H), 8.21 (d, *J* = 2.4 Hz, 1H), 7.70 (dd, *J* = 8.5, 2.5 Hz, 1H), 7.60 (d, *J* = 3.8 Hz, 1H), 7.00 (d, *J* = 3.8 Hz, 1H), 6.76 (d, *J* = 8.6 Hz, 1H). ^{13}C NMR [101 MHz, $(CD_3)_2SO$] δ 176.7 (CHO), 170.8 (CO), 165.5 (C), 159.8 (C), 150.8 (C), 129.2 (CH), 127.1 (CH), 120.0 (C), 117.3 (CH), 116.64, 116.62 (C, CH), 105.9 (CH). HRMS (TOF ES$^-$): calcd for $C_{12}H_7O_5$ $(M\text{-}H^+)^-$ 231.0300, found; 231,0293. HPLC (λ=254): 100%; (λ=214): 100% purity, t_R 11.02 min.

5-(Furan-2-yl)-2-hydroxybenzoic acid (**27**). Method C (SM). Reagents: Methyl 2-hydroxy-5-iodobenzoate (**18a**) (50 mg, 0.180 mmol), 2-furanboronic acid (**19b**) (24.2 mg, 0.216 mmol), PPh_3 (7.1 mg, 0.027 mmol), $Pd(OAc)_2$ (2 mg, 0.009 mmol), K_2CO_3 (74.6 mg, 0.540 mmol), H_2O/DMF 1/1 (2 mL). Column chromatography: EtOAc/CH_3CN/MeOH/H_2O (70:2.5:1.25:1.25 to 70:10:5:5). Brown solid, 83% yield (30 mg, 0.147 mmol), mp > 300 ºC. ^{1}H NMR (400 MHz, CD_3OD): δ = 8.20 (s, 1H), 7.67 (d, *J* = 7.9 Hz, 1H), 7.50-7.44 (m, 1H), 6.88 (d, *J* = 8.5 Hz, 1H), 6.58 (d, *J* = 3.3 Hz, 1H), 6.45 (dd, *J* = 3.4, 1.8 Hz, 1H). ^{13}C NMR (101 MHz, CD_3OD) δ 174.9 (CO), 162.2 (C), 155.2 (C), 142.5 (CH), 130.2 (CH), 127.1 (CH), 123.3 (C), 118.3 (C), 117.9

(CH), 112.5 (CH), 104.1 (CH). HRMS (TOF ES$^-$): *m/z* calcd for $C_{11}H_7O_4$ $(M\text{-}H^+)^-$ 203.0344, found 203.0350. HPLC (λ=214, 254): 97% purity, t_R 14.04 min.

4-(2-Furyl)-2-hydroxybenzoic acid (**28**). Method C (SM). Reagents: 2-Hydroxy-4-iodobenzoic acid (**18g**) (50 mg, 0.189 mmol), **19b** (38.6 mg, 0.227 mmol), K_2CO_3 (91.4 mg, 0.662 mmol), PPh_3 (7.4 mg, 0.028 mmol), $Pd(OAc)_2$ (2.12 mg, 0.010 mmol) and DMF/H_2O 1/1 (2 mL). Column chromatography: EtOAc/CH_3CN/MeOH/H_2O (70:5:2.5:2.5). Yellow solid, 50% yield (25 mg, 0.122 mmol) mp 220 ºC. ^{1}H NMR [400 MHz, $(CD_3)_2CO$] δ = 11.19 (bs, 1H), 7.92 (d, *J* = 8.31 Hz, 1H), 7.72 (m, 1H), 7.31 (dd, *J* = 8.3, 1.6 Hz, 1H), 7.27 (bd, *J* = 1,6 Hz, 1H), 7.07 (d, *J* = 3,5 Hz, 1H), 6.61 (dd, *J* = 3.5, 1.8 Hz, 1H). 13 C NMR [101 MHz, $(CD_3)_2CO$] δ = 172.4 (C), 163.5 (C), 153.3 (C), 144.8 (CH), 138.4 (C), 131.9 (CH), 115.4 (CH), 113.1 (CH), 112.2 (CH), 111.8 (C), 109.4 (CH). HRMS (TOF, ES$^-$): *m/z* calcd for $C_{11}H_7O_4$ $(M\text{-}H^+)^-$ 203.0344, found 203.0346. HPLC (λ = 214): 96.0%, (λ = 254): 95.6% purity; t_R 8.61 min.

2-Hydroxy-5-(5-hydroxymethylfuran-2-yl)benzoic acid (**29**). Compound **26** (40 mg, 0.172 mmol, 1 equiv) was dissolved in MeOH (2.5 mL). The solution was cooled down to 0 ºC and $NaBH_4$ (13.0 mg, 0.344 mmol, 2 equiv) was slowly added in small portions. After the addition, the reaction was stirred at rt and monitored by TLC till full starting material consumption (3.5 h). The reaction was quenched by addition of HCl (5%) until pH 5.0 and filtered. The filtrate was concentrated, and the crude was purified by flash column chromatography using EtOAc/CH_3CN/MeOH/H_2O (70:10:5:5→60:10:10:10) to afford **29** as a yellowish solid in 64% yield (25.6 mg, 0.109 mmol), mp > 300 ºC. ^{1}H NMR (400 MHz, CD_3OD) δ = 8.32-7.90 (m, 1H), 7.73 (dd, *J* = 8.7, 2.3 Hz, 1H), 6.92 (d, *J* = 8.7 Hz, 1H), 6.54 (d, *J* = 3.3 Hz, 1H), 6.20 (dd, *J* = 3.3, 0.9 Hz, 1H), 4.10 (s, 2H). ^{13}C NMR (101 MHz, CD_3OD) δ = 171.8 (CO), 160.8 (C), 152.0 (C), 150.8 (C), 134.3 (C), 130.4 (CH), 124.7 (CH), 122.7 (C), 117.3 (CH), 108.2 (CH), 104.4

(CH), 26.8 (CH_2). HRMS (TOF, ES^-): *m/z* calcd for $C_{12}H_9O_5$ $(M\text{-}H^+)^-$ 233.0442, found 233.0450. HPLC (λ = 254): 91.5% purity, t_R 9.4 min.

2-Hydroxy-4-(5-hydroxymethylfuran-2-yl)benzoic acid (**30**). Compound **8** (33mg, 0.142 mmol, 1 equiv) was dissolved in MeOH (2.5 mL). The solution was cooled down to 0 ºC and $NaBH_4$ (10.8 mg, 0.284 mmol, 2 equiv) was slowly added in small portions. After the addition, the reaction was stirred at rt and monitored by TLC till full starting material consumption (1 h). The reaction was quenched by addition of HCl (5%) until pH 5.0 and filtered. The filtrate was concentrated, and the crude was purified by flash column chromatography using EtOAc/CH_3CN/MeOH/H_2O (70:5:2.5:2.5→60:10:10:10) to afford **30** as a yellowish solid in 38% yield (12.5 mg, 0.053 mmol), mp > 300 ºC. ^{1}H NMR (400 MHz, $CDCl_3$) δ = 7.87 (d, *J* = 8.6 Hz, 1H), 7.19 (dt, *J* = 4.4, 2.2 Hz, 2H), 6.82 (d, *J* = 3.4 Hz, 1H), 6.44 (d, *J* = 3.3 Hz, 1H), 4.61 (s, CH_2, 2H). HRMS (TOF, ES^-): *m/z* calcd. for $C_{12}H_{10}O_5$ $(M\text{-}H^+)^-$ 233.0450, found 233.0450. HPLC (λ = 280): 95.1% purity, t_R 8.9 min.

5-(5-Carboxyfuran-2-yl)-2-hydroxybenzoic acid (**31**). Method B (SM). Reagents: 2-Hydroxy-5-iodobenzoic acid (**18h**) (15 mg, 0.057 mmol), 5-boronofuran-2-carboxylic acid (**19d**) (13.26 mg, 0.085 mmol), K_2CO_3 (23.63 mg, 0.171 mmol), PdEnCat® 30 (8.5 mg, 0.003 mmol; 0.4 mmol/g Pd), and EtOH/H_2O 1/1 (2 mL). Column chromatography: EtOAc/CH_3CN/MeOH/H_2O (70:5:2.5:2.5→70:10:10:10). White solid, quantitative yield (14 mg, 0.056 mmol). ^{1}H NMR (400 MHz, CD_3OD) δ = 8.34 (s, 1H), 7.84 (d, *J* = 8.5 Hz, 1H), 7.23 (d, *J* = 3.3 Hz, 1H), 6.94 (d, *J* = 8.6 Hz, 1H), 6.76 (d, *J* = 3.3 Hz, 1H). ^{13}C NMR (101 MHz, CD_3OD) δ = 174.7, 163.5, 162.8, 158.5, 145.4, 131.4, 128.2, 122.0, 120.8, 118.4, 117.6, 106.4. HRMS (TOF, ES^-): *m/z* calcd for $C_{12}H_7O_6$ $(M\text{-}H^+)^-$ 247.0243, found 247.0226. HPLC (λ= 254nm): 100%; (λ= 214 nm): 100%; t_R 10.05 min.

4-(5-Carboxyfuran-2-yl)-2-hydroxybenzoic acid (**32**). Method B (SM). Reagents: 5-Bromofuran-2-carboxylic acid (**18i**) (60 mg, 0.314 mmol), methyl 2-hydroxy-4-(4,4,5,5-tetramethyl-1,3,2-dioxaborolan-2-yl)benzoate (**19e**) (131 mg, 0.471 mmol), K_2CO_3 (130.19, 0.942 mmol), PdEnCat® 30 (47.5 mg, 0.19 mmol; 0.4 mmol/g Pd) and EtOH/H_2O 1/1 (2 mL). The crude residue was purified by flash chromatography on silica gel using EtOAc/CH_3CN/MeOH/H_2O (70:2.5:1.25:1.25→60:10:10:10). White solid, 28% yield (22 mg, 0.089 mmol), mp 250-252 ºC. ^{1}H NMR (400 MHz, D_2O) δ = 7.89 (d, *J* = 8.1 Hz, 1H), 7.45-7.32 (m, 2H), 7.13 (d, *J* = 3.6 Hz, 1H), 7.01 (d, *J* = 3.6 Hz, 1H). ^{13}C NMR (101 MHz, D_2O) δ = 175.0, 166.2, 159.9, 154.1, 148.7, 134.5, 131.0, 117.4, 117.0, 115.1, 111.4, 108.9. HRMS (TOF, ES$^-$): *m/z* calcd for $C_{12}H_7O_6$ $(M\text{-}H^+)^-$ 247.0243, found 247.0256. HPLC (λ= 214 nm): 95.5%; t_R 9.51 min.

4-(Furan-3-yl)-2-hydroxybenzoic acid (**33**). Method A (SM). Reagents: **18g** (60 mg, 0.227 mmol), 3-furanboronate pinacol ester (**19f**) (52.77 mg, 0.272 mmol), K_2CO_3 (94.12 mg, 0.681 mmol), PPh_3 (8.92 mg, 0.034 mmol), $Pd(OAc)_2$ (2.47 mg, 0.011 mmol) and DMF/H_2O 1/1 (2 mL). Column chromatography: DCM/MeOH (20:1→9:1) followed by EtOAc/CH_3CN/MeOH/H_2O (70:2.5:1.25:1.25→70:5:2.5:2.5). Brown solid, 45% yield (21 mg, 0.103 mmol), mp >300 ºC. ^{1}H NMR [400 MHz, $(CD_3)_2CO$] δ = 8.14 (s, 1H), 7.93 (d, *J* = 6.8 Hz, 1H), 7.66 (s, 1H), 7.15 (d, *J* = 8.7 Hz, 2H), 6.93 (s, 1H). ^{13}C NMR [101 MHz, $(CD_3)_2CO$] δ = 167.4, 163.0, 145.1, 141.3, 140.1, 132.1, 126.5, 117.1, 114.2, 110.8, 109.4. HRMS (TOF, ES$^-$): *m/z* calcd for $C_{11}H_7O_4$ $(M\text{-}H^+)^-$ 203.0344, found 203.0347. HPLC (λ= 254nm): 100%; (λ= 214 nm): 97.5%; t_R 13.67 min.

5-(Furan-3-yl)-2-hydroxybenzoic acid (**34**). Method A (SM). Reagents: **18a** (60 mg, 0.216 mmol), **19f** (50.25 mg, 0.259 mmol), K_2CO_3 (89.56 mg, 0.648 mmol), PPh_3 (8.39 mg, 0.032

mmol), $Pd(OAc)_2$ (2.47 mg, 0.011 mmol),) and DMF/H_2O 1/1 (2 mL). Column chromatography: DCM/MeOH (20:1→9:1) followed by EtOAc/CH_3CN/MeOH/H_2O (70:2.5:1.25:1.25→70:5:2.5:2.5). Brown solid, 34% yield (15 mg, 0.073 mmol), mp >300 ºC. ^{1}H NMR [400 MHz, $(CD_3)_2SO$] δ = 7.74 (d, *J* = 8.4 Hz, 1H), 7.57 (dd, *J* = 5.1, 1.1 Hz, 1H), 7.54 (dd, *J* = 3.6, 1.1 Hz, 1H), 7.13 (dd, *J* = 5.1, 3.7 Hz, 1H), 7.03 (dd, *J* = 3.3, 2.2 Hz, 2H). ^{13}C NMR [101 MHz, $(CD_3)_2SO$] 171.5, 162.5, 142.9, 137.8, 130.9, 128.5, 126.3, 124.4, 116.9, 114.5, 112.5. HRMS (TOF, ES^-): *m/z* calcd for $C_{11}H_7O_4$ $(M\text{-}H^+)^-$ 203.0344, found 203.0345. HPLC (λ= 254nm): 99.8%; (λ= 214 nm): 99.6%; t_R = 6.71 min.

4-(5-Formylthien-2-yl)-2-hydroxybenzoic acid (**35**). Method A (SM). Reagents: **18g** (70 mg, 0.265 mmol), 5-formyl-2-thiopheneboronic acid (**19g**) (49.61 mg, 0.318 mmol), K_2CO_3 (109.87 mg, 0.795 mmol), PPh_3 (10.49 mg, 0.040 mmol), $Pd(OAc)_2$ (2.92 mg, 0.013 mmol) and DMF/H_2O 1/1 (2 mL). Column chromatography: DCM/MeOH (20:1→9:1). Brown solid, 45% yield (30 mg, 0.121 mmol), mp > 300 °C. ^{1}H NMR [400 MHz, $(CD_3)_2SO$] δ = 9.92 (s, 1H), 8.04 (d, *J* = 4.0 Hz, 1H), 7.83-7.77 (m, 2H), 7.24-7.17 (m, 2H). ^{13}C NMR [101 MHz, $(CD_3)_2SO$] δ = 184.1, 171.0, 162.4, 151.7, 142.4, 139.0, 136.9, 131.1, 126.2, 117.5, 115.5, 113.6. HRMS (TOF, ES^-): *m/z* calcd for $C_{12}H_7O_4S$ $[M\text{-}H^+]^-$ 247.0065, found 247.0060. HPLC (λ= 254nm): 92.6%; (λ= 214 nm): 94.1%; t_R = 13.93 min.

5-(5-Formylthien-2-yl)-2-hydroxybenzoic acid (**36**). Method A (SM). Reagents: **18a** (60 mg, 0.216 mmol), **19g** (40.39 mg, 0.259 mmol), K_2CO_3 (89.56 mg, 0.648 mmol), PPh_3 (8.40 mg, 0.032 mmol), $Pd(OAc)_2$ (2.47 mg, 0.011 mmol) and DMF/H_2O 1/1 (2 mL). Column chromatography: DCM/MeOH (15:1→9:1) followed by EtOAc/CH_3CN/MeOH/H_2O (70:2.5:1.25:1.25→70:5:2.5:2.5). Brown solid, 46 % yield (25 mg, 0.101 mmol), mp > 300 °C. ^{1}H NMR [400 MHz, $(CD_3)_2SO$] δ = 9.86 (s, 1H), 8.10 (d, *J* = 2.4 Hz, 1H), 7.99 (d, *J* = 4.0 Hz,

1H), 7.79 (dd, *J* = 8.6, 2.4 Hz, 1H), 7.58 (d, *J* = 4.0 Hz, 1H), 6.90 (d, *J* = 8.6 Hz, 1H). ^{13}C NMR [101 MHz, $(CD_3)_2SO$] δ = 183.6, 170.7, 163.8, 153.3, 140.4, 139.6, 131.4, 127.8, 123.5, 121.8, 117.8, 117.3. HRMS (TOF, ES$^-$): *m/z* calcd for $C_{12}H_7O_4S$ $(M\text{-}H^+)^-$ 247.0065, found 247.0077. HPLC (λ= 254nm): 96.8%; (λ= 214 nm): 95.0%; t_R = 12.25 min.

2-Hydroxy-4-(thien-2-yl)benzoic acid (**37**). Method A (SM). Reagents: **18g** (70 mg, 0.265 mmol), 2-thiopheneboronic acid (**19h**) (40.69 mg, 0.318 mmol), K_2CO_3 (109.89 mg, 0.795 mmol), PPh_3 (10.49 mg, 0.040 mmol), $Pd(OAc)_2$ (2.91 mg, 0.013 mmol) and DMF/H_2O 1/1 (2 mL). Column chromatography: DCM/MeOH (20:1→9:1). Yellow solid, 51% yield (30 mg, 0.136 mmol), mp 225 ºC. ^{1}H NMR [400 MHz, $(CD_3)_2SO$] δ = 7.74 (d, *J* = 8.4 Hz, 1H), 7.57 (dd, *J* = 5.1, 1.1 Hz, 1H), 7.54 (dd, *J* = 3.6, 1.1 Hz, 1H), 7.13 (dd, *J* = 5.1, 3.7 Hz, 1H), 7.05 – 6.99 (m, 2H). ^{13}C NMR [101 MHz, $(CD_3)_2SO$] δ = 171.5, 162.5, 142.9, 137.8, 130.9, 128.5, 126.3, 124.4, 116.9, 114.5, 112.5. HRMS (TOF, ES$^-$): *m/z* calcd for $C_{11}H_7O_3S$ $(M\text{-}H^+)^-$ 219.0116, found 219.0105. HPLC (λ= 254nm): 90.7%; (λ= 214 nm): 90.4%; t_R = 15.09 min.

2-Hydroxy-5-(thien-2-yl)benzoic acid (**38**). Method A (SM). Reagents: **18a** (60 mg, 0.216 mmol), **19h** (33.14 mg, 0.259 mmol), K_2CO_3 (89.56 mg, 0.648 mmol), PPh_3 (8.40 mg, 0.032 mmol), $Pd(OAc)_2$ (2.47 mg, 0.011 mmol) and DMF/H_2O 1/1 (2 mL). Column chromatography: DCM/MeOH (20:1→9:1) followed by EtOAc/CH_3CN/MeOH/H_2O (70:2.5:1.25:1.25→70:5:2.5:2.5). Yellow solid, 63% yield (30 mg, 0.136 mmol), mp > 300 ºC. ^{1}H NMR [400 MHz, $(CD_3)_2CO$] δ = 8.19 (s, 1H), 7.79 (d, *J* = 6.5 Hz, 1H), 7.37 (s, 2H), 7.07 (s, 1H), 6.99 (d, *J* = 8.4 Hz, 1H).; ^{13}C NMR [101 MHz, $(CD_3)_2CO$] δ = 173.1, 162.2, 143.9, 133.6, 129.0, 128.3, 126.6, 125.1, 123.5, 118.7, 114.7. HRMS (TOF, ES$^-$): *m/z* calcd for $C_{11}H_7O_3S$ $(M\text{-}H^+)^-$ 219.0116, found 219.0100. HPLC (λ= 254nm): 99.0%; (λ= 214 nm): 98.7%; t_R = 14.37 min.

2-Hydroxy-4-(thien-3-yl)benzoic acid (**potassium salt**) (**39**): Method C (SM). Reagents: **18g** (50 mg, 0.189 mmol), 3-thiopheneboronic acid (**19i**) (29.0 mg, 0.227 mmoL), K_2CO_3 (91.4 mg, 0.662 mmol), PPh_3 (7.4 mg, 0.028 mmol), $Pd(OAc)_2$ (2.12 mg, 0.010 mmol) and DMF/H_2O 1/1 (2 mL). The reaction crude was not acidified. Column chromatography: EtOAc/CH_3CN/MeOH/H_2O (70:10:5:5). Brownish solid, 74% yield (36 mg, 0.139 mmol), mp > 300 ºC. ^{1}H NMR (500 MHz, CD_3OD) δ = 7.78 (dd, *J* = 8.4, 4.0 Hz, 1H), 7.61 (dd, *J* = 2.9, 1.4 Hz, 1H), 7.37 (m, 2H), 7.09-7.03 (m, 2H). ^{13}C NMR (126 MHz, CD_3OD) δ = 161.82, 141.51, 141.16, 130.82, 126.08, 125.71, 121.53, 116.41, 113.53; HRMS (TOF, ES^-): *m/z* calcd. for $C_{11}H_7O_3S$ $(M\text{-}H^+)^-$ 219.0116, found 219.0122. HPLC (λ= 280nm): 100%; t_R = 12.63 min.

2-Hydroxy-5-(thien-3-yl)benzoic acid (**40**): Method A (SM). Reagents: **18a** (70 mg, 0.252 mmol), **19i** (38.69 mg, 0.302 mmol), K_2CO_3 (104.49 mg, 0.756 mmol), PPh_3 (9.97 mg, 0.038 mmol), $Pd(OAc)_2$ (2.92 mg, 0.013 mmol) and DMF/H_2O 1/1 (2 mL). Column chromatography: DCM/MeOH (20:1→9:1) followed by EtOAc/CH_3CN/MeOH/H_2O (70:2.5:1.25:1.25→70:5:2.5:2.5). Brown solid, 72% yield (40 mg, 0.182 mmol), mp 222 °C. ^{1}H NMR [400 MHz, $(CD_3)_2CO$] δ = 11.08 (br, s, 1H), 8.18 (d, *J* = 2.4 Hz, 1H), 7.88 (dd, *J* = 8.6, 2.3 Hz, 1H), 7.71-7.64 (m, 1H), 7.55 (dd, *J* = 5.0, 2.9 Hz, 1H), 7.52-7.46 (m, 1H), 7.01 (d, *J* = 8.7 Hz, 1H). ^{13}C NMR [101 MHz, $(CD_3)_2CO$] δ = 172.6, 162.1, 141.7, 134.7, 128.4, 128.2, 127.5, 126.7, 120.4, 118.6, 113.3. HRMS (TOF, ES^-): *m/z* calcd for $C_{11}H_7O_3S$ $(M\text{-}H^+)^-$ 219.0116, found 219.0104. HPLC (λ= 254nm): 98.8%; (λ= 214 nm): 97.1%; t_R = 14.64 min.

4-(5-Acetylthien-2-yl)-2-hydroxybenzoic acid (**potassium salt**) (**41**). Method C (SM). Reagents: **18g** (50 mg, 0.189 mmol), 5-acetylthiophene-2-boronic acid (**19j**) (38.6 mg, 0.227 mmoL), K_2CO_3 (91.4 mg, 0.662 mmol), PPh_3 (7.4 mg, 0.028 mmol), $Pd(OAc)_2$ (2.12 mg, 0.0095 mmol) and DMF/H_2O 1/1 (2 mL). The reaction crude was not acidified. Column

chromatography: EtOAc/CH_3CN/MeOH/H_2O (70:5:2.5:2.5). Yellow solid, 44% yield (25 mg, 0.083 mmol), mp > 300 ºC. ^{1}H NMR (400 MHz, CD_3OD) δ = 7.79 (d, *J* = 8.6 Hz, 1H), 7.74 (d, *J* = 4.0 Hz, 1H), 7.43 (d, *J* = 4.0 Hz, 1H), 7.11-7.07 (m, 2H), 2.47 (s, 3H, CH_3). ^{13}C NMR (100 MHz, CD_3OD) δ = 191.6 (CO), 173.0 (CO), 161.8 (C), 151.7 (C), 143.2 (C), 138.0 (C), 134.3 (CH), 131.1 (CH), 125.1 (CH), 116.9 (C), 115.8 (CH), 113.3 (CH), 25.1 (CH_3). HRMS (TOF, ES^-): *m/z* calcd. for $C_{13}H_9O_4S$:$(M-H^+)^-$ 261.0222, found 261.0218. HPLC (λ= 254nm): 100%; (λ= 214 nm): 97.0%; (λ= 280 nm): 100%; t_R = 11.28 min.

2-Hydroxy-4-(5-methylthien-2-yl)benzoic acid (**potassium salt**) (**42**). Method C (SM). Reagents: **18g** (50 mg, 0.189 mmol), 5-methylthiophene-2-boronic acid pinacol ester (**19k**) (50.8 mg, 0.227 mmoL), K_2CO_3 (91.4 mg, 0.662 mmol), PPh_3 (7.4 mg, 0.028 mmol), $Pd(OAc)_2$ (2.12 mg, 0.010 mmol) and DMF/H_2O 1/1 (2 mL). The reaction crude was not acidified. Column chromatography: EtOAc/CH_3CN/MeOH/H_2O (70:5:2.5:2.5→70:10:5:5). Yellow solid, 64% yield (33 mg, 0.121 mmol), mp > 300 ºC. ^{1}H NMR (500 MHz, CD_3OD) δ = 7.72 (d, *J* = 8.1 Hz, 1H), 7.14 (d, *J* = 3.6 Hz, 1H), 7.02-6.87 (m, 2H), 6.73-6.60 (m, 1H), 2.55-2.30 (m, 3H). ^{13}C NMR (126 MHz, CD_3OD) δ = 161.8, 140.6, 140.6, 140.2, 130.8, 126.2, 124.1, 115.2, 112.1, 13.9 (CH_3). HRMS (TOF, ES^-): *m/z* calcd. for $C_{12}H_9O_3S$ $(M-H^+)^-$ 233.0272, found 233.0280. HPLC (λ= 254nm): 100%; t_R = 13.48 min.

2-Hydroxy-4-(1-methyl-1*H*-pyrazol-5-yl)benzoic acid (**potassium salt**) (**43**): Method C (SM). Reagents: **18g** (50 mg, 0.189 mmol), 1-methyl-1*H*-pyrazole-5-boronic acid pinacol ester (**19l**) (47.2 mg, 0.227 mmoL), K_2CO_3 (91.4 mg, 0.662 mmol), PPh_3 (7.4 mg, 0.028 mmol), $Pd(OAc)_2$ (2.12 mg, 0.0095 mmol) and DMF/H_2O 1/1 (2 mL). The reaction crude was not acidified. Column chromatography: EtOAc/CH_3CN/MeOH/H_2O (60:10:10:10). Crystalline solid, 27% yield (13 mg, 0.051 mmol), mp > 300 ºC. ^{1}H NMR (400 MHz, CD_3OD) δ = 7.95 (d, *J* = 8.0 Hz,

1H), 7.47 (d, *J* = 2.0 Hz, 1H), 7.03-6.84 (m, 2H), 6.37 (d, *J* = 2.0 Hz, 1H), 3.87 (s, 3H, CH_3). ^{13}C NMR (101 MHz, CD_3OD) δ = 173.5 (CO), 161.4, 143.3, 138.0 (CH), 135.3, 130.8 (CH), 118.3 (CH), 116.2 (CH), 105.8 (CH), 36.4 (CH_3). HRMS (TOF, ES^-): *m/z* calcd. for $C_{11}H_9N_2O_3$ $(M-H^+)^-$ 217.0613, found 217.0615. HPLC (λ= 254nm): 96.6%; (λ= 280 nm): 96.1%; t_R = 9.27 min.

2-Hydroxy-4-(4-pyridyl)benzoic acid (**potassium salt**) (**44**). Method C (SM). Reagents: **18g** (50 mg, 0.189 mmol), pyridin-4-ylboronic acid pinacol ester (**19m**) (47.2 mg, 0.227 mmol), K_2CO_3 (91.4 mg, 0.662 mmol), PPh_3 (7.4 mg, 0.028 mmol), $Pd(OAc)_2$ (2.12 mg, 0.0095 mmol) and DMF/H_2O 1/1 (2 mL). The reaction crude was not acidified. Column chromatography: EtOAc/CH_3CN/MeOH/H_2O (70:10:5:5→60:10:10:10). Solid, 49% yield (23.5 mg, 0.093 mmol), mp = 268 ºC. ^1H NMR (500 MHz, CD_3OD) δ = 8.64-8.51 (m, 2H), 7.97 (d, *J* = 8.0 Hz, 1H), 7.76-7.66 (m, 2H), 7.21-7.12 (m, 2H). ^{13}C NMR (101 MHz, CD_3OD) δ = 174.1 (CO), 161.8, 149.1 (CH), 149.0, 141.5, 131.2 (CH), 130.2 (CH), 121.8 (CH), 119.7, 117.5 (CH), 116.1 (CH), 114.2 (CH). HRMS (TOF, ES^-): *m/z* calcd. for $C_{12}H_8NO_3$ $(M-H^+)^-$ 214.0504, found 214.0507. HPLC (λ= 254nm): 95.3%; (λ= 280 nm): 98.0%; t_R = 1.90 min.

2-Hydroxy-4-(4-nitrophenyl)benzoic acid (**potassium salt**) (**45**): Method C (SM). Reagents: **18g** (50 mg, 0.189 mmol), 4-nitrobenzeneboronic acid (**19n**) (37.9 mg, 0.227 mmol), K_2CO_3 (91.4 mg, 0.662 mmol), PPh_3 (7.4 mg, 0.028 mmol), $Pd(OAc)_2$ (2.12 mg, 0.0095 mmol) and DMF/H_2O 1/1 (2 mL). The reaction crude was not acidified. Column chromatography: EtOAc/CH_3CN/MeOH/H_2O (70:10:5:5). Yellow solid, 60% yield (34 mg, 0.114 mmol), mp > 300 ºC. ^1H NMR (400 MHz, CD_3OD) δ = 8.31-8.12 (m, 2H), 7.90-7.82 (m, 1H), 7.81-7.73 (m, 2H), 7.09-6.99 (m, 2H). ^{13}C NMR (101 MHz, CD_3OD) δ = 174.1 (CO), 161.7 (C), 147.2 (C), 147.0 (C), 142.8 (C), 131.0 (CH), 127.6 (2CH), 123.5 (2CH), 118.9 (C), 116.5 (CH), 114.5

(CH). HRMS (TOF, ES^-): *m/z* calcd. for $C_{13}H_8NO_5$ $(M-H^+)^-$ 258.0402, found 258.0411. HPLC (λ= 254nm): 94.4%; (λ= 280 nm): 95.5%; t_R = 11.88 min.

2-Hydroxy-4-(3-methoxyphenyl)benzoic acid (potassium salt) (46): Method C (SM). Reagents: **18g** (50 mg, 0.189 mmol), 3-methoxyphenylboronic acid (**19o**) (34.5 mg, 0.227 mmoL), K_2CO_3 (91.4 mg, 0.662 mmol), PPh_3 (7.4 mg, 0.028 mmol), $Pd(OAc)_2$ (2.12 mg, 0.0095 mmol) and DMF/H_2O 1/1 (2 mL). The reaction crude was not acidified. Column chromatography: EtOAc/CH_3CN/MeOH/H_2O (70:5:2.5:2.5→60:10:10:10). Brown solid, 47% yield (25 mg, 0.089 mmol), mp 185.1 ºC. ^{1}H (500 MHz, CD_3OD) δ = 7.92 (dd, *J* = 7.9, 1.5 Hz, 1H), 7.33 (t, *J* = 7.9 Hz, 1H), 7.22-7.16 (m, 1H), 7.13 (dd, *J* = 2.5, 1.7 Hz, 1H), 7.09 (d, *J* = 8.0 Hz, 2H), 6.92 (ddd, *J* = 8.3, 2.5, 0.9 Hz, 1H), 3.83 (s, 3H, OCH_3). ^{13}C NMR (126 MHz, CD_3OD) δ = 174.8 (CO), 163.0 (C), 161.5 (C), 148.3 (C), 142.8 (C), 132.1 (CH), 130.9 (CH), 120.4 (CH), 118.5 (CH), 115.8 (CH), 115.7 (C), 114.5 (CH), 113.7 (CH), 55.7 (CH_3). HRMS (TOF, ES^-): *m/z* calcd. for $C_{14}H_{11}O_4$ $(M-H^+)^-$ 243.0657, found 243.0659. HPLC (λ= 254nm): 100%; (λ= 214 nm): 100%; (λ= 280 nm): 100%; t_R = 12.64 min.

2-Hydroxy-4-(4-hydroxyphenyl)benzoic acid (potassium salt) (47): Method C (SM). Reagents: **18g** (50 mg, 0.189 mmol), (4-hydroxyphenyl) boronic acid (**19p**) (31.3 mg, 0.227 mmol), K_2CO_3 (91.4 mg, 0.662 mmol), PPh_3 (7.4 mg, 0.028 mmol), $Pd(AcO)_2$ (2.12 mg, 0.010 mmol) and DMF/H_2O 1/1 (2 mL). The reaction crude was not acidified. Column chromatography: EtOAc/CH_3CN/MeOH/H_2O (70:5:2.5:2.5→60:10:10:10). Solid, quantitative yield (44 mg, 0.191 mmol), mp 266 ºC. ^{1}H NMR (300 MHz, CD_3OD) δ = 7.77 (d, *J* = 8.6 Hz, 1H), 7.42-7.35 (m, 2H), 6.99-6.94 (m, 2H), 6.81-6.74 (m, 2H). ^{13}C NMR (101 MHz, CD_3OD) δ = 174.5 (CO), 163.0 (C), 158.9 (C), 148.6 (C), 133.0 (C), 131.9 (CH), 129.2 (2CH), 118.0 (CH),

116.6 (2CH), 114.8 (CH), 113.8 (C). HRMS (TOF, ES^-): *m/z* calcd. for $C_{13}H_9O_4$ $(M\text{-}H^+)^-$ 229.0501, found 229.0510.

4-(4-Benzyloxyphenyl)-2-hydroxybenzoic acid (**48**): Method C (SM). Reagents: **18g** (50 mg, 0.189 mmol), 4-(benzyloxy)phenyl boronic acid (**19q**) (51.8 mg, 0.227 mmol), K_2CO_3 (91.4 mg, 0.662 mmol), PPh_3 (7.4 mg, 0.028 mmol), $Pd(AcO)_2$ (2.12 mg, 0.0095 mmol) and DMF/H_2O 1/1 (2 mL). The reaction crude was not acidified. Column chromatography: EtOAc/CH_3CN/MeOH/H_2O (60:10:10:10). White solid (potassium salt), 92% yield (62 mg, 0.173 mmol), mp > 300 ºC. ^{1}H NMR (400 MHz, CD_3OD) δ = 7.76 (d, *J* = 8.6 Hz, 1H), 7.49-7.43 (m, 2H), 7.38-7.32 (m, 2H), 7.31-7.24 (m, 2H), 7.24-7.18 (m, 1H), 6.99-6.94 (m, 2H), 6.94-6.89 (m, 2H), 5.03 (s, 2H). ^{13}C NMR (101 MHz, CD_3OD) δ = 174.5 (CO), 161.4 (C), 158.7 (C), 145.3 (C), 137.2 (C), 133.1 (C), 130.6 (CH), 129.6 (CH), 128.1 (CH), 127.7 (CH), 127.7 (CH), 127.4 (CH), 127.1 (CH), 116.6 (CH), 116.0 (CH), 114.8 (CH), 114.8 (CH), 113.4 (CH), 110.0 (C), 69.6 (CH_2). HRMS (TOF, ES^-): *m/z* calcd. for $C_{20}H_{15}O_4$ $(M\text{-}H^+)^-$ 319.0970, found 319.0964. The white solid (20 mg, 0.056 mmol) was dissolved in acetone (10 mL) and the solution was acidified with HCl 10% (pH 1-2). The acetone was then evaporated under vacuum and the residue was taken in a small volume of water, transferred to an Eppendorf and centrifuged (5 min x 13000 rpm). The supernatant was discarded. This procedure was repeated three times. The final white solid (10 mg, 0.097 mmol) was characterised and subjected to biological assay. ^{1}H NMR [400 MHz, $(CD_3)_2CO$] δ = 7.93 (d, *J* = 8.3 Hz, 1H), 7.73-7.67 (m, 2H), 7.51 (d, *J* = 7.3 Hz, 2H), 7.45-7.38 (m, 2H), 7.37-7.31 (m, 1H), 7.23 (dd, *J* = 8.3, 1.8 Hz, 1H), 7.19 (d, *J* = 1.6 Hz, 1H), 7.17-7.12 (m, 2H), 5.21 (s, 2H). ^{13}C NMR [101 MHz, $(CD_3)_2CO$] δ = 172.5 (CO), 163.3 (C), 160.4 (C), 149.0 (C), 138.2 (C), 132.7 (C), 131.8(CH), 129.3 (CH), 129.2 (CH), 128.7 (CH), 128.5 (CH), 118.3 (CH), 116.2 (CH), 115.2 (CH), 111.4 (C), 70.6 (CH_2). HRMS (TOF, ES^-): *m/z*

calcd. for $C_{20}H_{15}O_4$ $(M\text{-}H^+)^-$ 319.0970, found 319.0964. HPLC: (λ= 254nm): 100%; (λ= 214 nm): 100 %; t_R= 15.26 min.

2-Hydroxy-4-[4-(4-methoxyphenylmethoxy)phenyl]benzoic acid (**potassium salt**) (**49**). Method C (SM). Reagents: **18g** (50 mg, 0.189 mmol), 4-(4-methoxyphenylmethoxy)phenylboronic acid (**19r**) (58.6 mg, 0.227 mmol), K_2CO_3 (91.4 mg, 0.662 mmol), PPh_3 (7.4 mg, 0.028 mmol), $Pd(AcO)_2$ (2.12 mg, 0.010 mmol) and DMF/H_2O 1/1 (2 mL). The reaction crude was not acidified. Column chromatography: EtOAc/CH_3CN/MeOH/H_2O (70:5:2.5:2.5→60:10:10:10). Solid, 15% yield (11 mg, 0.028 mmol), mp 200 ºC. ^{1}H NMR (300 MHz, CD_3OD) δ = 7.81-7.71 (m, 1H), 7.50-7.42 (m, 2H), 7.28 (d, *J* = 8.5 Hz, 2H), 6.99-6.88 (m, 4H), 6.88-6.80 (m, 2H), 4.95 (s, 2H, CH_2), 3.70 (s, 3H, CH_3). ^{13}C NMR (151 MHz, CD_3OD) δ = 131.8, 130.3, 129.4, 117.6, 116.3, 114.9, 114.8, 70.8 (CH_2), 55.7 (CH_3). HRMS (TOF, ES^-): *m/z* calcd. for $C_{21}H_{17}O_5$ $(M\text{-}H^+)^-$ 349.1076, found 349.1071. HPLC: (λ= 214 nm): 95.0%; t_R= 14.16 min.

5-(4-Benzyloxyphenyl)-2-hydroxybenzoic acid (**50**): Method A (SM). Reagents: **18a** (50 mg, 0.18 mmol), **19q** (50 mg, 1.2 mmol), K_2CO_3 (104 mg, 0.76 mmol), PPh_3 (7.45 mg, 0.03 mmol), $Pd(AcO)_2$ (2.1 mg, 0.01 mmol) and DMF/H_2O 1/1 (2 mL). Column chromatography: DCM/MeOH (10:0.25→9:1). White solid, 80% (46 mg, 0.144 mmol). ^{1}H-NMR [400 MHz, $(CD_3)_2SO$] δ = 7.97 (bs, 1H), 7.67-7.60 (m, 1H), 7.55-7.30 (m, 7H), 7.06 (d, *J* = 8.5 Hz, 2H), 6.90 (d, *J* = 8.5 Hz, 1H), 5.13 (s, 2H). ^{13}C NMR [101 MHz, $(CD_3)_2SO$] δ = 171.8 (CO), 160.8 (C), 157.4 (C), 137.1 (C), 132.4 (C), 131.8 (CH), 129.8 (C), 128.4 (CH), 127.8 (CH), 127.6 (CH), 127.5 (CH), 127.1 (CH), 117.1 (CH), 116.2 (C), 115.2 (CH), 69.2 (CH_2). HRMS (TOF, ES^-): *m/z* calcd. for $C_{20}H_{15}O_4$ $(M\text{-}H^+)^-$ 319.0976, found 319.0959. HPLC: (λ= 254nm): 100%; (λ= 214 nm): 100 %; t_R= 11.44 min.

2-Hydroxy-5-[4-(4-methoxyphenylmethoxy)phenyl]benzoic acid (**51**). Method C (SM). Reagents: **18a** (50 mg, 0.189 mmol), **19r** (44.9 mg, 0.216 mmol), K_2CO_3 (87.1 mg, 0.63 mmol), PPh_3 (7.1 mg, 0.027 mmol), $Pd(AcO)_2$ (2.02 mg, 0.009 mmol) and DMF/H_2O 1/1 (2 mL). The reaction crude was not acidified. Column chromatography: EtOAc/CH_3CN/MeOH/H_2O (70:10:5:5→60:10:10:10). Yellow solid (potassium salt), 17% yield (12.8 mg, 0.033 mmol), mp 177.8 ºC. ^{1}H NMR (400 MHz, CD_3OD) δ = 7.96 (s, 1H), 7.53(m, 1H), 7.38 (m, 2H), 7.27 (m, 2H), 6.93 (m, 2H), 6.83 (m, 3H), 4.93 (s, 2H, CH_2), 3.70 (s, 3H, CH_3). HRMS (TOF, ES^-): *m/z* calcd. for $C_{21}H_{17}O_5$ $(M\text{-}H^+)^-$ 349,1076, found 349,1084. The yellow solid (13 mg, 0.033 mmol) was disolved in acetone (10 mL) and the solution was acidified with HCl 10% (pH 1-2). The acetone was then evaporated under vacuum and the residue was taken in a small volume of water, transferred to an Eppendorf and centrifuged (5 min x 13000 rpm). The supernatant was discarded. This procedure was repeated three times. The final solid (10 mg, 0.029 mmol) was characterised and subjected to biological assay. ^{1}H NMR [400 MHz, $(CD_3)_2CO$] δ 8.10 (d, *J* = 2.3 Hz, 1H), 7.80 (dd, *J* = 8.7, 2.5 Hz, 1H), 7.59-7.54 (m, 2H), 7.45-7.40 (m, 2H), 7.12-7.07 (m, 2H), 7.03 (d, *J* = 8.6 Hz, 1H), 6.98-6.94 (m, 2H), 5.09 (s, 2H), 3.81 (s, 3H). ^{13}C NMR [101 MHz, $(CD_3)_2CO$] δ 192.3, 179.9, 172.6, 159.3, 134.9, 133.17, 132.8, 130.1, 128.6, 128.3, 118.6, 116.2, 116.0, 114.6, 113.3, 70.3, 55.6.

4-[2-(3,5-Difluorophenoxymethyl)phenyl]-2-hydroxybenzoic acid (**52**). Method A (SM). Reagents: **18g** (50 mg, 0.19 mmol), 2-(3,5-difluorophenoxymethyl)benzene boronic acid (**19s**) (60 mg, 1.2 mmol), K_2CO_3 (104 mg, 0.76 mmol), PPh_3 (7.45 mg, 0.03 mmol), $Pd(AcO)_2$ (2.1 mg, 0.01 mmol) and DMF/H_2O 1/1 (2 mL). Column chromatography: EtOAc/MeOH (10:1→9:1). White solid, 65% yield (44 mg, 0.123 mmol). ^{1}H NMR [500 MHz, $(CD_3)_2SO$] δ = 7.77 (d, *J* = 3.4 Hz, 1H), 7.57 (dd, *J* = 7.5, 1.6 Hz, 1H), 7.46-7.38 (m, 3H), 7.32 (dd, *J* = 7.6, 1.5 Hz, 1H),

6.86 (d, J = 8.4 Hz, 1H), 6.75 (tt, *J* = 9.4, 2.3 Hz, 1H), 6.70-6.65 (m, 2H), 4.93 (s, 2H). ^{13}C NMR [101 MHz, $(CD_3)_2CO$] δ = 175.2 (CO), 164.5 (dd, $J_{C\text{-}F}$ = 244.6, 16 Hz, 2C-F), 162.1 (C), 161.7 (t, $J_{C\text{-}F}$ = 13.9 Hz, C), 146.6 (C), 142.5 (C), 134.1(C), 132.4 (CH), 130.6 (CH), 130.3 (CH), 129.2 (CH), 128.7 (CH), 120.0 (CH), 117.9 (CH), 117.3 (C), 99.6 (dd, $J_{C\text{-}F}$ = 20.5, 7.9 Hz, 2-CH), 96.8 (t, $J_{C\text{-}F}$ = 26.3 Hz, CH), 69.5 (CH_2). ^{19}F NMR [376 MHz, $(CD_3)_2SO$] δ = -109.35 (m, 2F). HRMS (TOF, ES$^-$): *m/z* calcd. for $C_{20}H_{13}0_4F_2$ $(M\text{-}H^+)^-$ 355.0782, found 355.0796. HPLC: (λ= 254nm): 100%; (λ= 214 nm): 100 %; t_R= 12.19 min.

5-[2-(3,5-Difluorophenoxymethyl)phenyl]-2-hydroxybenzoic acid (**53**). Method A (SM). Reagents: **18a** (50 mg, 0.19 mmol), **19s** (57 mg, 0.21 mmol), K_2CO_3 (99 mg, 0.72 mmol), PPh_3 (7.10 mg, 0.27 mmol), $Pd(AcO)_2$ (0.2 mg, 0.01 mmol) and DMF/H_2O 1/1 (2 mL). Column chromatography: DCM/MeOH (10:1→9:1). White solid, 62% yield (40 mg, 0.112 mmol). ^{1}H NMR [500 MHz, $(CD_3)_2SO$] δ = 7.70 (d, *J* = 7.8 Hz, 1H), 7.56 (dd, *J* = 7.0, 3.0 Hz, 1H), 7.46-7.39 (m, 2H), 7.33 (m, 1H), 6.75 (tt, *J* = 9.4, 2.3 Hz, 1H), 6.70-6.64 (m, 4H), 4.97 (s, 2H). ^{13}C NMR [101 MHz, $(CD_3)_2CO$] δ = 183.1 (CO), 164.5 (dd, $J_{C\text{-}F}$ = 244.5, 16 Hz, 2C-F), 162.1 (C), 161.7 (t, $J_{C\text{-}F}$ = 13.8 Hz, C), 142.4 (C), 141.4 (C), 136.9 (C), 134.3 (C), 131.8 (CH), 131.1 (CH), 129.5 (CH), 128.4 (CH), 117.8 (CH), 99.5 (dd, $J_{C\text{-}F}$ = 20.3, 8.0 Hz, 2-CH), 96.8 (t, $J_{C\text{-}F}$ = 26.3 Hz, CH), 69.8 (CH_2). ^{19}F NMR [376 MHz, $(CD_3)_2SO$] δ = -109.29 (m, 2F). HRMS (TOF, ES$^-$): *m/z* calcd. for $C_{20}H_{13}0_4F_2$ $(M\text{-}H^+)^-$ 355.0782, found 355.0796. HPLC: (λ= 254nm): 100%; t_R= 12.12 min.

2-Hydroxy-4-[2-(3-trifluoromethylphenoxymethyl)phenyl]benzoic acid (**54**). Method C (SM). Reagents: **18g** (50 mg, 0.189 mmol), 2-[3-(trifluoromethyl)phenoxymethyl]benzeneboronic acid (**19t**) (67.2 mg, 0.227 mmoL), K_2CO_3 (91.4 mg, 0.662 mmol), PPh_3 (7.4 mg, 0.028 mmol), $Pd(AcO)_2$ (2.12 mg, 0.0095 mmol) and

DMF/H_2O 1/1 (2 mL). The reaction crude was not acidified. Column chromatography: EtOAc/CH_3CN/MeOH/H_2O (70:2.5:2.5:1.25→70:10:5:5). Solid (potassium salt), 72% yield (58 mg, 0.136 mmol), mp 83.8 ºC. ^{1}H NMR (300 MHz, CD_3OD) δ = 7.87 (d, *J* = 8.0 Hz, 1H), 7.57-7.53 (m, 1H), 7.41-7.33 (m, 3H), 7.29 (m, 1H), 7.16 (bd, *J* = 7.4 Hz, 1H), 7.06-7.02 (m, 2H), 6.87 (bd, *J* = 1.6 Hz, 1H), 6.83 (dd, *J* = 7.9, 1.7 Hz, 1H), 4.99 (s, 2H). ^{13}C NMR (101 MHz, CD_3OD) δ = 174.8 (CO), 162.5 (C), 160.1 (C), 147.9 (C), 142.8 (C), 134.7 (C), 132.6 (c, J_{C-F} = 32.1 Hz, C), 131.6 (CH), 131.3 (CH), 130.68 (m, CH), 130.65 (CH), 129.5 (CH), 129.1 (CH), 125.4 (c, J_{C-F} = 271.6 Hz, CF_3), 120.6 (CH), 119.42 (CH), 119.4 (m, CH), 118.4 (c, J_{C-F} = 3.9 Hz, CH), 118.3 (CH), 116.1 (C), 112.8 (c, J_{C-F} = 3.9 Hz, CH), 69.5 (CH_2). HRMS (TOF, ES$^-$): *m/z* calcd. for $C_{21}H_{14}O_4F_3$ (M-H$^+$)$^-$ 387.0844, found 387.0845. HPLC: (λ= 254nm): 99.8%; (λ= 214 nm): 98.8 %; t_R= 13.97 min. The solid (25 mg, 0.059 mmol) was disolved in acetone (10 mL) and the solution was acidified with HCl 10% (pH 1-2). The acetone was then evaporated under vacuum and the residue was taken in a small volume of water, transferred to an Eppendorf and centrifuged (5 min x 13000 rpm). The supernatant was discarded. This procedure was repeated three times. The final syrup (22 mg, 0.057 mmol) was characterised and subjected to biological assay. ^{1}H NMR [400 MHz, $(CD_3)_2CO$] δ = 7.91 (d, *J* = 8.5 Hz, 1H), 7.68 (m, 1H), 7.51-7.45 (m, 3H), 7.39 (m, 1H), 7.25 (d, *J* = 8.0 Hz, 1H), 7.22–7.18 (m, 2H), 7.03-7.00 (m, 2H), 5.14 (s, 2H). ^{13}C NMR [101 MHz, $(CD_3)_2CO$] δ = 172.3 (CO), 162.6 (C), 159.8 (C), 149.3 (C), 141.9 (C), 134.5 (C), 132.1 (c, J_{C-F} = 32.0 Hz, C), 131.3 (CH), 131.2 (CH), 130.8 (CH), 130.5 (CH), 129.4 (CH), 129.2 (CH), 125.1 (c, J_{C-F} = 271.6 Hz, CF_3), 121.1 (CH), 119.6 (m, CH), 118.5 (CH), 118.3 (c, J_{C-F} = 3.9 Hz, CH), 112.4 (c, J_{C-F} = 3.9 Hz, CH), 112.1 (C), 69.2 (CH_2). HRMS (TOF, ES$^-$): *m/z* calcd. for $C_{21}H_{14}O_4F_3$ (M-H$^+$)$^-$ 387.0844, found 387.0845. HPLC: (λ= 254nm): 100%; (λ= 214 nm): 100%; t_R= 16.89 min.

2-Hydroxy-5-[2-(3-trifluoromethylphenoxymethyl)phenyl]benzoic acid (**55**). Method C (SM). Reagents: **18a** (50 mg, 0.189 mmol), **19t** (63.9 mg, 0.216 mmol), K_2CO_3 (87.1 mg, 0.63 mmol), PPh_3 (7.1 mg, 0.027 mmol), $Pd(AcO)_2$ (2.02 mg, 0.009 mmol) and DMF/H_2O 1/1 (2 mL). The reaction crude was not acidified. Column chromatography: EtOAc/CH_3CN/MeOH/H_2O (70:5:2.5:2.5→60:10:10:10). Solid (potassium salt), 73% (59 mg, 0.138 mmol), mp 154.8 ºC. ^{1}H NMR (300 MHz, CD_3OD) δ = 7.89 (d, *J* = 2.3 Hz, 1H), 7.56 (bd, *J* = 7.3 Hz, 1H), 7.48 (m, 1H), 7.43-7.35 (m, 3H), 7.31 (m, 1H), 7.18 (bd, *J* = 7.7 Hz, 1H), 7.10-7.05 (m, 2H), 6.94 (bd, *J* = 8.5 Hz, 1H), 4.97 (s, 2H). ^{13}C NMR (101 MHz, CD_3OD) δ = 173.3 (CO), 162.5 (C), 160.1 (C), 142.7(C), 137.3 (CH), 135.0 (C), 132.7 (c, J_{C-F} = 32.1 Hz, C), 132.6 (C), 132.0 (CH), 131.3 (CH), 131.2 (2 CH), 129.7 (CH), 128.7 (CH), 125.4 (c, J_{C-F} = 271.6 Hz, CF_3), 119.5 (CH), 118.4 (c, J_{C-F} = 4.0 Hz, CH), 118.1 (m, CH), 113.7 (C), 112.7 (c, J_{C-F} = 4.0 Hz, CH), 69.8 (CH_2). HRMS (TOF, ES^-): *m/z* calcd. for $C_{21}H_{14}O_4F_3$ $(M\text{-}H^+)^-$ 387.0844, found 387.0843. The solid (50 mg, 0.059 mmol) was disolved in acetone (10 mL) and the solution was acidified with HCl 10% (pH 1-2). The acetone was then evaporated under vacuum and the residue was taken in a small volume of water, transferred to an Eppendorf and centrifuged (5 min x 13000 rpm). The supernatant was discarded. This procedure was repeated three times. The final solid (16 mg, 0.057 mmol) (mp 158.0 ºC) was characterised and subjected to biological assay. ^{1}H NMR [400 MHz, $(CD_3)_2CO$] δ = 11.14 (s, 1H), 7.98 (d, *J* = 2.4 Hz, 1H), 7.67 (dd, *J* = 7.1, 1.8 Hz, 1H), 7.61 (dd, *J* = 8.5, 2.3 Hz, 1H), 7.50-7.42 (m, 3H), 7.38 (dd, *J* = 7.1, 1.9 Hz, 1H), 7.25 (d, *J* = 7.6 Hz, 1H), 7.20 (d, *J* = 6.5 Hz, 2H), 7.00 (d, *J* = 8.5 Hz, 1H), 5.09 (s, 2H). ^{13}C NMR [101 MHz, $(CD_3)_2CO$] δ = 172.5 (CO), 162.3 (C), 159.7 (C), 142.1 (C), 137.5 (CH), 134.7 (C), 132.2 (C), 132.0 (c, J_{C-F} = 32.1 Hz, C), 131.7 (CH), 131.3 (CH), 131.1 (CH), 131.0 (CH), 129.5 (CH), 128.5 (CH), 125.1 (c, J_{C-F} = 271.6 Hz, CF_3), 119.6 (CH), 118.2 (c, J_{C-F} = 4.0 Hz,

CH), 118.1 (CH), 112.9 (C), 112.4 (c, J_{C-F} = 3.9 Hz, CH), 69.4 (CH_2). HPLC: (λ= 254nm): 100%; (λ= 214 nm): 95.7%; t_R= 16.82 min.

Metabolic profiling and metabolic stability of compounds 26 and 27. Stocks solutions of **26** and **27** were prepared in DMSO at 25 mM. The final concentration in the assay was 2 µM. A stock solution of 2.66 mM NADPH was prepared by dissolving the appropriate amount of NADPH in 100 mM potassium phosphate buffer. The reaction was initiated by adding a mouse liver microsomes solution (1 mg/mL) to an equal volume of buffer solution containing test compound and cofactor at the proper concentrations. Reactions without NADPH were also incubated to rule out non NADPH metabolism or chemical instability in the incubation buffer. One positive control compound (Verapamil) was included to monitor incubation course. All reactions were terminated using 60 µL of ice cold acetonitrile at 0, 5, 15, 30, 45, and 60 min. The plates were centrifuged at 3700 rpm for 15 minutes. All experiments were conducted in triplicates. Samples were analyzed by LC-HRMS, ionization by electrospray in negative mode (Agilent 1290 Infinity UHPLC; AB Sciex Triple TOF 5600 Mass Spectrometer) (metabolite chromatograms for **26** and **27** in Figures S5 and S6). Compound incubations without NADPH and compound reference standard were used as interference control for each incubation sample.

LC-HRMS Method:

Ionization mode: Electrospray Negative; Acquisition mode: TOF MS with IDA MS/MS; Column: Atlantis T3 C18, 2.1 X 15 mm, 3 µm; Mobile phase: Water: Acetonitrile: 0.1% Formic Acid; Flow rate: 0.3 mL/min; Source Temperature: 500 ºC; Column Temperature: 30ºC; Injection Volume: 5 µL; Run time: 20 min.

Metabolic profiling: Metabolites elucidation was made after accurate mass MS and MS/MS data in a single injection and analysis using Metabolite Pilot V 1.5 Software, at each time point.

Metabolic stability of **26** and **27**: Samples were monitored for parent compound disappearance by LC-HRMS (method above) according to a previously verified quantification method for **26** and **27**. The peak area of analyte was used to calculate the percentage of remaining compound at each incubation time (Tables S8 and S9). Positive control (Verapamil) showed a half life value according to the validation and published results. Compound **27** displayed a half-life of 61.9 min and **26** of 13.3 min. Consequently, the predicted intrinsic clearance calculated for this compound are 40.3 µL/min/mg protein and 187.5 µL/min/mg protein respectively (equations in Figure S7).

Mouse glycolate oxidase enzymatic assays. Mouse glycolate oxidase was purified by affinity chromatography as described previously from transformed *E.coli* bacteria carrying pET15b vector recombinant with *Hao1* cDNA.[11] Protein concentration was measured by bicinchoninic acid assay (Sigma Aldrich). Enzymatic activity of purified mGO was determined in the presence of glycolate as substrate in 50 mM potassium phosphate buffer pH 7. The addition of sulfonated-dichloroindophenol (DCIP) and 4-aminoantipyrine (Sigma Aldrich) in a coupled horseradish peroxidase (HRP) reaction using the hydrogen peroxide produced in the GO reaction, yields a dye that is measured at 515 nm.[17] IC_{50} values were calculated using 10 µL of mGO at 0.1 µg/µl with increasing concentrations of compounds between 0.2 µM and 0.2 mM in saturated conditions of substrate (22.2 mM). To determine the type of inhibition of **26** with glycolate oxidase and to calculate the corresponding K_i, increasing concentrations of the inhibitor at different concentrations of substrate with a constant enzyme concentration were plotted in a Cornish-Bowden plot and Dixon plot, in which K_i was calculated as the intersection of all lines.

Hepatocytes isolation and culture. Hepatocytes were isolated by *in situ* collagenase perfusion method7[v] from male C57BL/6 *Agxt1*$^{-/-}$ mice liver. Culture of primary hepatocytes was performed as described previously.[11] Briefly, $3.0x10^5$ cells/well were cultured in 6-well plates with Williams E medium supplemented with 5% fetal bovine serum, 2 mM L-glutamine, 100 U/mL penicillin, 100 µg/mL streptomycin, 2.2 mUI/mL insulin and 0.3 µg/mL hydrocortisone. After 5 h, medium was changed to Williams E complete medium (Biochrom, Cambridge, UK) without serum and cells were treated with compounds in the presence of 5 mM glycolate. Culture medium was harvested at 24 h after treatment for oxalate quantification on secondary assays, and also at 48 and 72 h for full dose-response curves.

Cell viability and cytotoxicity. $1.0x10^4$ cells/well were seeded in 96-well plates and treated with the same concentrations of compounds as in 6-well plates. At each time point, 20 µl of Cell Titer 96® Aqueous One Solution Reagent (Promega, Madison, WI) was added to the medium, incubated 2 h at 37°C 5% CO_2 and measured at 493 nm.

Oxalate determination. Determination of oxalate excreted to the medium was measured by the oxalate oxidase assay using a commercial kit (Trinity Biotech, Co Wicklow, Ireland), following manufacturer's instructions. The method involves oxidation of oxalate (1 equiv) by oxalate oxidase with formation of H_2O_2 (1 equiv) and subsequent utilization of the generated H_2O_2 for the formation of a dye (absorbance at 595 nm) in a HRP catalyzed reaction with the substrates 3-methyl-2-benzothiazolinone hydrazone (MBTH) and 3-(dimethylamino) benzoic acid (DMAB).

Assay interference test. Those compounds presenting the best activities in the mGO enzymatic assay and oxalate determination assay were tested for possible interference in the biological assays.

Test for colorimetric interferences: Compounds **21**, **26** and **27** (0.1 mg) were dissolved in a water/acetonitrile 80/20 mixture (1 mL), filtered and transferred into separate HPLC vials. The resulting solutions were injected in HPLC and analyzed for absorbance at 515 and 590 nm (see General Experimental Methods for HPLC set up). Compounds **54** and **55** (0.1 mg) were dissolved in a water/acetonitrile 60/40 mixture (1 mL), filtered and transferred into separate HPLC vials. The resulting solutions were injected in HPLC and analyzed for absorbance at 515 and 590 nm (see General Experimental Methods for HPLC set up). No absorbance could be observed for any of the tested compounds.

Test for interferences by HRP inhibition:

a) Detection of interferences in mGO-inhibition test: A standard curve (R^2 = 0.9999) was built using 0, 5, 10, 15, 20 and 30 µL of a solution of H_2O_2 (1:10 000) and measuring absorbance at 515 nm after 1 min in the presence of HRP, sulfonated-DCIP and 4-aminoantipyrine, using the same conditions as for mGO enzymatic assay. For the construction of the standard curve, the process was carried out in duplicate. The interference detection assay was performed by measuring HRP reaction in the absence of mGO and glycolate, using 10 µL of H_2O_2 (1:10 000) as subtrate and 5 µL of a stock solution (1 mM) of the tested compound (**21**, **26**, **27**, **53**, **54** and **55**) in DMSO (final concentration of the tested compound = 22.2 µM). Absorbance was measured at 515 nm after 1 min. The process was carried out in duplicate. Diminution of the standard absorbance, indicating HRP inhibition, was only observed for compound **27**, for which an inhibition value of 12.61 % at 20 µM was determined (Table S4).

b) Detection of interferences in the oxalate determination test: The most active compounds decreasing oxalate production (**21**, **26** and **27**) were subjected to determination of interferences with the commercial kit. A standard absorbance *vs.* oxalate curve was built using the commercial kit for oxalate determination and growing amounts of oxalate (0, 0.5, 1, 2, 4 and 5 nmol). The same culture medium used in the cellular assay was used here as a solvent. The average absorbance was calculated from triplicate experiments. The interference detection assay was performed by construction of an absorbance *vs.* oxalate curve for each tested compounds at 10 μM in the cell-culture medium. Deviations from the standard curve were only observed for compound **27**, agreeing with the HRP inhibition capacity found for this compound in the former experiment (paragraph above) (Table S5).

c) Calculation of EC_{50} against oxalate detection commercial kit for compound **27**: A value of EC_{50} was calculated for compound **27** against the mixture of enzymes contained in the commercial kit for oxalate determination (oxalate oxidase and HRP), with 5 nmol of the substrate oxalate, the highest point on the standard curve, dissolved in culture media. The standard curve was built using the commercial kit, by measuring absorbance at 595 nm in the presence of 0, 0.5, 1, 2, 4, 5 nmol oxalate and in the absence of **27** ($R^2 = 0.9948$). The EC_{50} value was calculated by measuring absorbance in mixtures containing different concentrations of **27** (0, 1, 2.5, 5, 7.5, 10, 20 and 40 μM), 5 nmol oxalate in culture media and the components of the commercial kit. EC_{50} for **27** was determined to be 18 μM (Table S4).

***In silico* studies**. Interactions of GO with the compounds were analyzed by computational docking using Maestro software (Schrödinger). Crystallographic structure of human GO (hGO) was obtained from Protein Data Bank (PDB ID: 2RDT). Protein structure was energetically minimized using OPSL3 force field and a maximum RMSD of 0.3 Å from crystallographic

positions was selected. Grid generation for ligand binding was established around the volume where CDST was co-crystallized with hGO; exclusion volumes were not established and rotation of hydroxyl and thiol groups of serine, threonine, tyrosine and cysteine was blocked. Ligand structures were drawn in HyperChem (Hypercube Inc.) software and their energy was minimized using OPSL3 force field. Molecules geometry was optimized using the Polak-Ribiere conjugated gradient algorithm, with an atomic gradient convergence of RMS < 0.01 kcal/Å mol. The energy of the interaction was defined by the equation $\Delta G_{bind} = \Delta G_{electrostatic} + \Delta G_{vdW} \sim \alpha\Delta G_{electrostatic} + \beta\Delta G_{vdW.}$ β scaling factor of non-polar interactions was set on 0.8, with a partial charge limit of 0.15. Standard precision method was configured for docking calculations, allowing total flexibility of the ligands. Non-planar conformations of amides were penalized, as well as low probability tautomers. Their docking score values were penalized using Epik algorithm. Post-docking energy minimization was also performed. 2D diagrams were obtained from Maestro software (Schrödinger). 3D illustrations of hGO and ligands were performed using Pymol software, and polar interactions were analyzed.

Statistical analysis. Descriptive data are expressed as mean ± SD and plotted in GraphPad Prism 5 software. Non-linear regression analysis was used for dose-response curve fitting of logarithm of inhibitor concentration *vs.* normalized enzymatic activity to calculate IC_{50} values, generating also the proper curve. One-way ANOVA test was used for comparison between independent groups. Tukey's range test was chosen as *post-hoc* analysis. All data were analyzed using SPSS v.19 statistical package. A *p-value* <0.05 was considered significant.

ASSOCIATED CONTENT

Supporting Information. The following files are available free of charge.

Complementary experimental data

Full biological data and interference tests

Docking information (2D-diagrams). Atomic coordinates for hGO (.pdb)

Interaction tables for all the tested compounds

NMR Spectra

Molecular Formula Strings

Corresponding Author Information:

* For M.D.G.: E-mail: monicadg@ugr.es. Phone: (+34) 958240726.

For E.S.: E-mail: esalido@ull.es. Phone: (+34) 922 679 731

Current addresses:

[#]Instituto Universitario de Bio-Orgánica "Antonio González" (IUBO-AG), C/ Astrofísico Francisco Sánchez 2, Universidad de La Laguna, 38200 La Laguna, Tenerife, Spain.

[§]Instituto de Parasitología y Biomedicina "López-Neyra". Parque Tecnológico de Ciencias de la Salud, Avenida del Conocimiento 17. 18016 Armilla, Granada. Spain.

Author Contributions:

[¥]These authors contributed equally.

Notes:

All authors have given approval to the final version of the manuscript.

The authors declare no competing financial interest.

Authorization number for animal studies: CEIBA2015-0163.

Funding Sources:

This research was supported by the Oxalosis and Hyperoxaluria Foundation (OHF) (OHF Research Grant Program 2013, IP M.D.G.). Authors E.S. (research project SAF2015-69796) and C.M.H. (Predoctoral FPI Fellowship BES-2012-052719) received funding from the Spanish Ministry of Economy. Authors M.D.M.G. (Predoctoral FPU Fellowship) and M.D.G. (Research Grant PP2016-PIP05) received funding from the University of Granada.

Acknowledgment:

We would like to acknowledge the Oxalosis and Hyperoxaluria Foundation (OHF) for supporting this investigation through a Research Grant to our team. We thank the Spanish Ministry of Economy for a predoctoral FPI fellowship to C.M.H. (BES-2012-052719) and a research project to E.S. (SAF2015-69796), and the University of Granada for a predoctoral FPU fellowship to M.D.M.G and a research grant to M.D.G. (PP2016-PIP05).

ABBREVIATIONS USED:

ADME, Absortion-distribution-metabolism-excretion; AGT, alanine-glyoxylate aminotransferase; Bn, benzyl; CCPST, 4-carboxy-5-[(4-chlorophenyl)sulfanyl]-1,2,3-thiadiazole; CDST, 4-carboxy-5-dodecylsulfanyl-1,2,3-triazole; DMAB, 3-(dimethylamino)benzoic acid; GO, glycolate oxidase; GOi, glycolate oxidase inhibitor; hGO, human glycolate oxidase; mGO,

mouse glycolate oxidase; sGO, spinach glycolate oxidase; HRP, horse radish peroxidase; Hy, hydrophobic interaction; HYPDH, hydroxiproline dehydrogenase; LDH, lactate dehydrogenase; MBTH, 3-methyl-2-benzothiazolinone hydrazine; Me, methyl; PH1, primary hyperoxaluria type 1; SM, Suzuki-Miyaura cross-coupling; SRT, substrate reduction therapy.

REFERENCES

[1] Zhang, X.; Roe, S.M.; Hou, Y.; Bartlam, M.; Rao, Z.; Pearl, L.H.; Danpure, C.J. Crystal Structure of Alanine:Glyoxylate Aminotransferase and the Relationship Between Genotype and Enzymatic Phenotype in Primary Hyperoxaluria Type 1. *J. Mol. Biol.* **2003**, *331*, 643-652.

[2] Monico, C. G.; Rossetti, S.; Olson, J. B.; Milliner, D. S. Pyridoxine Effect in Type I Primary Hyperoxaluria Is Associated with the Most Common Mutant Allele. *Kidney Int.* **2005**, *67* (5), 1704–1709.

[3] Fargue, S.; Rumsby, G.; Danpure, C. J. Multiple Mechanisms of Action of Pyridoxine in Primary Hyperoxaluria Type 1. *BBA-Mol. Basis Dis.* **2013**, *1832* (10), 1776–1783.

[4] Salido, E.; Pey, A. L.; Rodriguez, R.; Lorenzo, V. Primary Hyperoxalurias: Disorders of Glyoxylate Detoxification. *BBA-Mol. Basis Dis.* **2012**, *1822* (9), 1453–1464.

[5] Beck, B. B.; Hoyer-Kuhn, H.; Göbel, H.; Habbig, S.; Hoppe, B. Hyperoxaluria and Systemic Oxalosis: An Update on Current Therapy and Future Directions. *Expert Opin. Investig. Drugs* **2013**, *22* (1), 117–129.

[6] Watts, R. W. E.; Danpure, C. J.; Pauw, L. D.; Toussaint, C. Combined Liver–Kidney and Isolated Liver Transplantations for Primary Hyperoxaluria Type 1: The European Experience. *Nephrol. Dial. Transplant.* **1991**, *6* (7), 502–511.

[7] (a) Roncador, A.; Oppici, E.; Talelli, M.; Pariente, A. N.; Donini, M.; Dusi, S.; Voltattorni, C. B.; Vicent, M. J.; Cellini, B. Use of Polymer Conjugates for the Intraperoxisomal Delivery of Engineered Human Alanine:glyoxylate Aminotransferase as a Protein Therapy for Primary Hyperoxaluria Type I. *Nanomedicine: NBM* **2017**, *13*(3), 879-907. (b) Castello, R.; Borzone, R.; D'Aria, S.; Annunziata, P.; Piccolo, P.; Brunetti-Pierri, N. Helper-Dependent Adenoviral Vectors for Liver-Directed Gene Therapy of Primary Hyperoxaluria Type 1. *Gene Ther* **2016**, *23* (2), 129–134. (c) Oppici, E.; Montioli, R.; Dindo, M.; Maccari, L.; Porcari, V.; Lorenzetto, A.; Chellini, S.; Voltattorni, C. B.; Cellini, B. The Chaperoning Activity of Amino-Oxyacetic Acid on Folding-Defective Variants of Human Alanine:Glyoxylate Aminotransferase Causing Primary Hyperoxaluria Type I. *ACS Chem. Biol.* **2015**, *10* (10), 2227–2236. (d) Salido, E.; Rodriguez-Pena, M.; Santana, A.; Beattie, S. G.; Petry, H.; Torres, A. Phenotypic Correction of a Mouse Model for Primary Hyperoxaluria With Adeno-Associated Virus Gene Transfer. *Mol Ther* **2011**, *19* (5), 870–875. (e) Salido, E. C.; Li, X. M.; Lu, Y.; Wang, X.; Santana, A.; Roy-Chowdhury, N.; Torres, A.; Shapiro, L. J.; Roy-Chowdhury, J. Alanine-Glyoxylate Aminotransferase-Deficient Mice, a Model for Primary Hyperoxaluria that Responds to Adenoviral Gene Transfer. *Proc. Natl. Acad. Sci. U.S.A.* **2006**, *103* (48), 18249–18254.

[8] Martin-Higueras, C.; Torres, A.; Salido, E. Molecular Therapy of Primary Hyperoxaluria. *J Inherit Metab Dis* **2017**, *40* (4), 481-489.

[9] Cellini, B. Treatment Options in Primary Hyperoxaluria Type I. *Exp. Opin. Orphan Drugs* **2017**, *5* (4), 309–319.

[10] Smid, B. E.; Aerts, J. M. F. G.; Boot, R. G.; Linthorst, G. E.; Hollak, C. E. M. Pharmacological Small Molecules for the Treatment of Lysosomal Storage Disorders. *Expert Opin Investig Drugs* **2010**, *19* (11), 1367–1379.

[11] Martin-Higueras, C.; Luis-Lima, S.; Salido, E. Glycolate Oxidase Is a Safe and Efficient Target for Substrate Reduction Therapy in a Mouse Model of Primary Hyperoxaluria Type I. *Mol. Ther*. **2016**, *24* (4), 719–725.

[12] Summitt, C. B.; Johnson, L. C.; Jönsson, T. J.; Parsonage, D.; Holmes, R. P.; Lowther, W. T. Proline Dehydrogenase 2 (PRODH2) Is a Hydroxyproline Dehydrogenase (HYPDH) and Molecular Target for Treating Primary Hyperoxaluria. *Biochem. J.* **2015**, *466* (2), 273–281.

[13] Fargue, S.; Milliner, D. S.; Knight, J.; Olson, J. B.; Lowther, W. T.; Holmes, R. P. Hydroxyproline Metabolism and Oxalate Synthesis in Primary Hyperoxaluria. *J. Amer. Soc. Nephrol.* **2018**, *29* (6), 1615–1623.

[14] Holmes, R. P. Pharmacological Approaches in the Treatment of Primary Hyperoxaluria. *J. Nephrol.* **1998**, *11 Suppl 1*, 32–35.

[15] Murray, M. S.; Holmes, R. P.; Lowther, W. T. Active Site and Loop 4 Movements within Human Glycolate Oxidase: Implications for Substrate Specificity and Drug Design. *Biochemistry* **2008**, *47* (8), 2439–2449.

[16] Stenberg, K.; Lindqvist, Y. Three-Dimensional Structures of Glycolate Oxidase with Bound Active-Site Inhibitors. *Protein Sci.* **1997**, *6* (5), 1009-1015.

[17] Vignaud, C.; Pietrancosta, N.; Williams, E. L.; Rumsby, G.; Lederer, F. Purification and Characterization of Recombinant Human Liver Glycolate Oxidase. *Arch. Biochem. Biophys.* **2007**, *465* (2), 410–416.

[18] Bourhis, J.-M.; Vignaud, C.; Pietrancosta, N.; Guéritte, F.; Guénard, D.; Lederer, F.; Lindqvist, Y. Structure of Human Glycolate Oxidase in Complex with the Inhibitor 4-Carboxy-5-[(4-Chlorophenyl)sulfanyl]-1,2,3-Thiadiazole. *Acta Cryst. F* **2009**, *65* (12), 1246–1253.

[19] Randall, W. C.; Streeter, K. B.; Cresson, E. L.; Schwam, H.; Michelson, S. R.; Anderson, P. S.; Cragoe, E. J.; Williams, H. W. R.; Eichler, E.; Rooney, C. S. Quantitative Structure-Activity Relationships Involving the Inhibition of Glycolic Acid Oxidase by Derivatives of Glycolic and Glyoxylic Acids. *J. Med. Chem.* **1979**, *22* (6), 608–614.

[20] Williams, H. W. R.; Eichler, E.; Randall, W. C.; Rooney, C. S.; Cragoe, E. J.; Streeter, K. B.; Schwam, H.; Michelson, S. R.; Patchett, A. A.; Taub, D. Inhibitors of Glycolic Acid Oxidase. 4-Substituted-2,4-Dioxobutanoic Acid Derivatives. *J. Med. Chem.* **1983**, *26* (8), 1196–1200.

[21] Rooney, C. S.; Randall, W. C.; Streeter, K. B.; Ziegler, C.; Cragoe, E. J.; Schwam, H.; Michelson, S. R.; Williams, H. W. R.; Eichler, E. Inhibitors of Glycolic Acid Oxidase. 4-Substituted 3-Hydroxy-1H-Pyrrole-2,5-Dione Derivatives. *J. Med. Chem.* **1983**, *26* (5), 700–714.

[22] Chen, Z.; Vignaud, C.; Jaafar, A.; Lévy, B.; Guéritte, F.; Guénard, D.; Lederer, F.; Mathews, F. S. High Resolution Crystal Structure of Rat Long Chain Hydroxy Acid Oxidase in Complex

with the Inhibitor 4-Carboxy-5-[(4-Chlorophenyl)sulfanyl]-1, 2, 3-Thiadiazole. Implications for Inhibitor Specificity and Drug Design. *Biochimie* **2012**, *94* (5), 1172–1179.

[23] Lowther, W. T.; Holmes, R. P. Hypdh Inhibitors and Methods of Use for the Treatment of Kidney Stones. WO2016123012 (A1), August 4, 2016.

[24] Dutta, C.; Avitahl-Curtis, N.; Pursell, N.; Larsson Cohen, M.; Holmes, B.; Diwanji, R.; Zhou, W.; Apponi, L.; Koser, M.; Ying, B.; Chen, D.; Shui, X.; Saxena, U.; Cyr, W.A.; Shah, A.; Nazef, N.; Wang, W.; Abrams, M.; Dudek, H.; Salido, E.; Brown, B.D.; Lai, C. Inhibition of Glycolate Oxidase with Dicer-Substrate siRNA Reduces Calcium Oxalate Deposition in a Mouse Model of Primary Hyperoxaluria Type 1. *Mol. Ther.* **2016**, *24* (4), 770–778.

[25] Li, X.; Knight, J.; Fargue, S.; Buchalski, B.; Guan, Z.; Inscho, E. W.; Liebow, A.; Fitzgerald, K.; Querbes, W.; Todd Lowther, W.; et al. Metabolism of 13C5-Hydroxyproline in Mouse Models of Primary Hyperoxaluria and Its Inhibition by RNAi Therapeutics Targeting Liver Glycolate Oxidase and Hydroxyproline Dehydrogenase. *BBA-Mol. Basis Dis.* **2016**, *1862* (2), 233–239.

[26] Querbes, W.; Fitzgerald, K.; Bettencourt, B.; Liebow, A.; Erbe, D. Compositions and Methods for Inhibition of Hao1 (Hydroxyacid Oxidase 1 (Glycolate Oxidase)) Gene Expression. WO2016057893 (A1), April 14, 2016.

[27] Brown, B.; Dudek, H. Methods and Compositions for the Specific Inhibition of Glycolate Oxidase (Hao1) by Double-Stranded Rna. WO2015100436 (A1), July 2, 2015.

[28] Liebow, A.; Li, X.; Racie, T.; Hettinger, J.; Bettencourt, B.R.; Najafian, N.; Haslett, P.; Fitzgerald, K.; Holmes, R.P.; Erbe, D.; Querbes, W.; Knight, J. An Investigational RNAi Therapeutic Targeting Glycolate Oxidase Reduces Oxalate Production in Models of Primary Hyperoxaluria. *J. Amer. Soc. Nephrol.* **2017**, *28*, 494-503.

[29] Hinkle, G. Polynucleotde Agents Targeting Hydroxyacid Oxidase (Glycolate Oxidase, Hao1) and Methods of Use Thereof. WO 2016205323 (A1) December 22, 2016.

[30] (a) Hennekens, C. H.; Buring, J. E.; Sandercock, P.; Collins, R.; Peto, R. Aspirin and Other Antiplatelet Agents in the Secondary and Primary Prevention of Cardiovascular Disease. *Circulation* **1989**, *80* (4), 749–756. (b) Yosipovitch, G.; Tang, M. B. Y. Practical Management of Psoriasis in the Elderly. *Drugs Aging* **2002**, *19* (11), 847–863. (c) Davies, S. L.; Moral, M. A.; Bozzo, J. Salicylates Targeting Insulin Resistance. *Drug Future* **2007**, *32* (4), 361. (d) Baltazar, T.; Dinis-Oliveira, R. J.; Duarte, J. A.; de Lourdes Bastos, M.; Carvalho, F. Paraquat Research: Do Recent Advances in Limiting Its Toxicity Make Its Use Safer? *Br. J. Pharmacol.* **2013**, *168* (1), 44-45. (e) Wang, W.; Ye, S.-D.; Zhou, K.-Q.; Wu, L.-M.; Huang, Y.-N. High Doses of Salicylate and Aspirin Are Inhibitory on Acid-Sensing Ion Channels and Protective against Acidosis-Induced Neuronal Injury in the Rat Cortical Neuron. *J. Neurosci. Res.* **2012**, *90* (1), 267-277. (f) Nam, J.; Kim, W.; Lee, S.; Jeong, S.; Yoo, J.-W.; Kim, M.-S.; Jung, Y. Dextran-5-(4-Ethoxycarbonylphenylazo)salicylic Acid Ester, a Polymeric Colon-Specific Prodrug Releasing 5-Aminosalicylic Acid and Benzocaine, Ameliorates TNBS-Induced Rat Colitis. *J. Drug Target.* **2016**, *24* (5), 468-474.

[31] Klessig, D. F.; Tian, M.; Choi, H. W. Multiple Targets of Salicylic Acid and Its Derivatives in Plants and Animals. *Front. Immunol.* **2016**, *7*:206, 1-10.

[32] Williams, E.; Cregeen, D.; Rumsby, G. Identification and Expression of a cDNA for Human Glycolate Oxidase. Biochim. Biophys. Acta **2000**, *1493*(1-2), 246-248.

[33] Stone C.A.; Van Arman C.G.; Lotti V.J.; Minsker D.H.; Risley E.A.; Bagdon W.J.; Bokelman D.L.; Jensen R.D.; Mendlowski B.; Tate C.L.; Peck H.M.; Zwickley R.E.; McKinney S.E. Pharmacology and Toxicology of Diflunisal. *Br. J. Clin. Pharmacol.* **1977***, 4*(S1), 19S-29S.

[34] (a) Ramarao, C.; Ley, S.V.; Smith, S.C.; Shiley, I.M.; DeAlmeida, N. Encapsulation of Palladium in Polyurea Microcapsules. *J. Chem. Soc., Chem. Commun.* **2002**, 1132-1133. (b) Silva, J. F. M. da; Perez, A. F. Y.; Almeida, N. P. de. Phosphine-Free Suzuki Cross-Coupling Reaction Using an Efficient and Reusable Pd Catalyst in an Aqueous Medium Under Microwave Irradiation. *Synthetic Communications* **2015**, *45* (17), 1995–2004. (c) Silva, J. F. M. da; Perez, A. F. Y.; Almeida, N. P. de. An Efficient and New Protocol for Phosphine-Free Suzuki Coupling Reaction Using Palladium-Encapsulated and Air-Stable MIDA Boronates in an Aqueous Medium. *RSC Advances* **2014**, *4* (53), 28148–28155.

[35] Katritzky, A. R.; Tala, S. R.; Lu, H.; Vakulenko, A. V.; Chen, Q.-Y.; Sivapackiam, J.; Pandya, K.; Jiang, S.; Debnath, A. K. Design, Synthesis, and Structure−Activity Relationship of a Novel Series of 2-Aryl 5-(4-Oxo-3-Phenethyl-2-Thioxothiazolidinylidenemethyl)furans as HIV-1 Entry Inhibitors. *J. Med. Chem.* **2009**, *52* (23), 7631–7639.

[36] Hosoya, T.; Aoyama, H.; Ikemoto, T.; Kihara, Y.; Hiramatsu, T.; Endo, M.; Suzuki, M. Dantrolene Analogues Revisited: General Synthesis and Specific Functions Capable of Discriminating Two Kinds of Ca2+ Release from Sarcoplasmic Reticulum of Mouse Skeletal Muscle. *Bioorg. Med. Chem.* **2003**, *11* (5), 663–673.

[37] Franchi, L.; Rinaldi, M.; Vignaroli, G.; Innitzer, A.; Radi, M.; Botta, M. Arylation of 2-Furyl 4-Fluorophenyl Ketone: An Extension of Heck Chemistry towards Novel Integrase Inhibitors. *Synthesis* **2010**, *2010* (22), 3927–3933.

[38] Xie, Y.; Liu, Y.; Gong, G.; Rinderspacher, A.; Deng, S.-X.; Smith, D. H.; Toebben, U.; Tzilianos, E.; Branden, L.; Vidović, D.; et al. Discovery of a Novel Submicromolar Inhibitor of the Lymphoid Specific Tyrosine Phosphatase. *Bioorg. Med. Chem. Letters* **2008**, *18* (9), 2840–2844.

[39] Jones, H.; Fordice, M. W.; Greenwald, R. B.; Hannah, J.; Jacobs, A.; Ruyle, W. V.; Walford, G. L.; Shen, T. Y. Synthesis and Analgesic-Antiinflammatory Activity of Some 4- and 5-Substituted Heteroarylsalicylic Acids. *J. Med. Chem.* **1978**, *21* (11), 1100–1104.

[40] (a) Wang, Z.; Yang, Z.; Zhang, L.; Wang, X.; Peng, C.; Meng, D.; Yan, D. Toxic Effects of Vinca Alkaloids from Catharanthus Roseus (L.) G. Don on Tetrahymena Thermophila BF5 Growth by Microcalorimetry. *Thermochim. Acta* **2017**, *651* (Supplement C), 53–57. (b) Miyamoto, M.; Fujiwara, A.; Tanaka, H.; Katagi, T. Acute Aquatic Toxicity of Metofluthrin Metabolites in the Environment. *J. Pestic. Sci.* **2013**, *38* (4), 173–180. (c) Rees, J. N.; Florang, V. R.; Eckert, L. L.; Doorn, J. A. Protein Reactivity of 3,4-Dihydroxyphenylacetaldehyde, a Toxic Dopamine Metabolite, Is Dependent on Both the Aldehyde and the Catechol. *Chem. Res. Toxicol.* **2009**, *22* (7), 1256–1263.

[41] Pan, P.; Knudson, S. E.; Bommineni, G. R.; Li, H.-J.; Lai, C.-T.; Liu, N.; Garcia-Diaz, M.; Simmerling, C.; Patil, S. S.; Slayden, R. A.; et al. Time-Dependent Diaryl Ether Inhibitors of

InhA: Structure–Activity Relationship Studies of Enzyme Inhibition, Antibacterial Activity, and in Vivo Efficacy. *ChemMedChem* **2014**, *9* (4), 776–791.

[42] Hathway, T.; Chernyshov, D. L.; Jenks, W. S. Selectivity in the Photo-Fenton and Photocatalytic Hydroxylation of Biphenyl-4-Carboxylic Acid and Derivatives (viz. 4-Phenylsalicylic Acid and 5-Phenylsalicylic Acid). *J. Phys. Org. Chem.* **2011**, *24* (12), 1151–1156.

[43] Vilaró, M.; Nieto, J.; La Parra, J. R.; Almeida, M. R.; Ballesteros, A.; Planas, A.; Arsequell, G.; Valencia, G. Tuning Transthyretin Amyloidosis Inhibition Properties of Iododiflunisal by Combinatorial Engineering of the Nonsalicylic Ring Substitutions. *ACS Comb. Sci.* **2015**, *17* (1), 32–38.

[44] Petros, A. M.; Swann, S. L.; Song, D.; Swinger, K.; Park, C.; Zhang, H.; Wendt, M. D.; Kunzer, A. R.; Souers, A. J.; Sun, C. Fragment-Based Discovery of Potent Inhibitors of the Anti-Apoptotic MCL-1 Protein. *Bioorg. Med. Chem. Letters* **2014**, *24* (6), 1484–1488.

[45] Hunter, C.A.; Sanders, J.K.M. the Nature of π-π Interactions. *J. Am. Chem. Soc.* **1990**, *112*, 5525-5534.

[46] (a) Flower, R. J. The Development of COX2 Inhibitors. *Nat. Rev. Drug Discov.* **2003**, *2* (3), 179–191. (b) Mitchell, J. A.; Akarasereenont, P.; Thiemermann, C.; Flower, R. J.; Vane, J. R. Selectivity of Nonsteroidal Antiinflammatory Drugs as Inhibitors of Constitutive and Inducible Cyclooxygenase. *Proc. Natl. Acad. Sci. U.S.A.* **1993**, *90* (24), 11693–11697.

[47] (a) Randjelović, P.; Veljković, S.; Stojiljković, N.; Sokolović, D.; Ilić, I.; Laketić, D.; Randjelović, D.; Randjelović, N. The Beneficial Biological Properties of Salicylic Acid. *Acta Facultatis Medicae Naissensis* **2015**, *32* (4), 259–265. (b) Choi, H. W.; Tian, M.; Song, F.; Venereau, E.; Preti, A.; Park, S.-W.; Hamilton, K.; Swapna, G. V. T.; Manohar, M.; Moreau, M.; et al. Aspirin′s Active Metabolite Salicylic Acid Targets High Mobility Group Box 1 to Modulate Inflammatory Responses. *Mol. Med*. **2015**, *21*, 526-535. (c) Fürst, R.; Blumenthal, S. B.; Kiemer, A. K.; Zahler, S.; Vollmar, A. M. Nuclear Factor-KB-Independent Anti-Inflammatory Action of Salicylate in Human Endothelial Cells: Induction of Heme Oxygenase-1 by the c-Jun N-Terminal Kinase/Activator Protein-1 Pathway. *J Pharmacol Exp Ther* **2006**, *318* (1), 389–394. (d) Wang, Z.; Brecher, P. Salicylate Inhibits Phosphorylation of the Nonreceptor Tyrosine Kinases, Proline-Rich Tyrosine Kinase 2 and c-Src. *Hypertension* **2001**, *37* (1), 148–153.

[48] Kenneth Kun-Yu Wu. Biochemical Pharmacology of Nonsteroidal Anti-Inflammatory Drugs. *Biochem. Pharmacol.* **1998**, *55* (5), 543–547.

[49] Cai, Q.; Dmitrieva, N. I.; Michea, L. F.; Rocha, G.; Ferguson, D.; Burg, M. B. Toxicity of Acetaminophen, Salicylic Acid, and Caffeine for First-Passage Rat Renal Inner Medullary Collecting Duct Cells. *J. Pharmacol. Exp. Ther.* **2003**, *306* (1), 35–42.

[50] Stupi, B. P.; Li, H.; Wang, J.; Wu, W.; Morris, S. E.; Litosh, V. A.; Muniz, J.; Hersh, M. N.; Metzker, M. L. Stereochemistry of Benzylic Carbon Substitution Coupled with Ring Modification of 2-Nitrobenzyl Groups as Key Determinants for Fast-Cleaving Reversible Terminators. *Angew. Chem. Int. Ed.* **2012**, *51* (7), 1724–1727.

[51] Vogrig, A.; Dorr, L.; Bouzidi, N.; Boucherle, B.; Wattiez, A.-S.; Cassier, E.; Vallon, G.; Ripoche, I.; Abrunhosa-Thomas, I.; Marin, P.; Nauton, L.; Thery, V.; Courteix, C.; Lian, L.-Y.; Ducki, S. Structure-Based Design of PDZ Ligands as Inhibitors of 5-HT2A Receptor/PSD-95 PDZ1 Domain Interaction Possessing Anti-Hyperalgesic Activity. *ACS Chem. Biol.* **2013**, *8* (10), 2209–2216.

Table of Contents graphic.